S1 Introduction of supplement

This document contains supplemental materials of the paper by Tsujino et al. “Evaluation of global ocean–sea-ice model simulations based on the experimental protocols of the Ocean Model Intercomparison Project phase 2 (OMIP-2)” submitted for possible publication in Geoscientific Model Development.

References

de Boyer-Montégut, C., Madec, G., Fischer A. S., Lazar, A., Iudicone, D.: Mixed layer depth over the global ocean: An examination of profile data and a profile-based climatology, J. Geophys. Res. 109, C12003, doi:10.1029/2004JC002378, 2004.

Ishii, M., Y. Fukuda, H. Hirahara, S. Yasui, T. Suzuki, and K. Sato: Accuracy of Global Upper Ocean Heat Content Estimation Expected from Present Observational Data Sets. SOLA, 13, 163–167, doi:10.2151/sola.2017-030, 2017.

Hurrell, J. W., Hack, J. J., Shea D., Caron, J. M., Rosinski, J.: A new sea surface temperature and sea ice boundary dataset for the community atmospheric model, J. Clim., 21, 5145–5153, https://doi.org/10.1175/2008JCLI2292.1, 2008.

Locarnini, R., Mishonov, A., Antonov, J. I., Boyer, T. P., Garcia, H., Baranova, O., Zweng, M. M., Paver, C. R., Reagan, J. R., Hamilton, D. J., and Seidov, D.: World Ocean Atlas 2013, Volume 1: Temperature, NOAA Atlas NESDIS 73, NOAA/NESDIS, U.S. Dept. of Commerce, Washington, D.C., 2013.

Macdonald, A. and Baringer, M.: Ocean Heat Transport. Ocean Circulation & Climate: A 21st Century Perspective. International geophysics series 103. Academic Press, pp.759–785, 2013.

McDonagh, E. L., King, B. A., Bryden, H. L., Courtois, P., Szuts, Z., Baringer, M., Cunningham, S. A., Atkinson, C., McCarthy, G.: Continuous estimate of Atlantic oceanic freshwater flux at 26.5°N, J. Clim. 28, 8888–8906. https://doi.org/10.1175/JCLI-D-14-00519.1, 2015.

Zweng, M., Reagan, J., Antonov, J., Locarnini, R., Mishonov, A., Boyer, T., Garcia, H., Baranova, O., Johnson, D., Seidov, D., and Biddle, M.: World Ocean Atlas 2013, Volume 2: Salinity, NOAA Atlas NESDIS 74, NOAA/NESDIS, U.S. Dept. of Commerce, Washington, D.C., 2013.

25

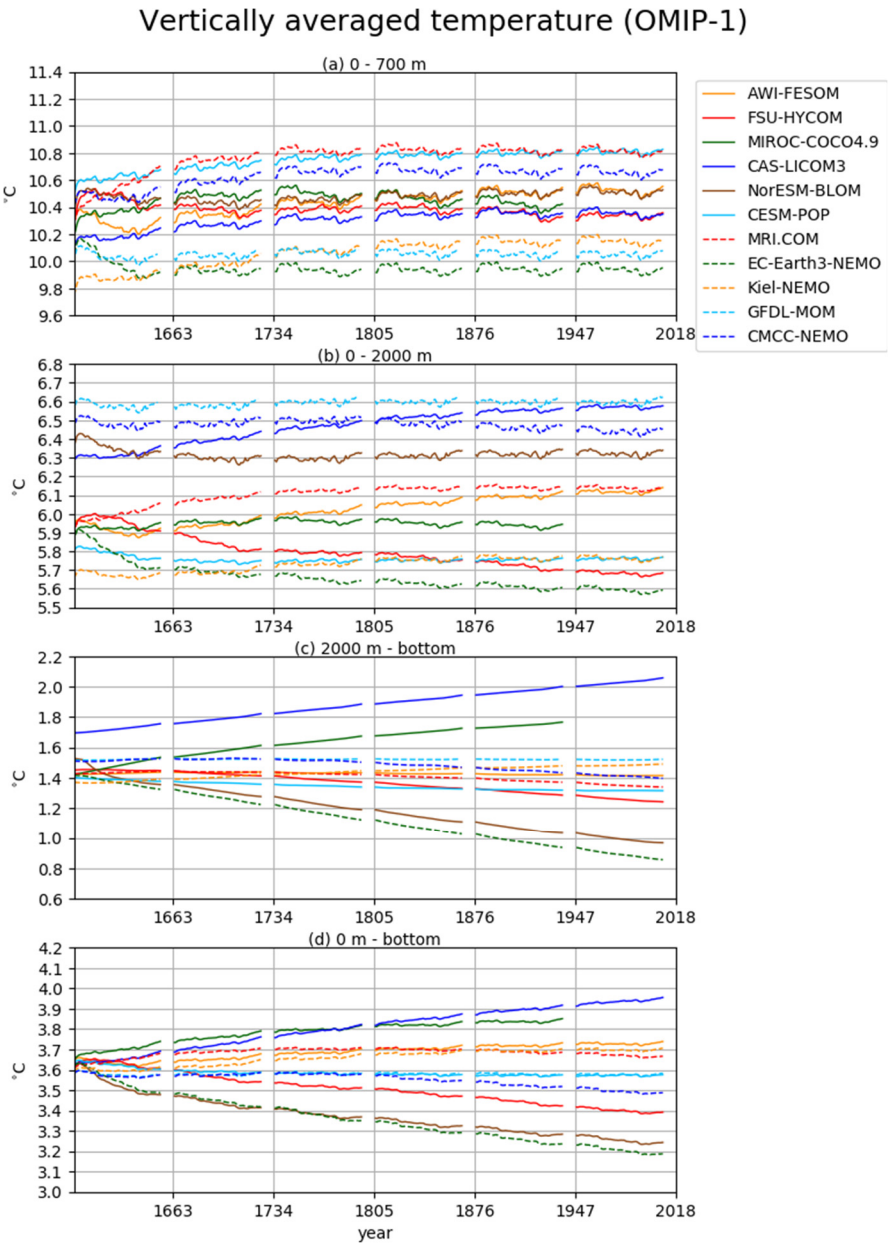

Figure S1: Drift of annual mean, global mean vertically averaged temperatures (°C) for four depth ranges of OMIP-1 simulations. (a) 0 – 700m, (b) 0 – 2000m, (c) 2000m – bottom, (d) 0 m – bottom.

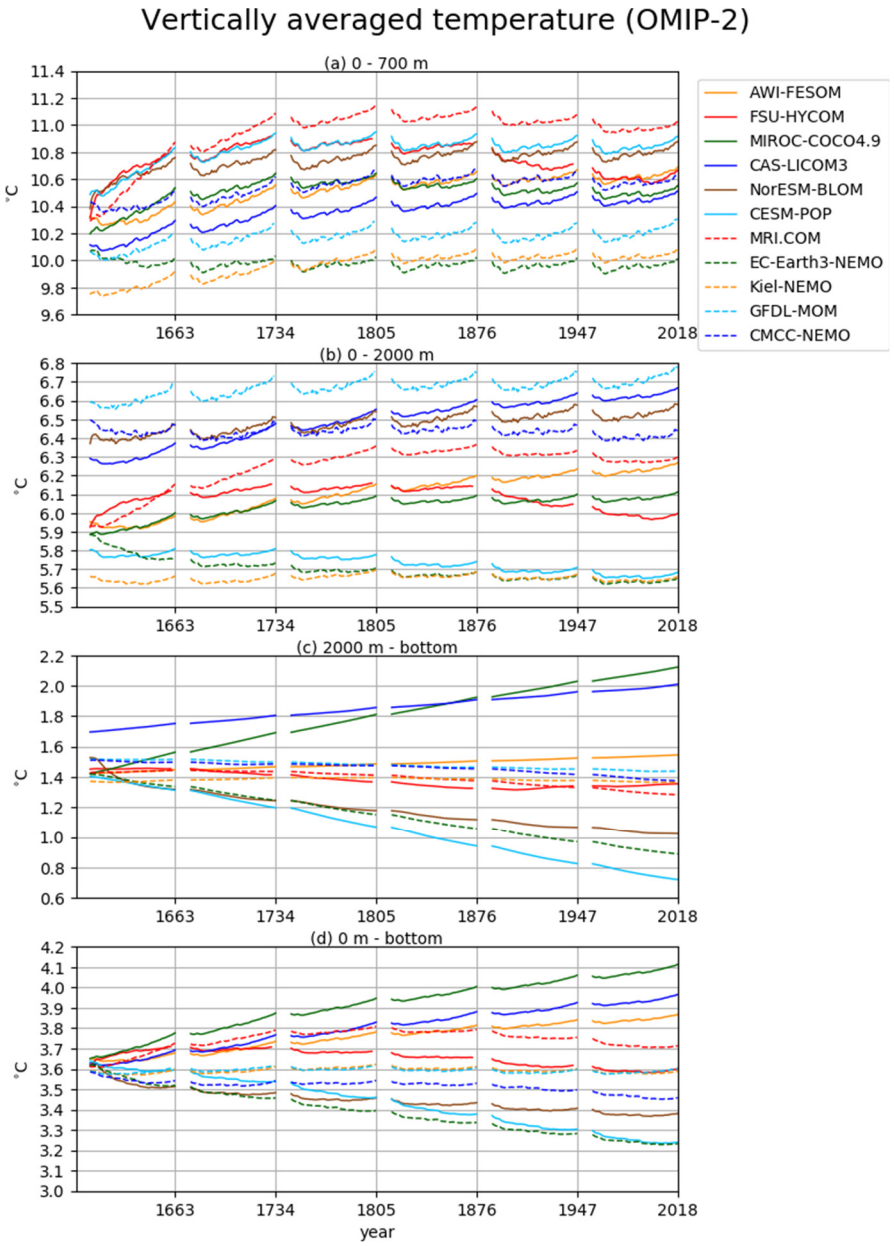

Figure S2: Same as Fig. S1 but for OMIP-2 simulations.

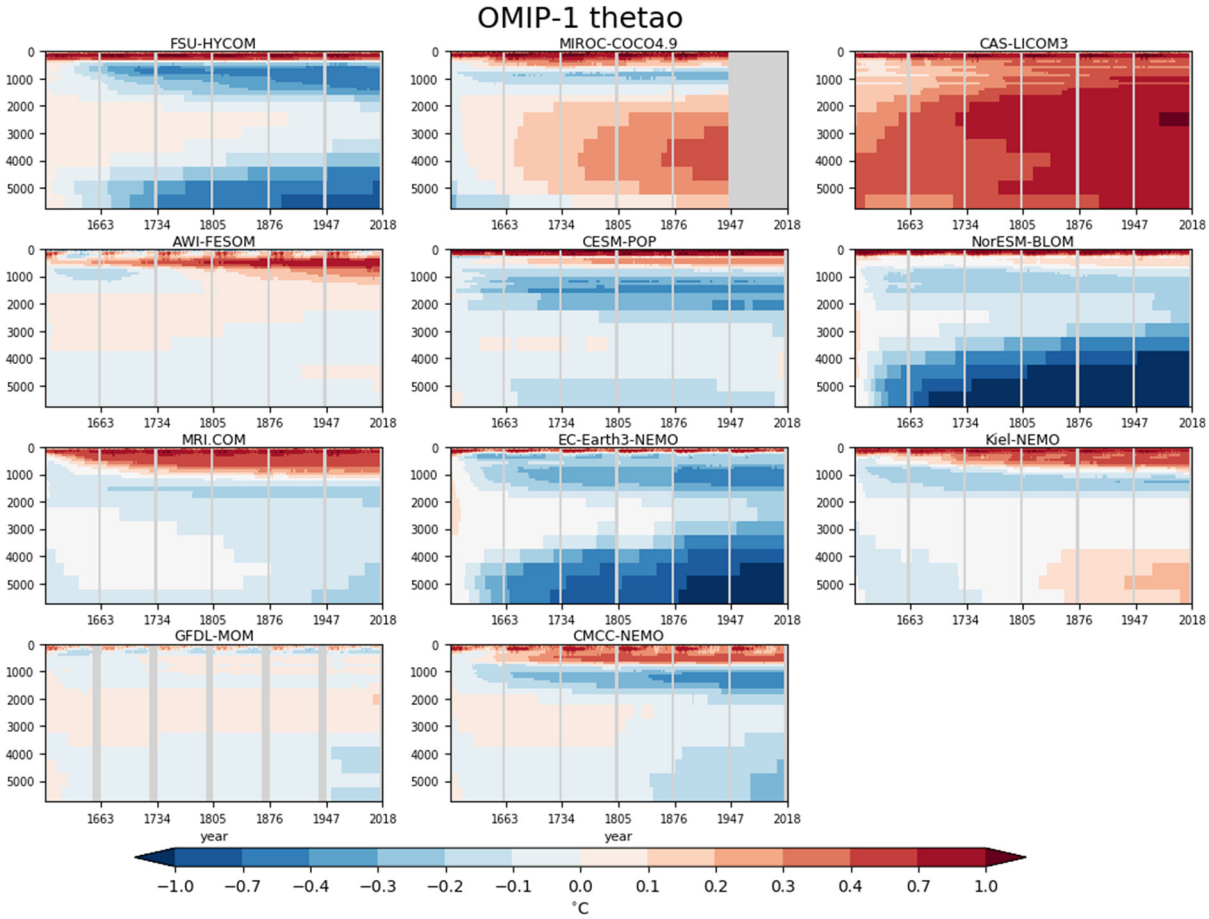

Figure S3: Globally averaged drift of annual mean temperature (°C) as a function of depth and time for OMIP-1 simulations. The drift is defined as the deviation from WOA13v2 (Locarnini et al. 2013).

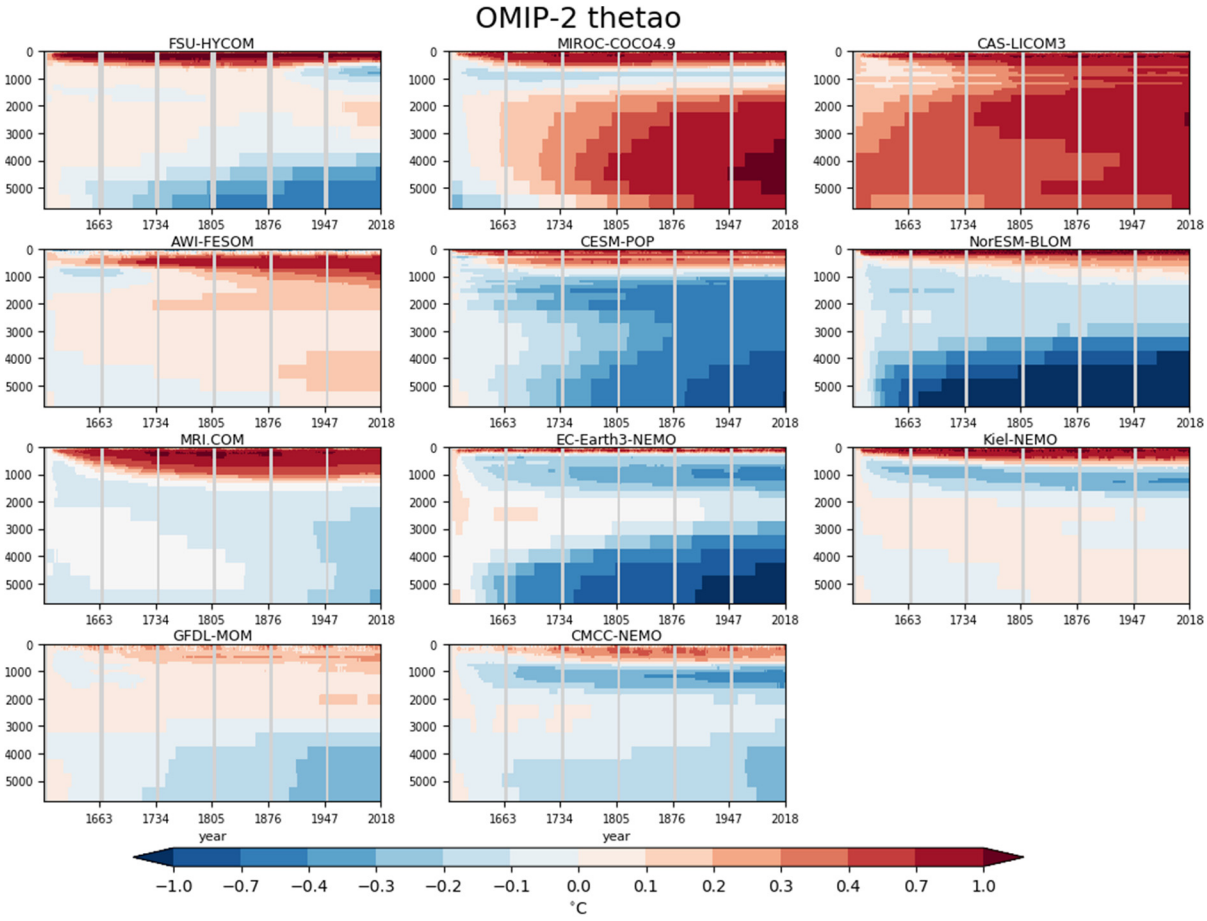

Figure S4: Same as Fig. S3 but for OMIP-2 simulations.

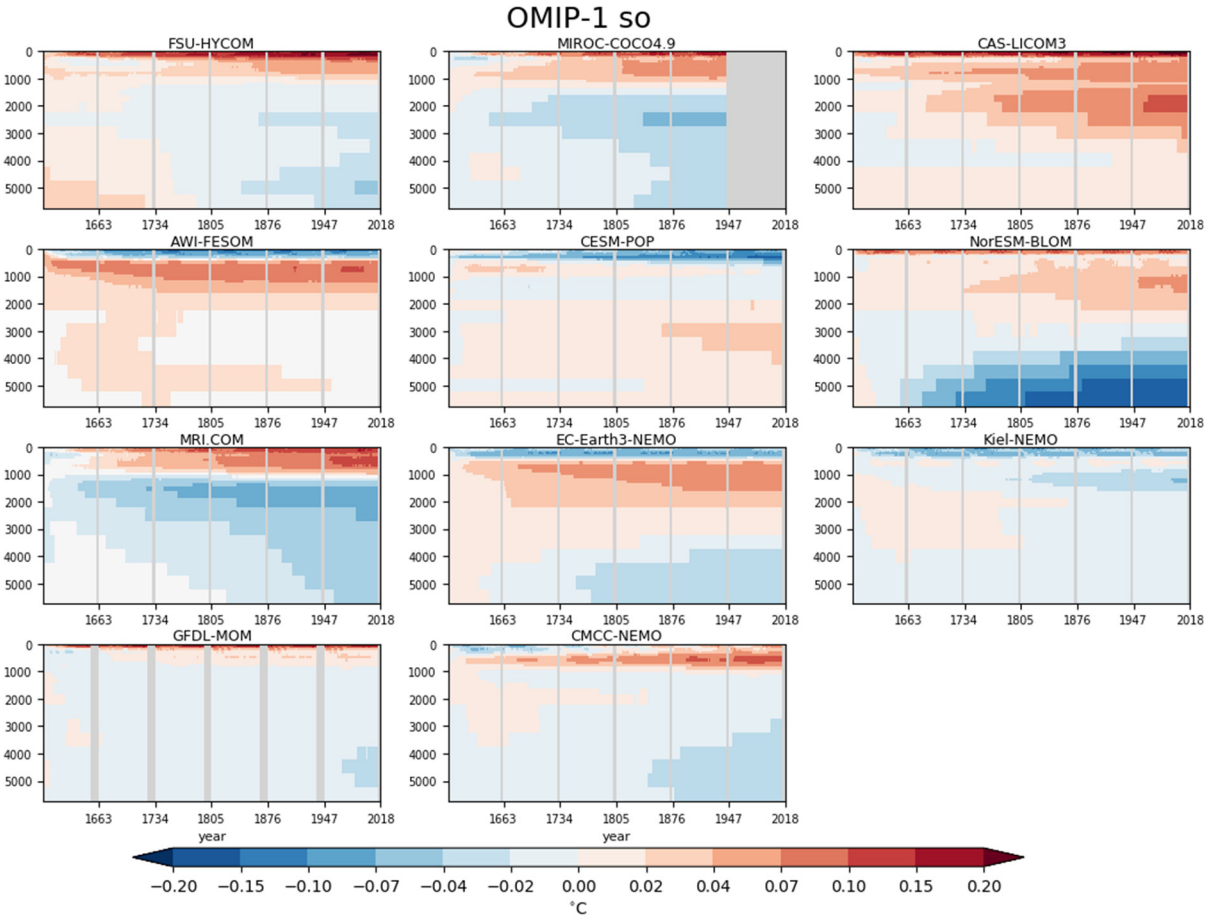

Figure S5: Globally averaged drift of annual mean horizontal mean salinity (psu) as a function of depth and time for OMIP-1 simulations. The drift is defined as the deviation from WOA13v2 (Zweng et al. 2013).

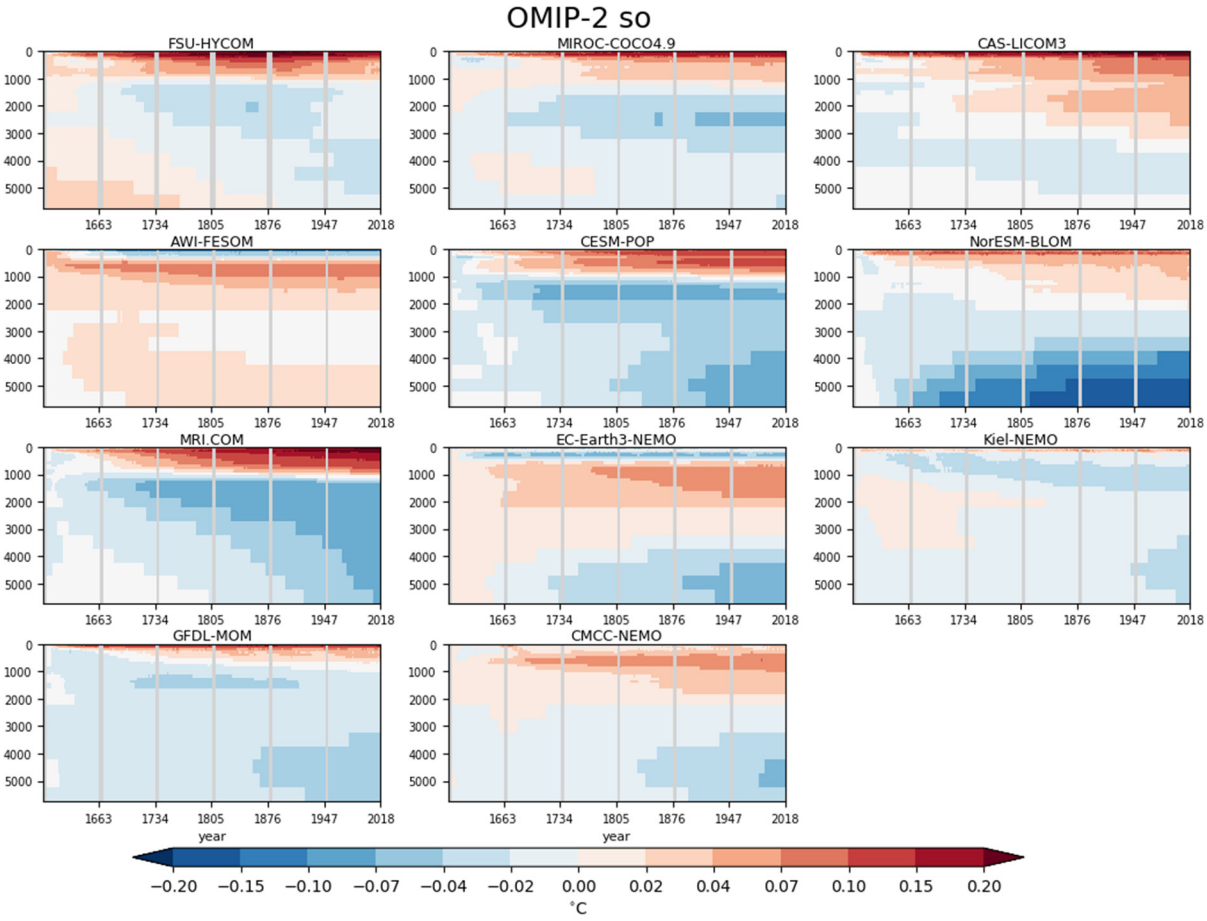

45 **Figure S6: Same as Fig. S5 but for OMIP-2 simulations.**

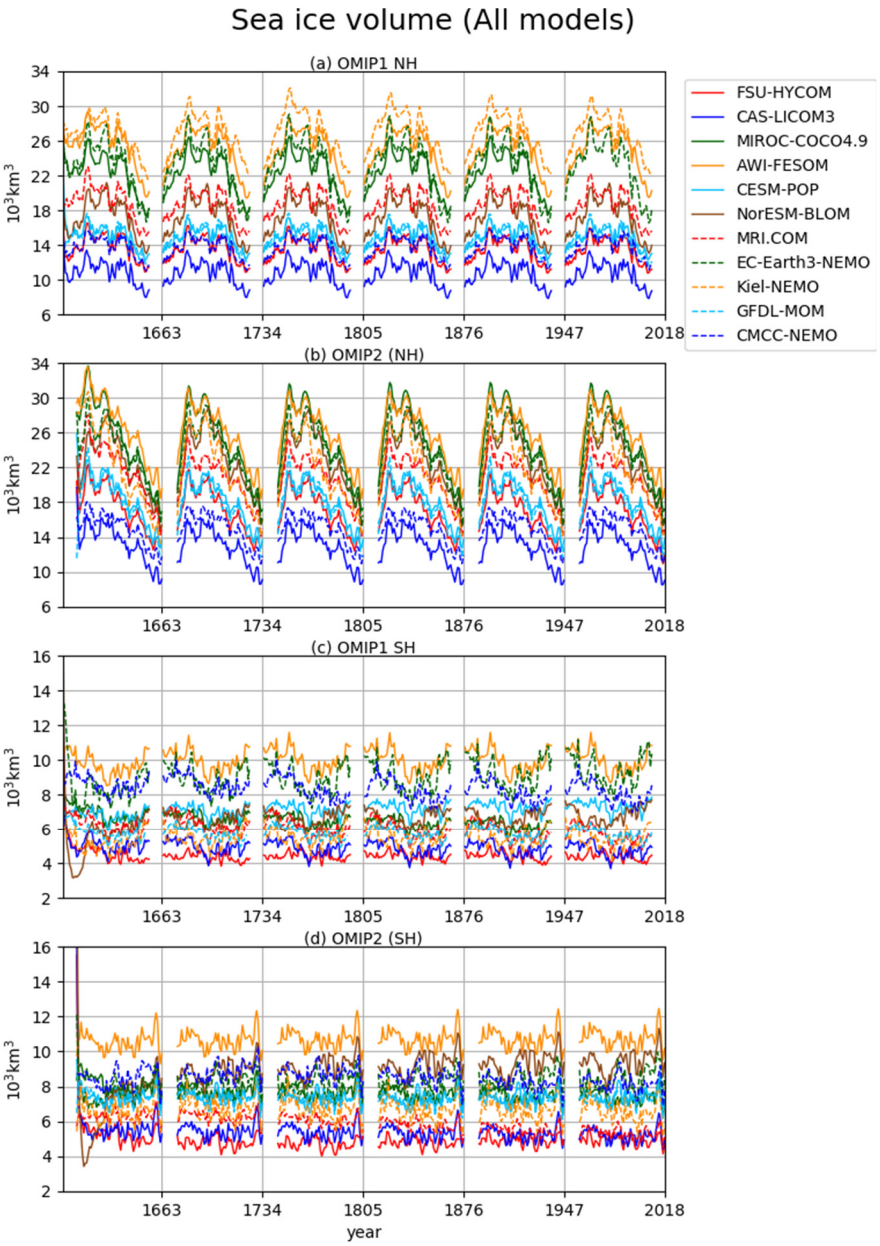

Figure S7: Time series of annual mean sea ice volume integrated over the Northern hemisphere (upper two panels) and the Southern hemisphere (lower two panels). Units are 10^3 km^3. (a, c) OMIP-1 and (b, d) OMIP-2 simulations.

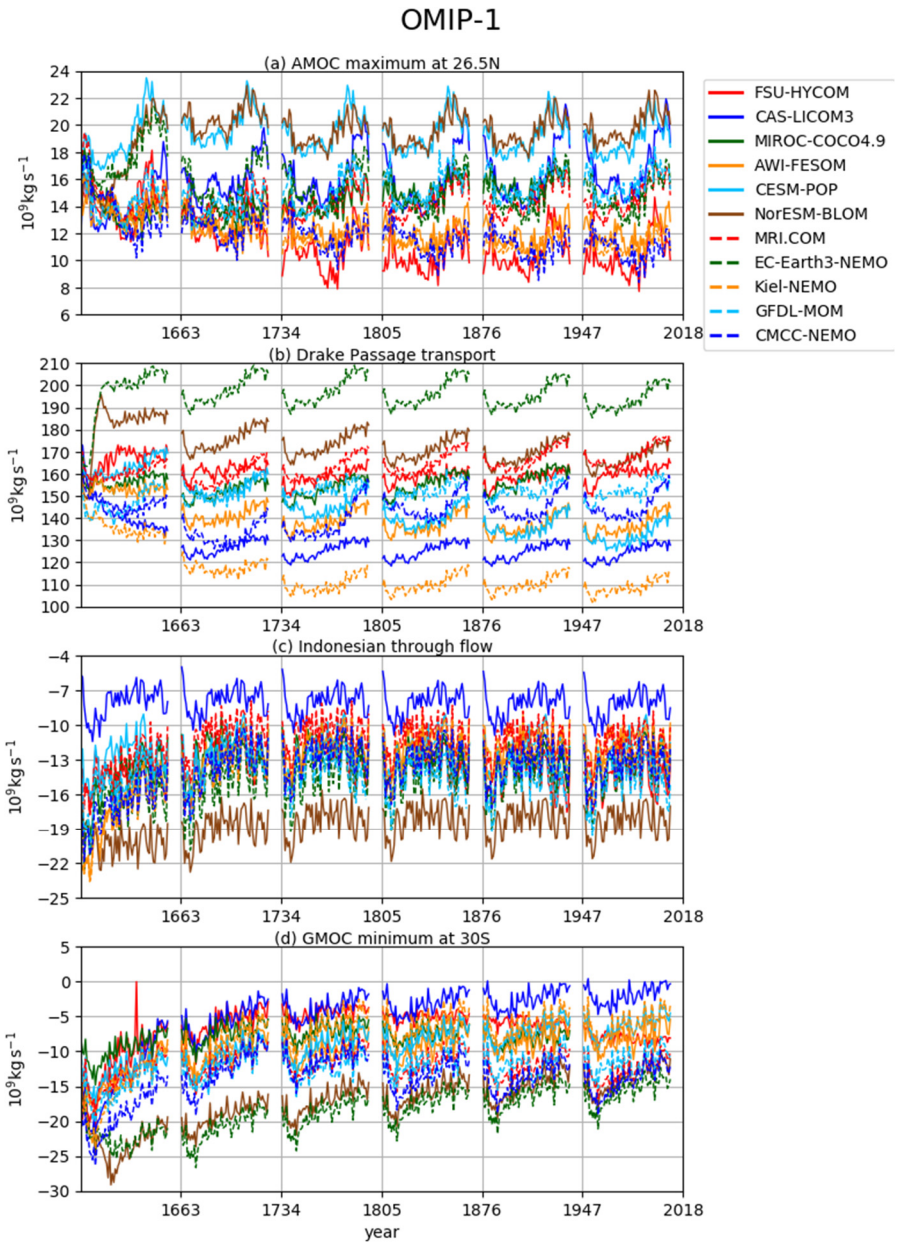

Figure S8: Time series of annual mean important ocean circulation metrics for OMIP-1 simulations. (a) Atlantic meridional overturning circulation (AMOC) maximum at 26.5°N, which represents the strength of AMOC associated with the North Atlantic Deep Water formation. (b) Drake passage transport (positive eastward), which represents the strength of Antarctic Circumpolar Current. (c) Indonesian Throughflow (negative into the Indian Ocean), which represents water exchange between the Pacific and Indian Ocean. (d) Global meridional overturning circulation (GMOC) minimum in 2000 m – bottom depths at 30°S, which represents the strength of deep to bottom layer GMOC associated with the Antarctic Bottom Water and Lower Circumpolar Deep Water formation. Units are 10^9 kg s^{-1}.

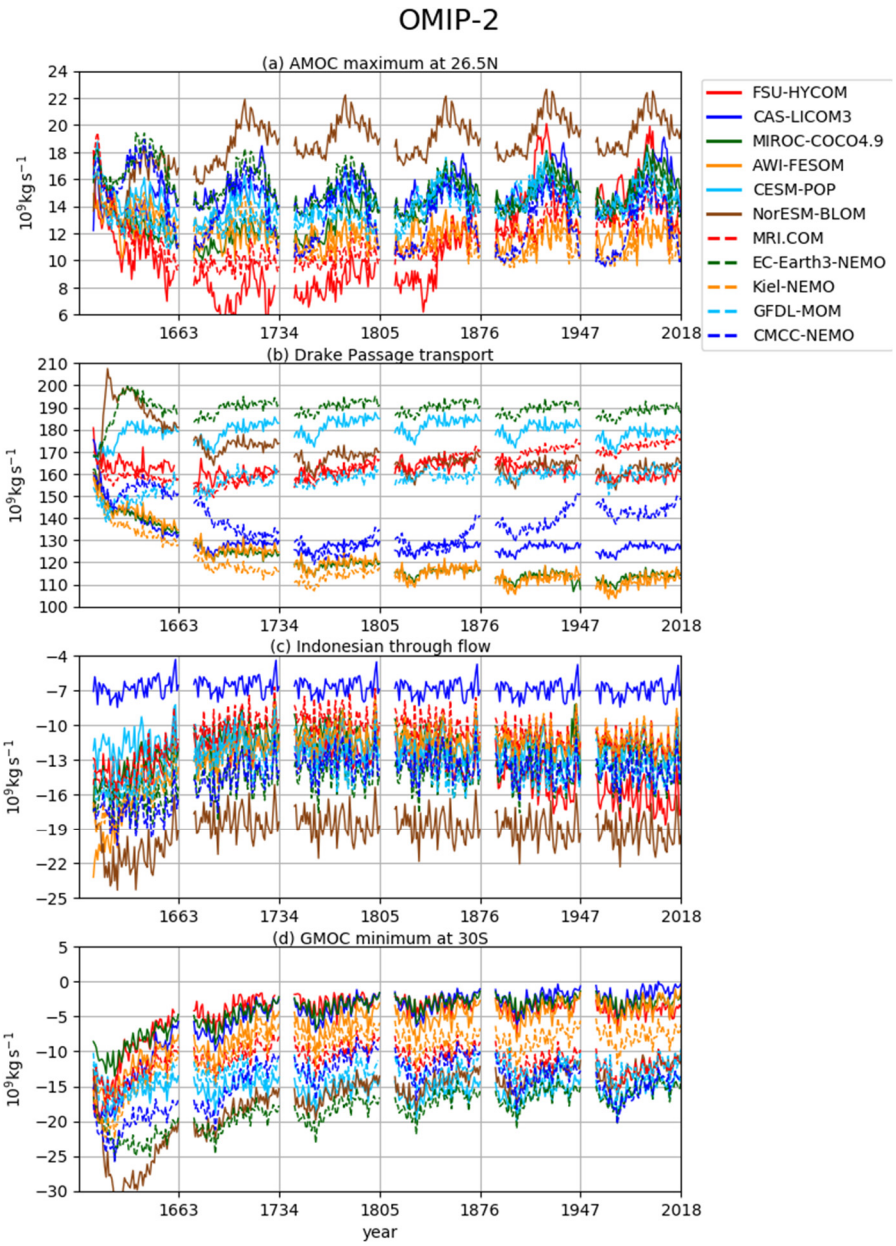

Figure S9: Same as Fig. S8 but for OMIP-2 simulations.

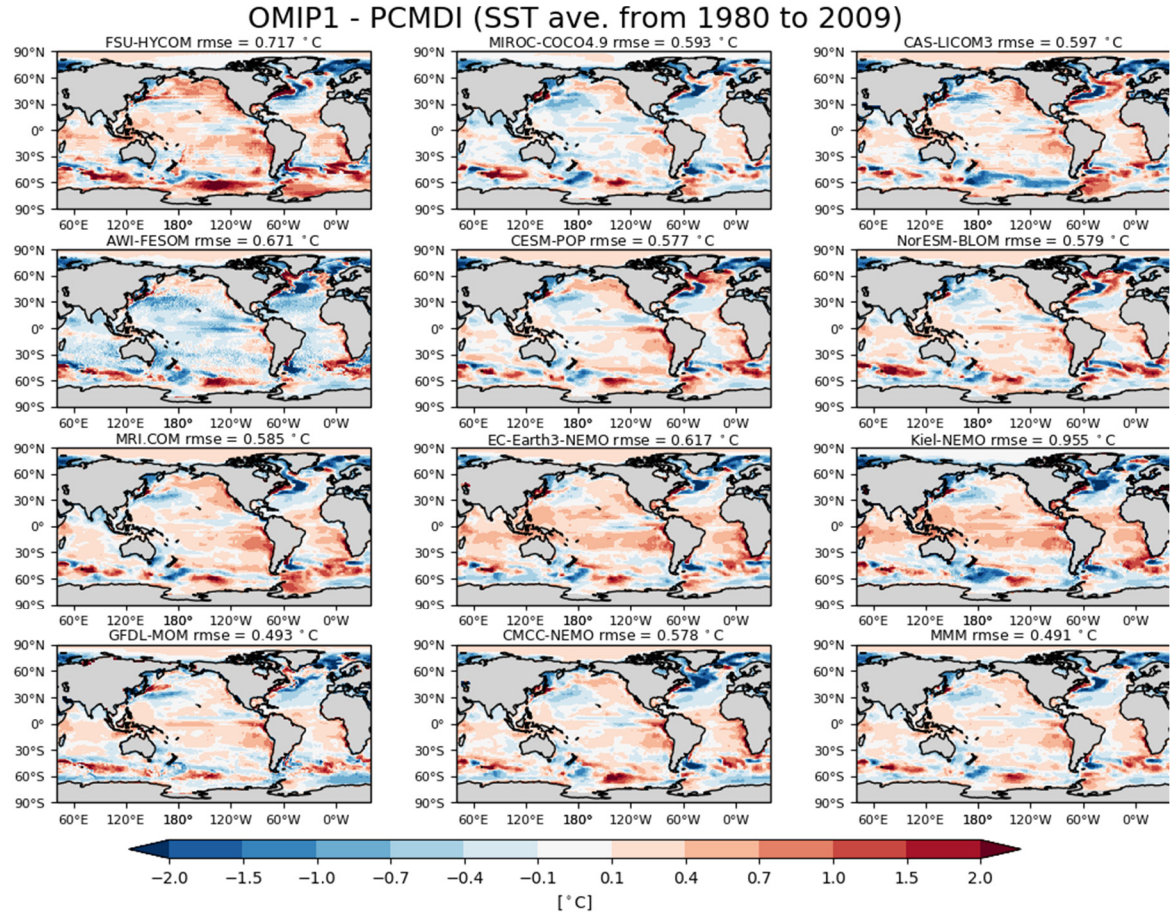

Figure S10: Bias of 30-year (1980-2009) mean sea surface temperature (SST) of OMIP-1 simulations relative to an observational estimate provided and updated by Program for Climate Model Diagnosis and Intercomprison (PCMDI) following a procedure described by Hurrell et al. (2008) (hereafter referred to as PCMDI-SST). Units are °C.

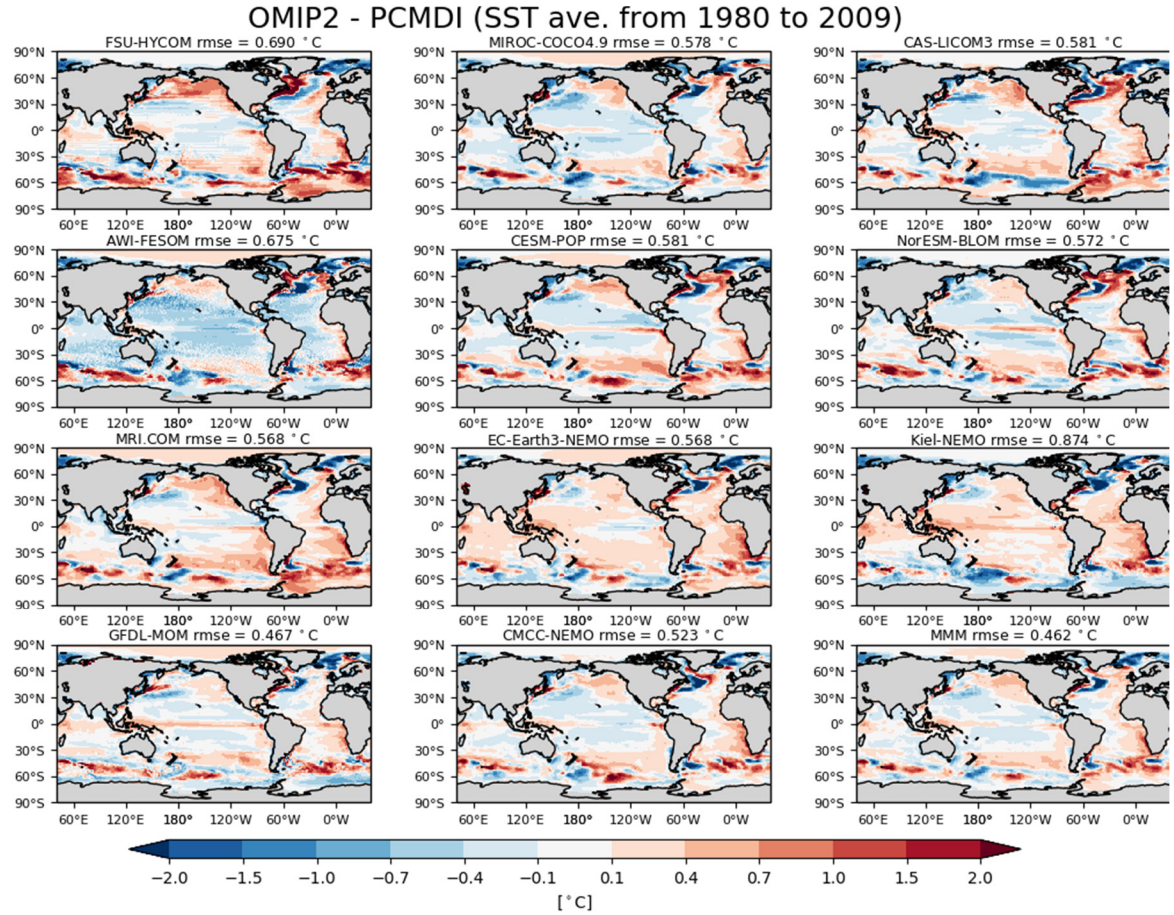

Figure S11: Same as Fig. S10 but for OMIP-2 simulations.

70

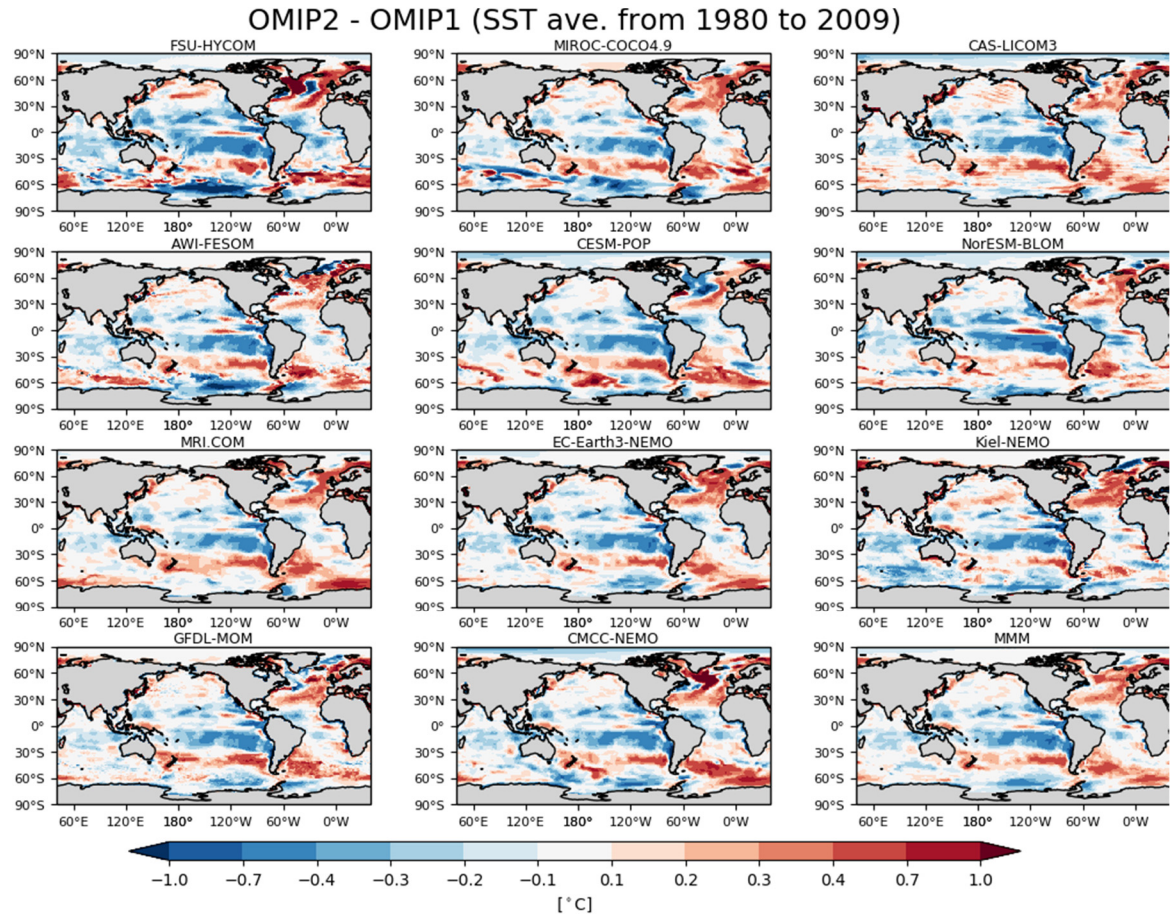

Figure S12: Difference of 30-year (1980-2009) mean SST between OMIP-1 and OMIP-2 simulations of individual models. Units are °C.

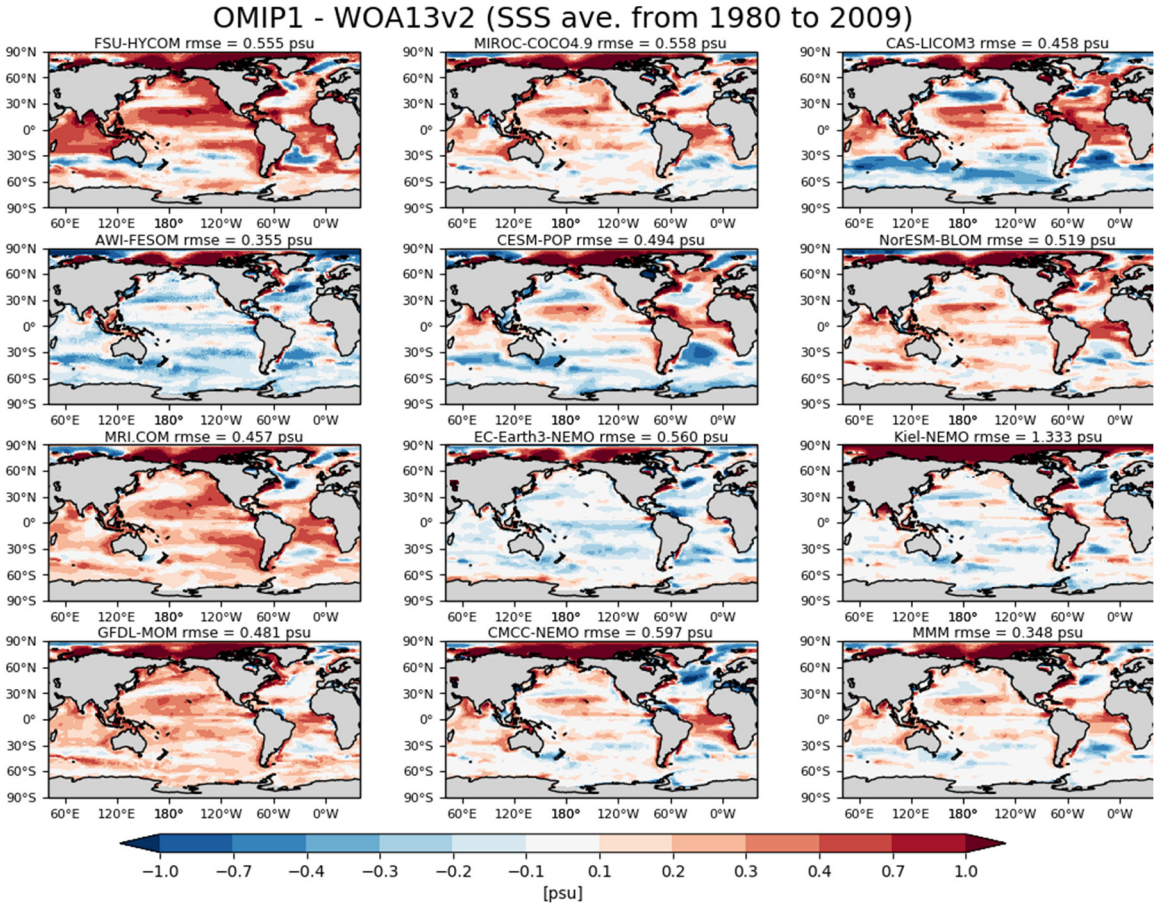

Figure S13: Bias of 30-year (1980-2009) mean sea surface salinity (SSS) of OMIP-1 simulations relative to WOA13v2 (Zweng et al. 2013). Units are psu.

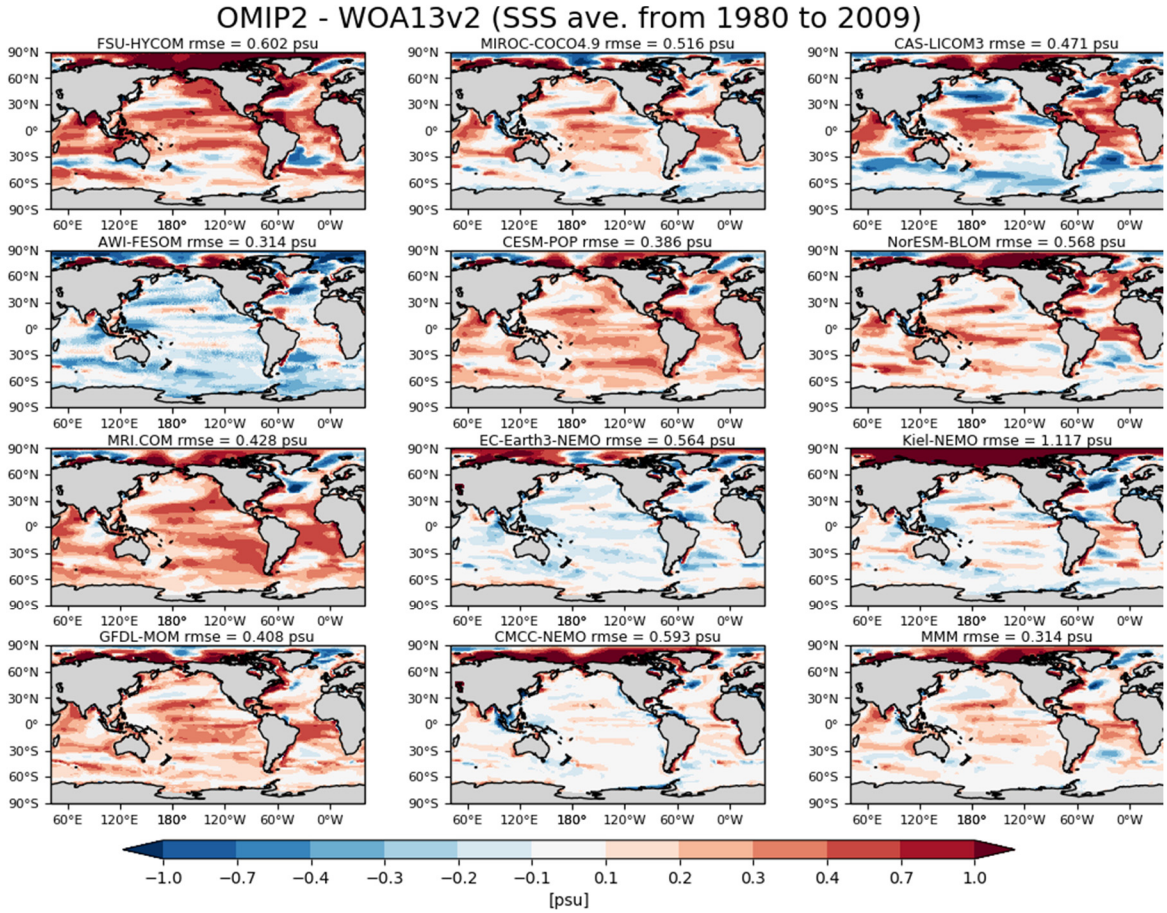

Figure S14: Same as Fig. S13 but for OMIP-2 simulations.

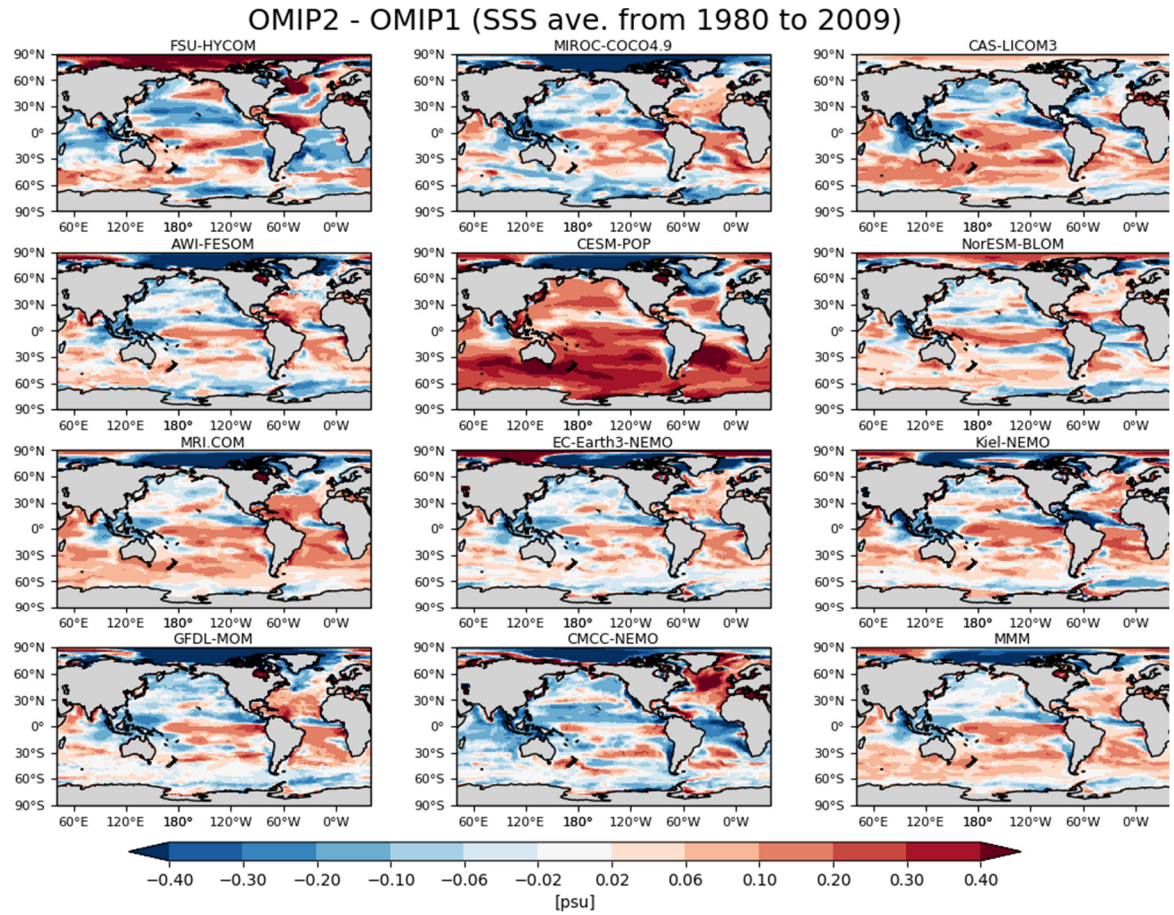

Figure S15: Difference of 30-year (1980-2009) mean SSS between OMIP-1 and OMIP-2 simulations of individual models. Units are psu.

85

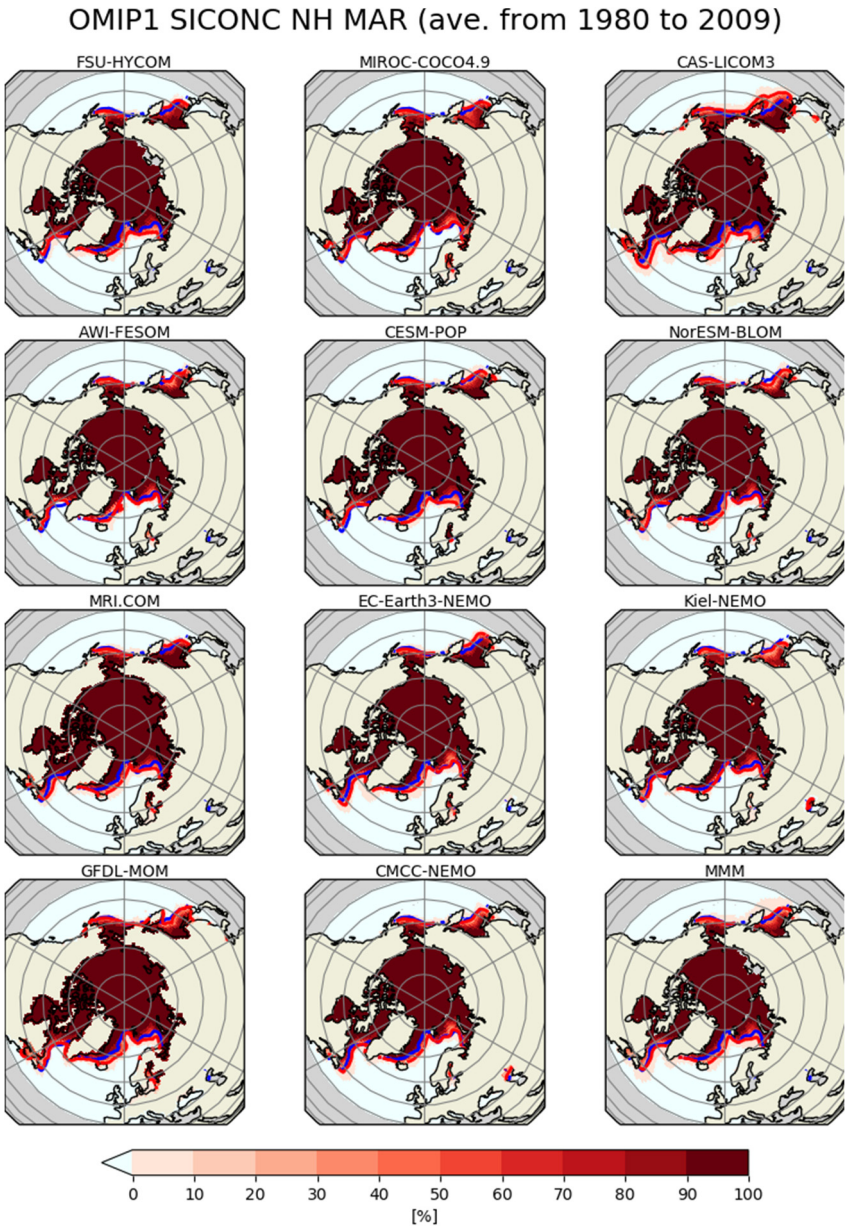

Figure S16: Thirty (30)-year (1980-2009) mean sea ice concentration (%) in March of Northern Hemisphere of OMIP-1 simulations. Blue lines are contours of 15 % concentration of an observational estimate from the PCMDI-SST dataset and red lines are those of the model.

90

Figure S17: Same as Fig. S16 but for OMIP-2 simulations. Blue and red lines as in Fig. S16.

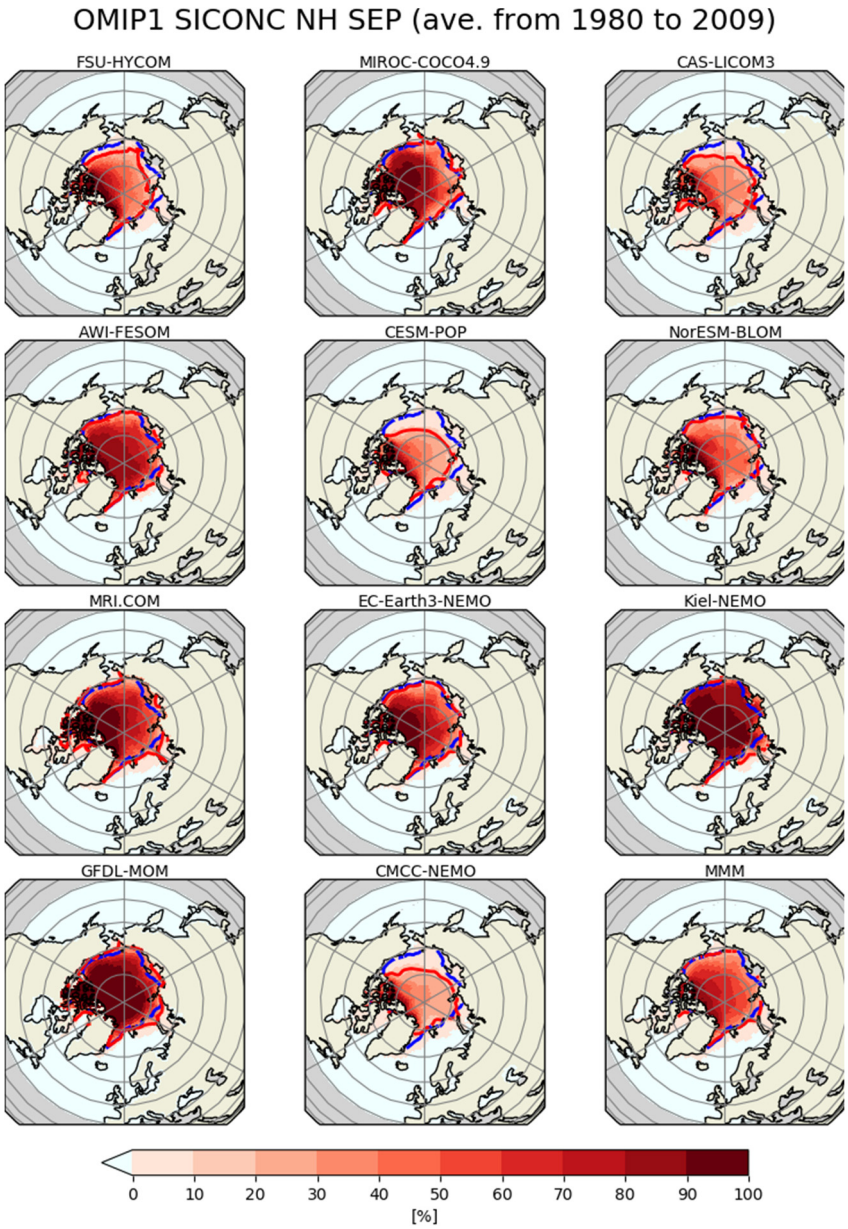

95 **Figure S18: Thirty (30)-year (1980-2009) mean sea ice concentration (%) in September of Northern Hemisphere of OMIP-1 simulations. Blue and red lines as in Fig. S16.**

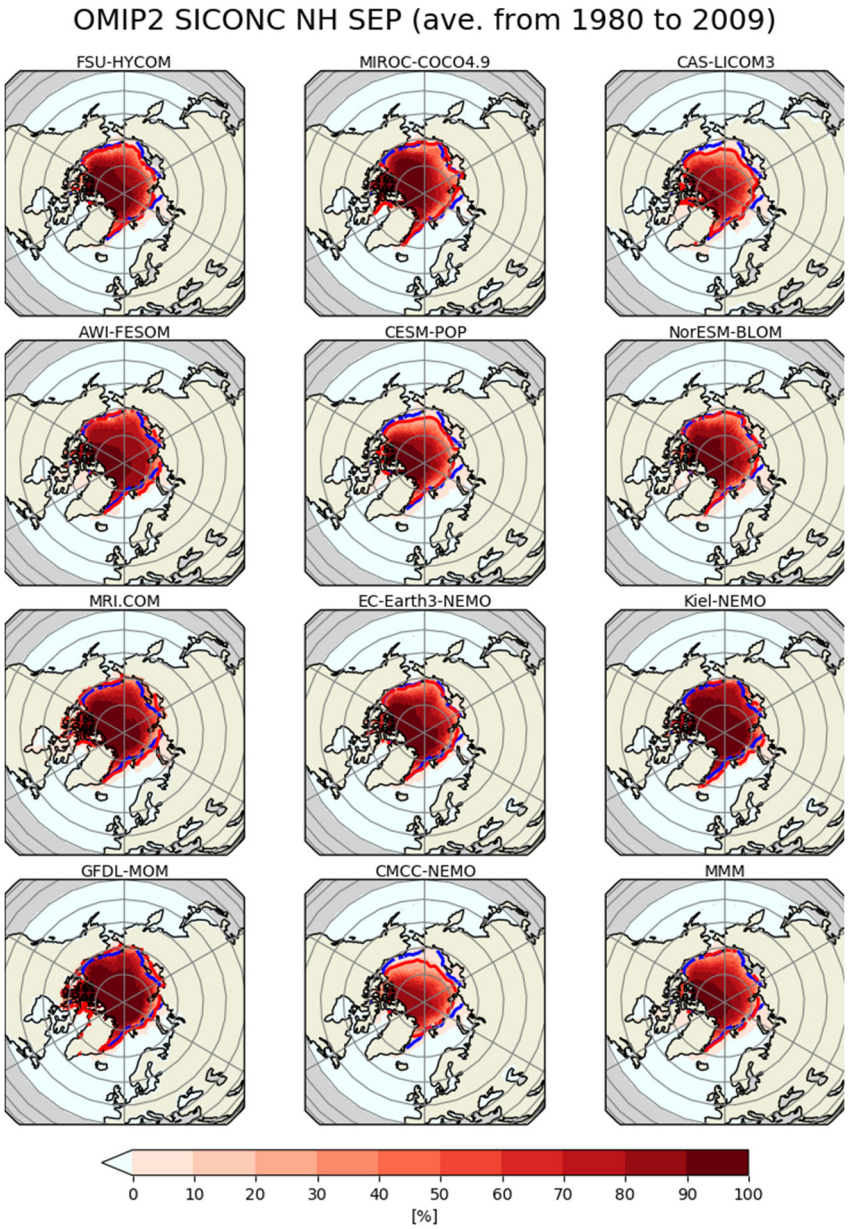

Figure S19: Same as Fig. S18 but for OMIP-2 simulations. Blue and red lines as in Fig. S16.

100

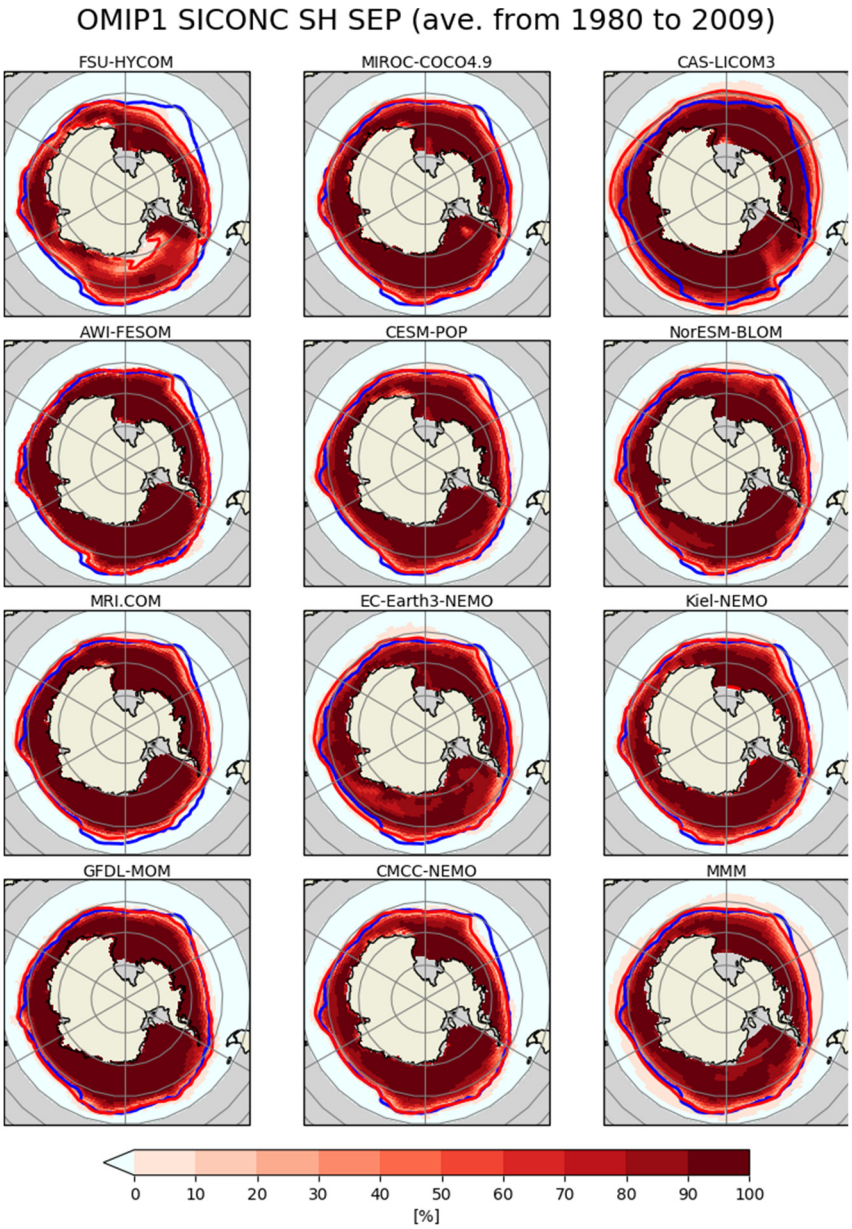

Figure S20: Thirty (30)-year (1980-2009) mean sea ice concentration (%) in September of Southern Hemisphere of OMIP-1 simulations. Blue lines are contours of 15 % concentration of an observational estimate from the PCMDI-SST dataset and red lines are those of the model.

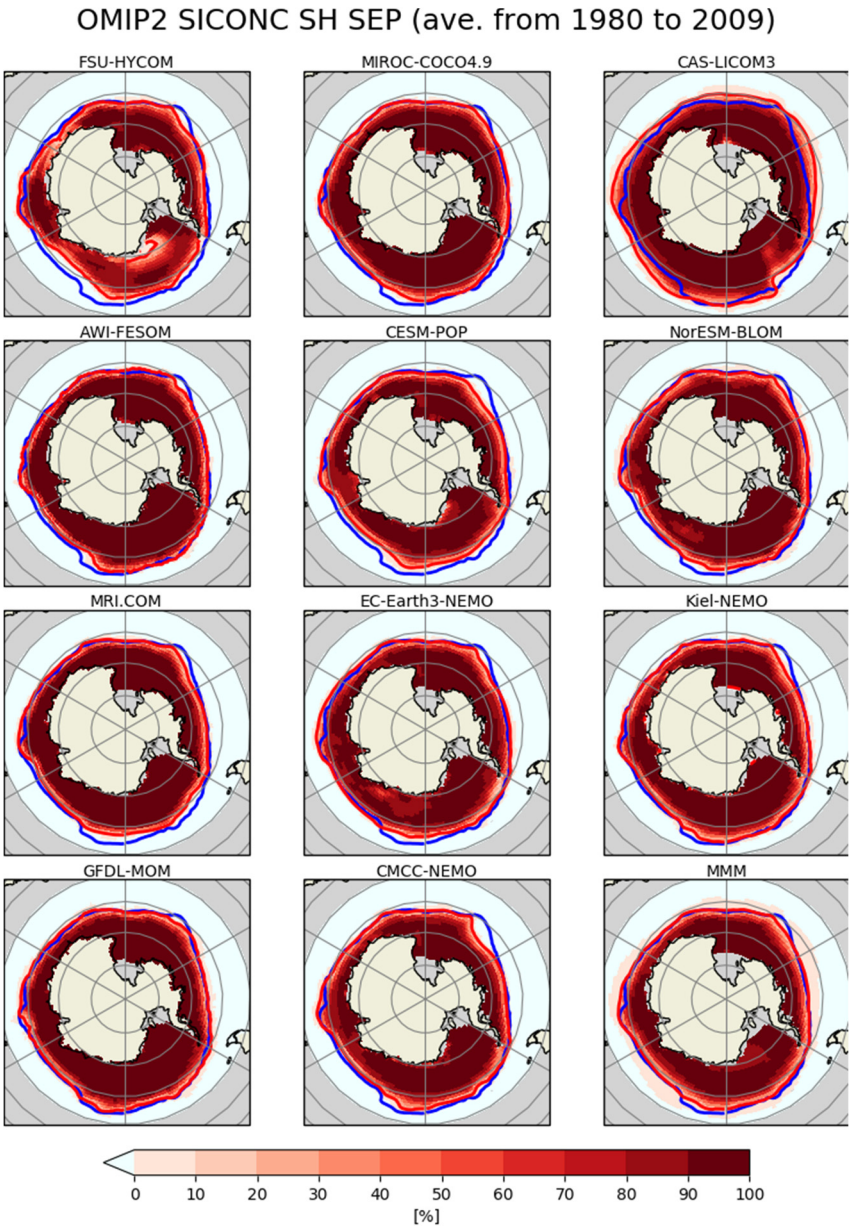

Figure S21: Same as Fig. S20 but for OMIP-2 simulations. Blue and red lines as in Fig. S20.

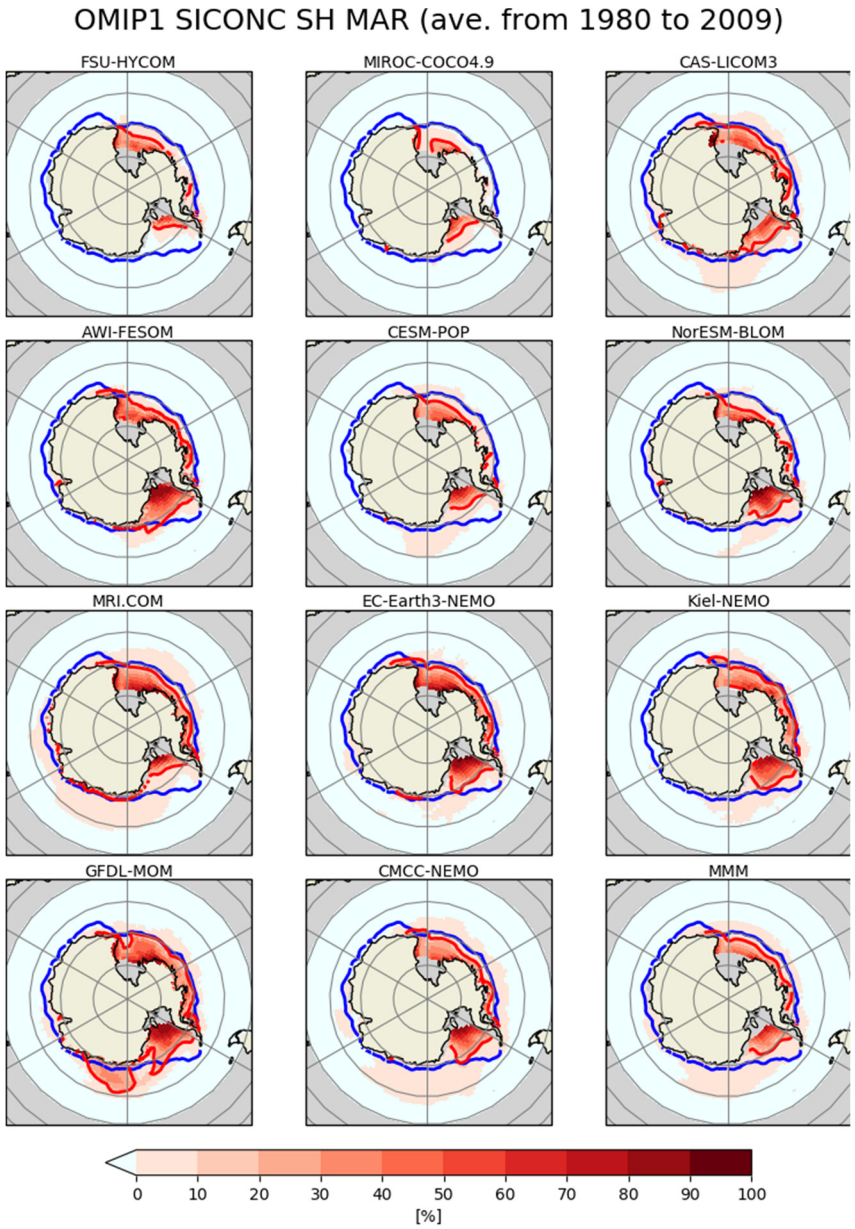

Figure S22: Thirty (30)-year (1980-2009) mean sea ice concentration (%) in March of Southern Hemisphere of OMIP-1 simulations. Blue and red lines as in Fig. S20.

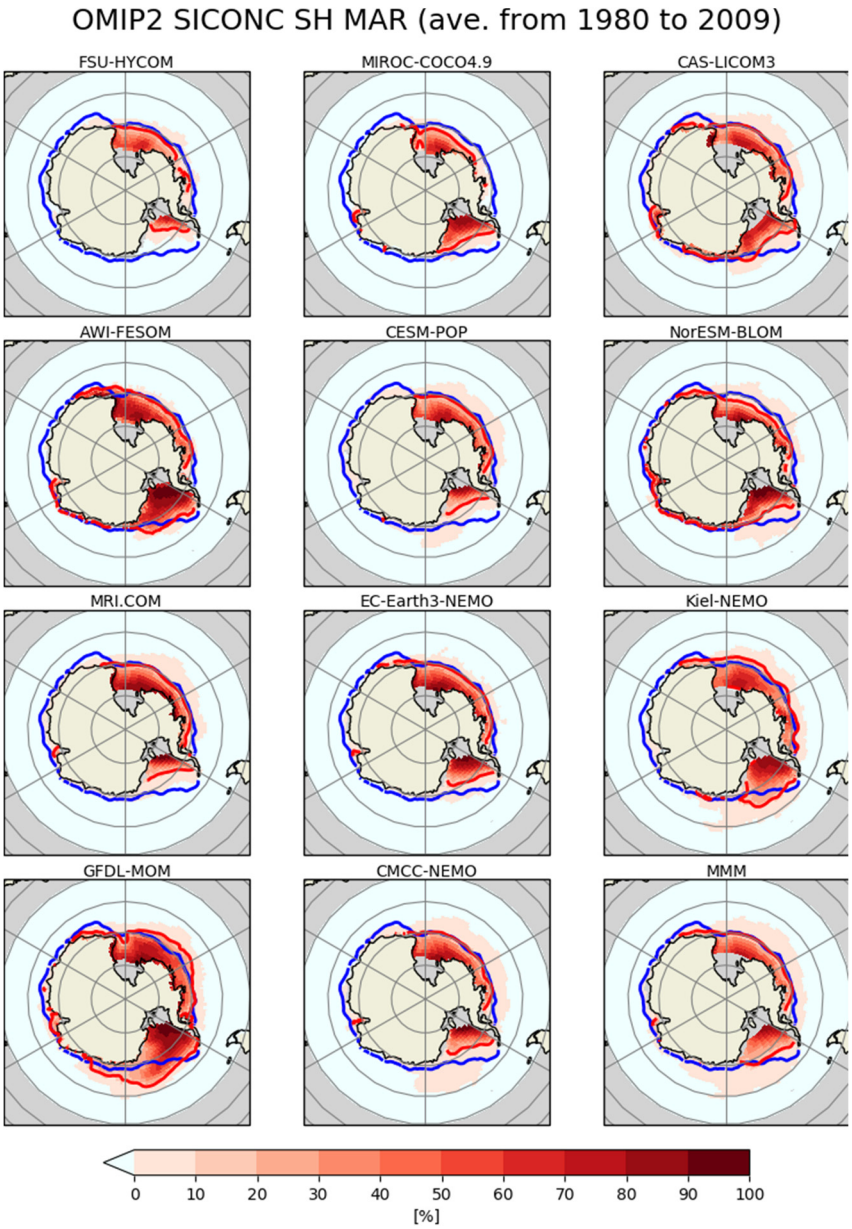

115 **Figure S23: Same as Fig. S22 but for OMIP-2 simulations. Blue and red lines as in Fig. S20.**

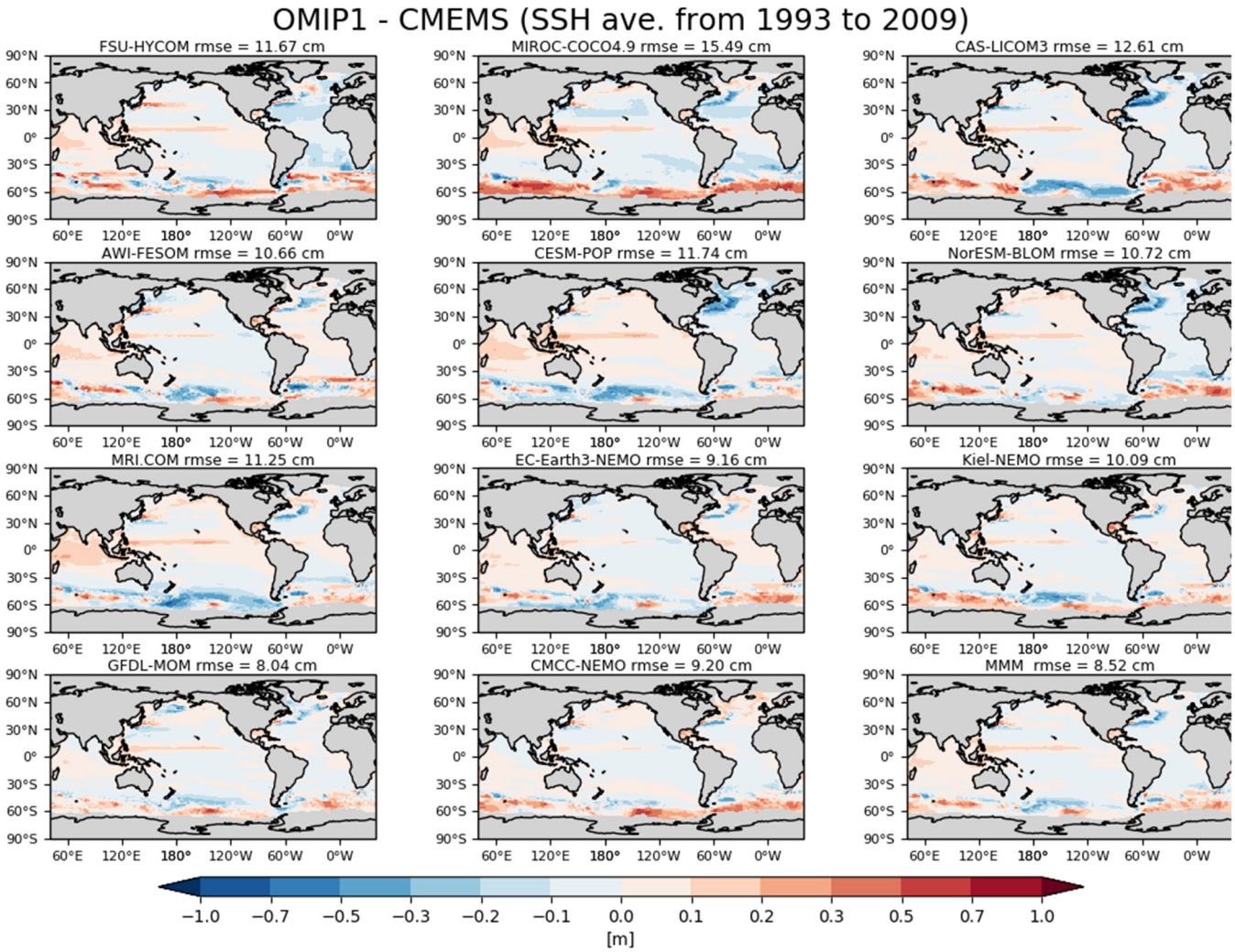

Figure S24: Bias of seventeen (17)-year (1993-2009) mean sea surface height (m) of OMIP-1 simulations relative to CMEMS.

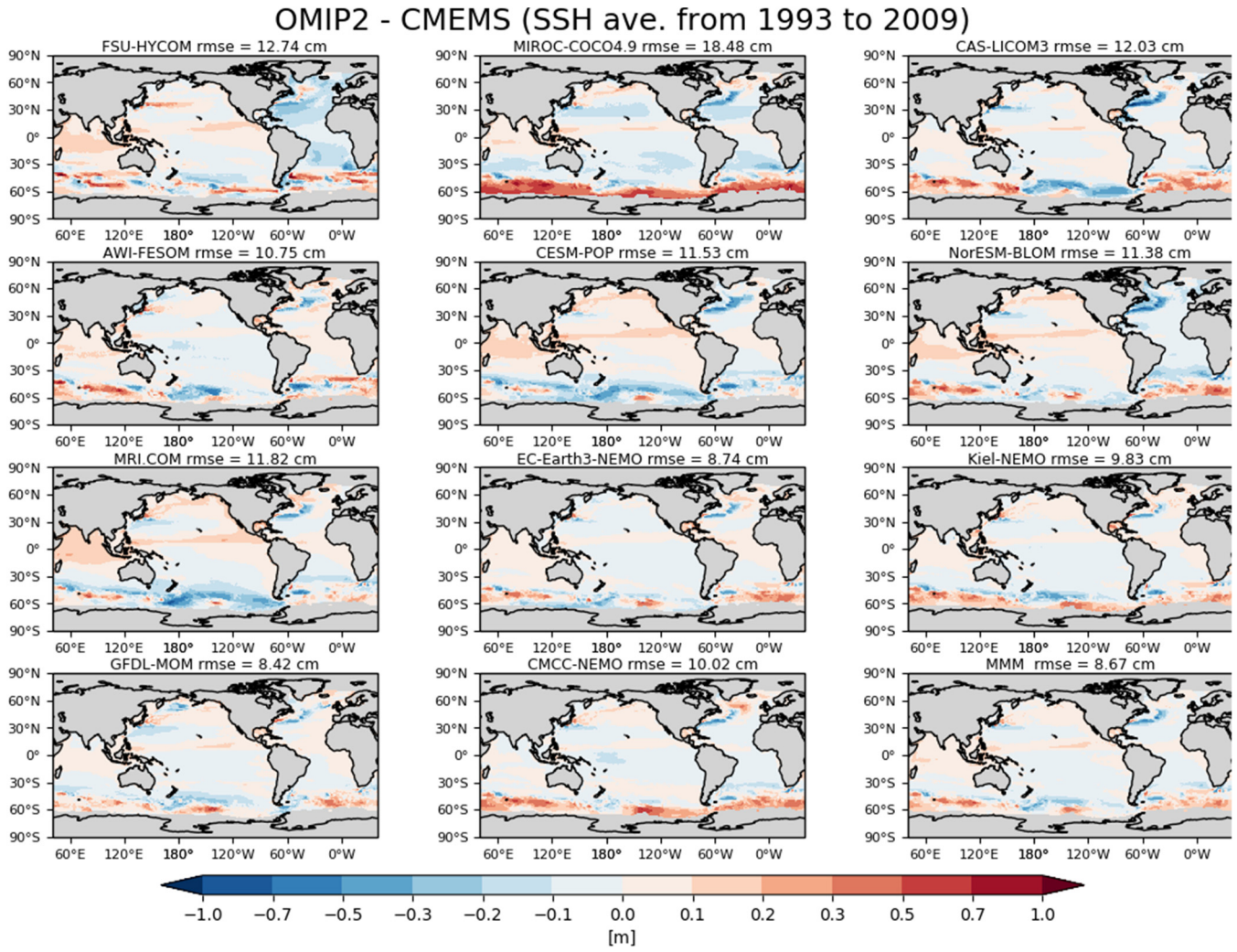

120

Figure S25: Same as Fig. S24 but for OMIP-2 simulations.

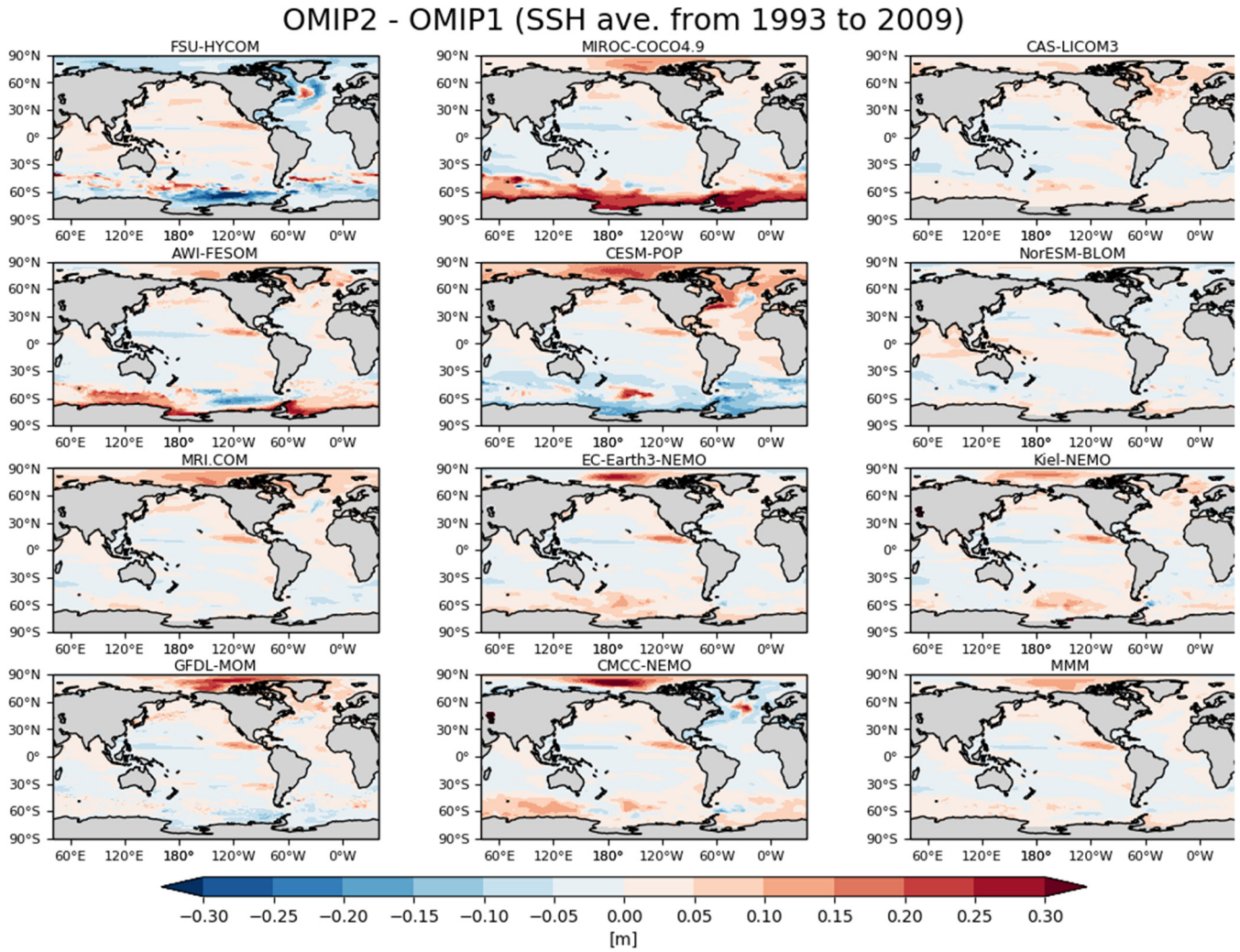

Figure S26: Difference of 17-year (1993-2009) mean sea surface height (m) between OMIP-1 and OMIP-2 simulations of individual models.

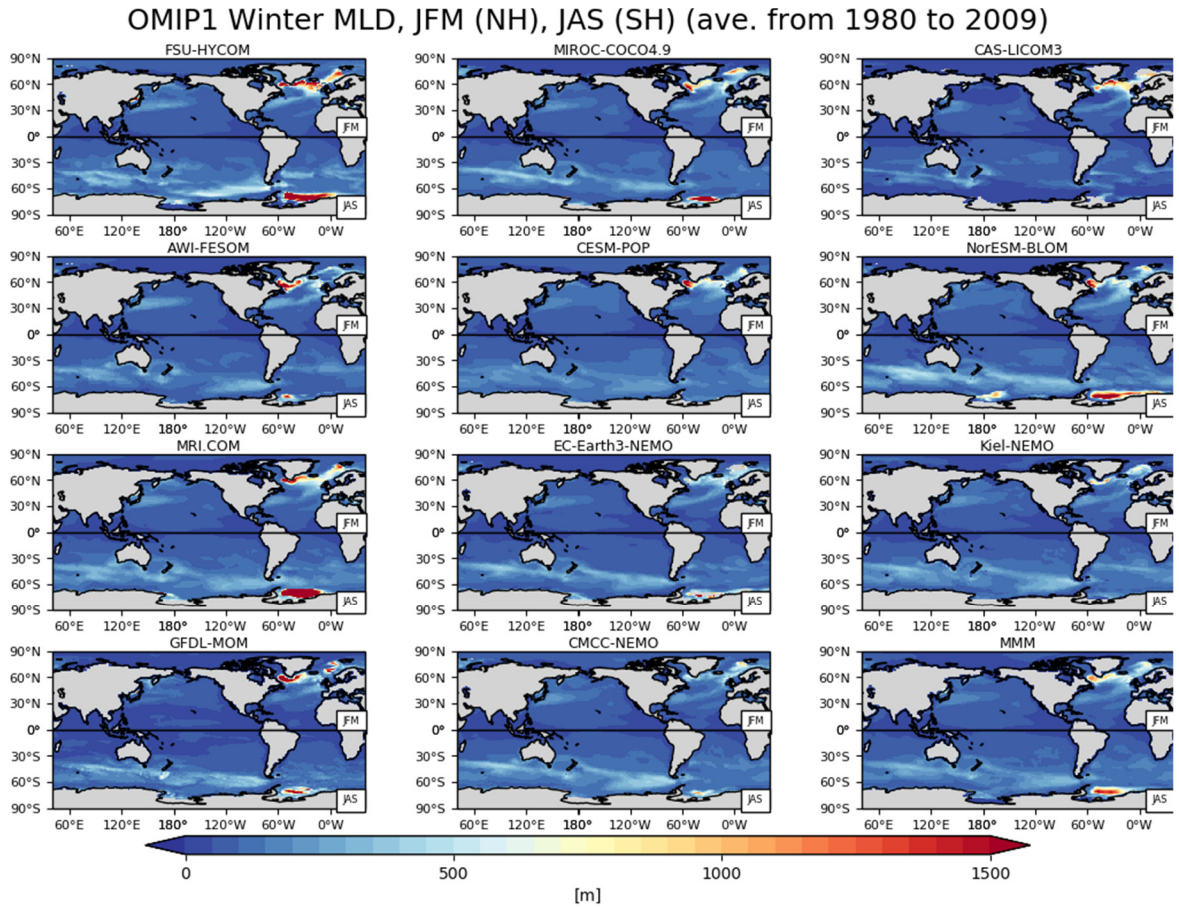

Figure S27: Thirty (30)-year (1980-2009) mean winter mixed layer depth (m) in both hemispheres of OMIP-1 simulations. January-February-March mean for the northern hemisphere and July-August-September mean for the southern hemisphere.

130

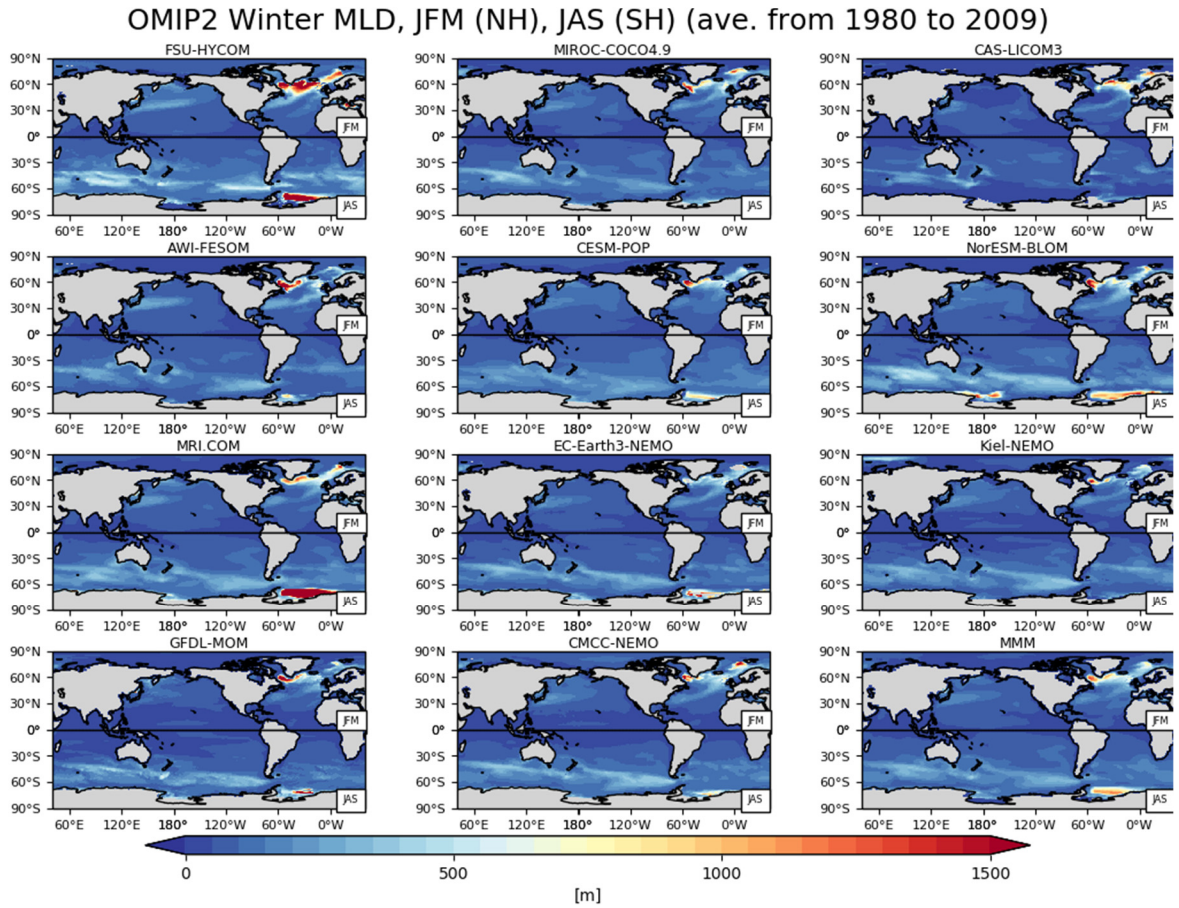

Figure S28: Same as Fig. S27 but for OMIP-2 simulations.

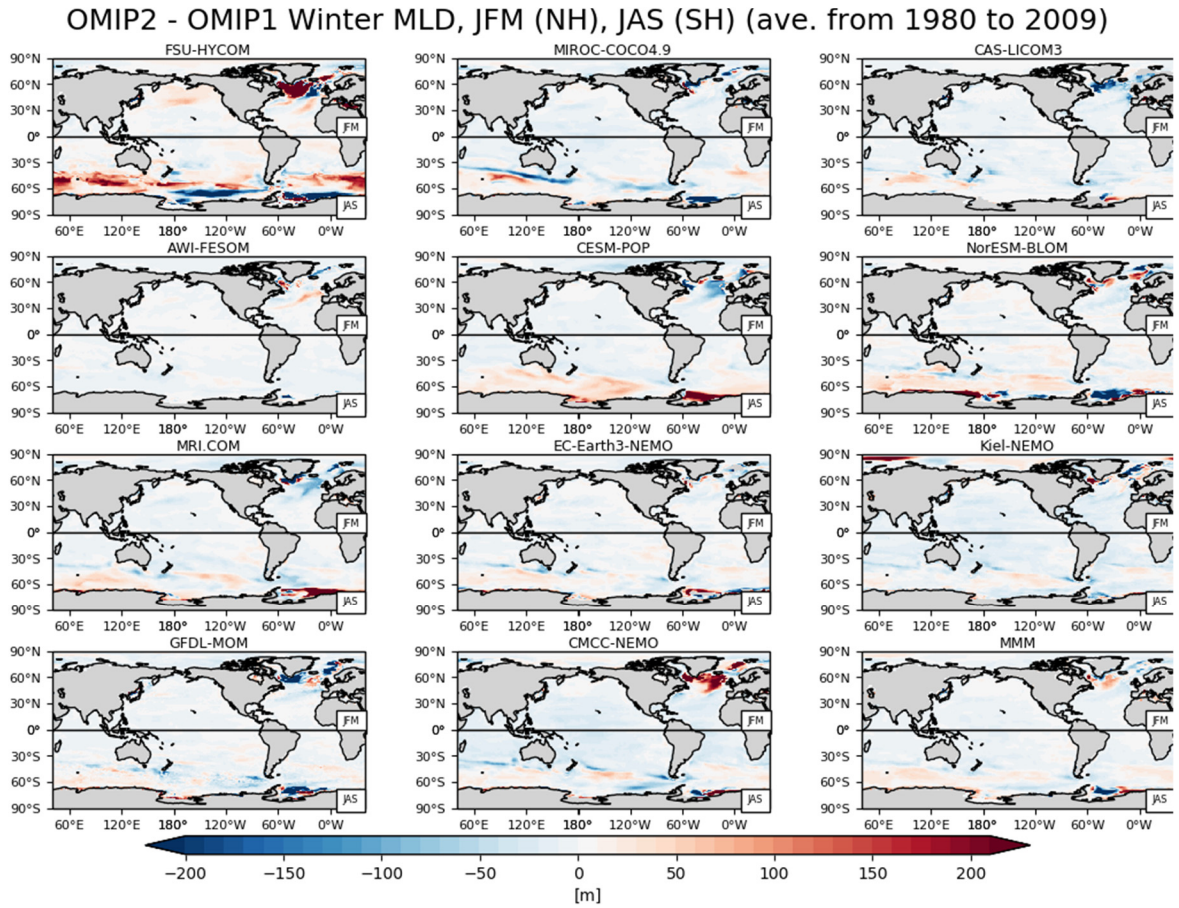

135 **Figure S29: Difference of 30-year (1980-2009) mean winter mixed layer depth (m) between OMIP-1 and OMIP-2 simulations (OMIP-2 minus OMIP-1) for individual models.**

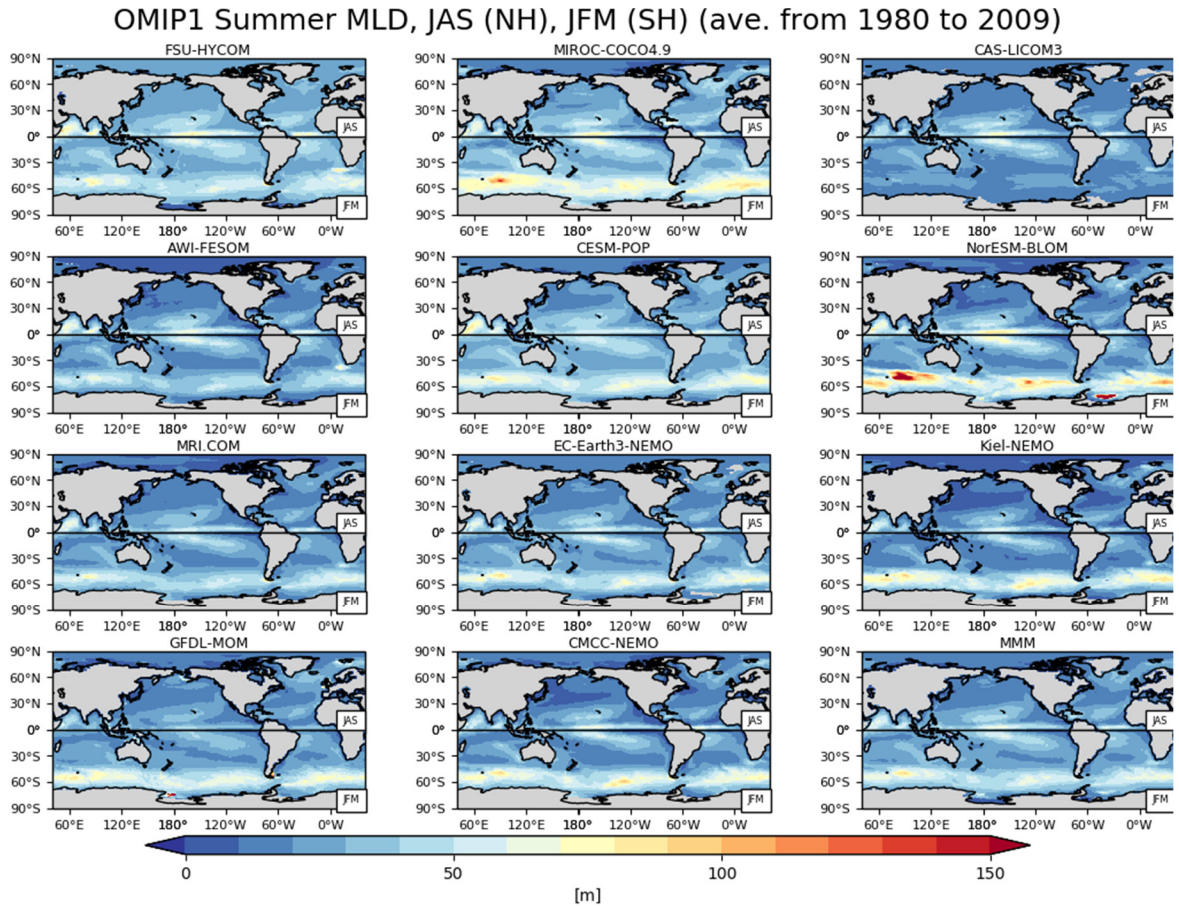

Figure S30: Thirty (30)-year (1980-2009) mean summer mixed layer depth (m) in both hemispheres of OMIP-1 simulations. July-August-September mean for the northern hemisphere and January-February-March mean for the southern hemisphere.

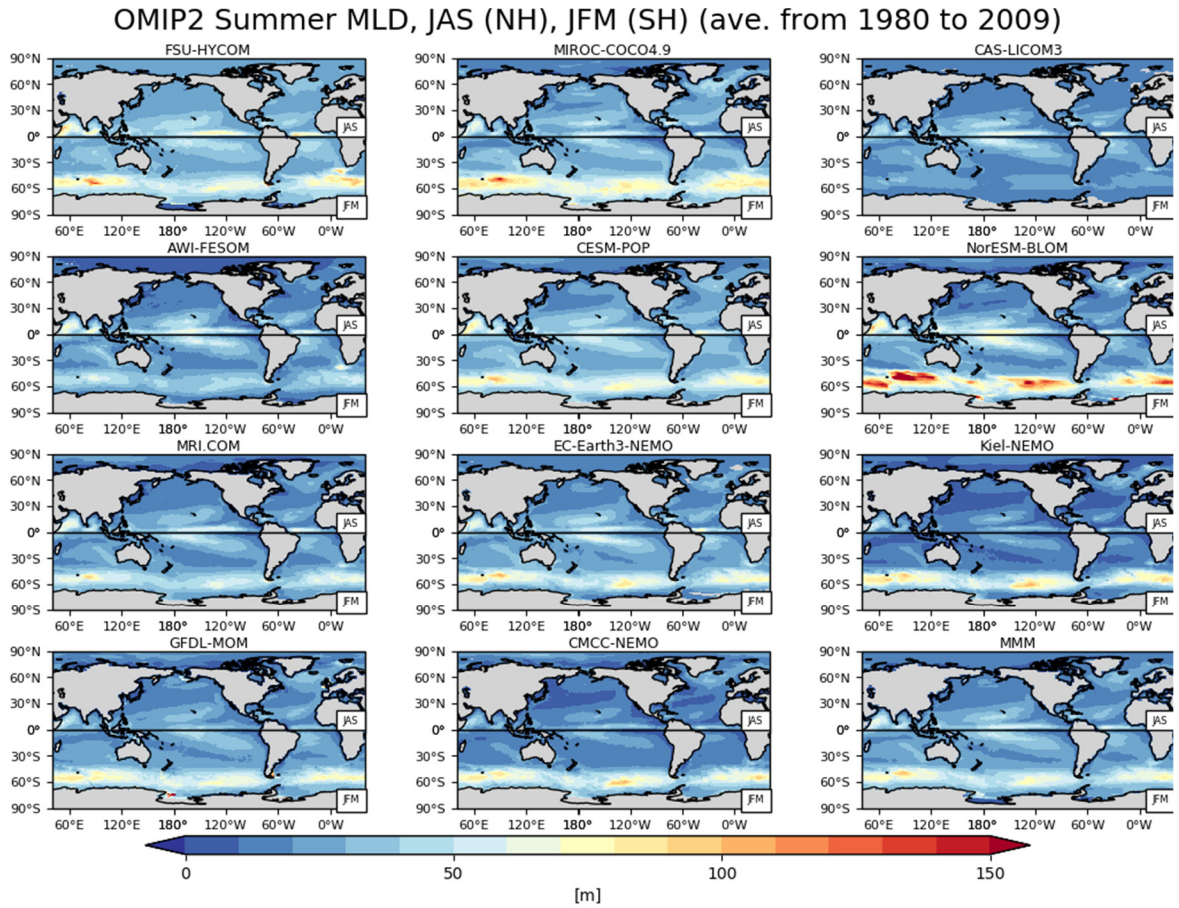

Figure S31: Same as Fig. S30 but for OMIP-2 simulations.

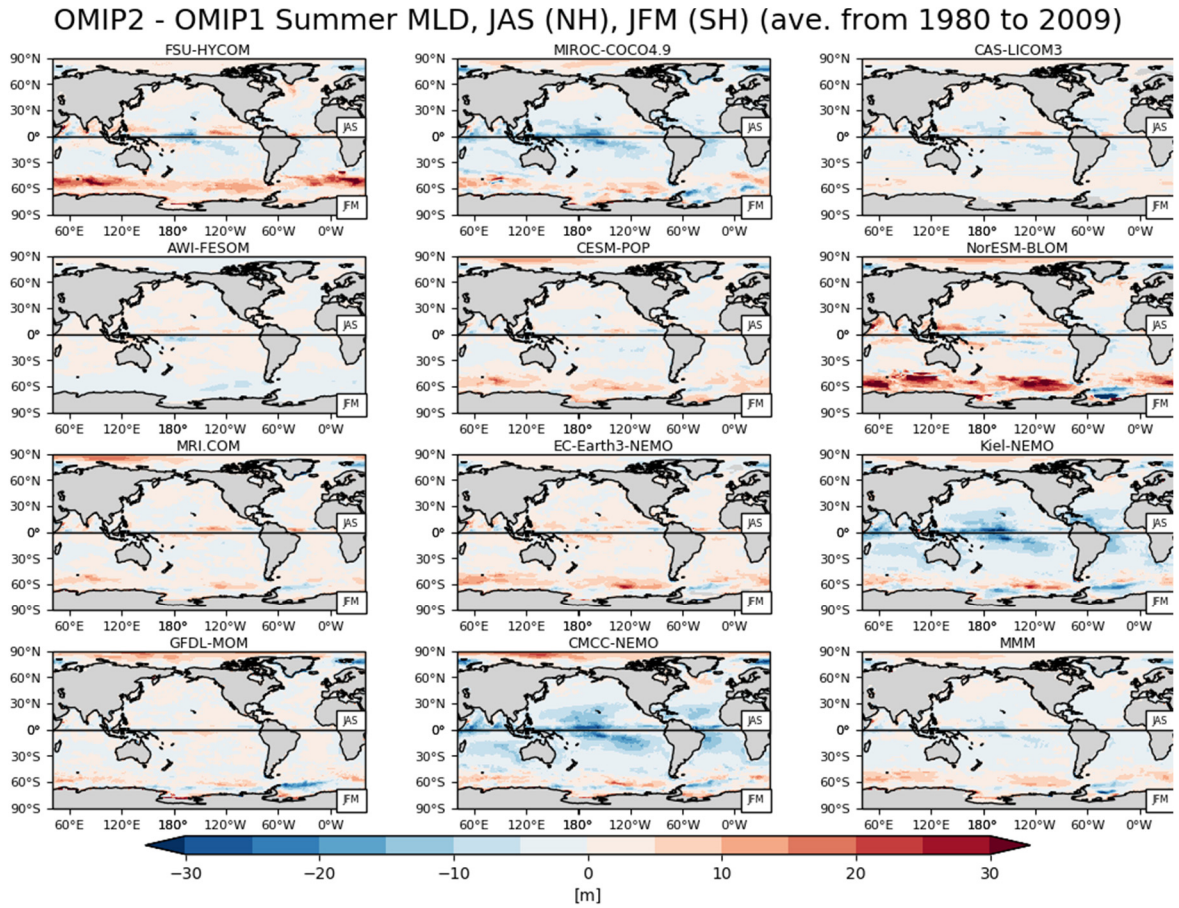

145

Figure S32: Difference of 30-year (1980-2009) mean summer mixed layer depth (m) between OMIP-1 and OMIP-2 simulations (OMIP-2 minus OMIP-1) for individual models.

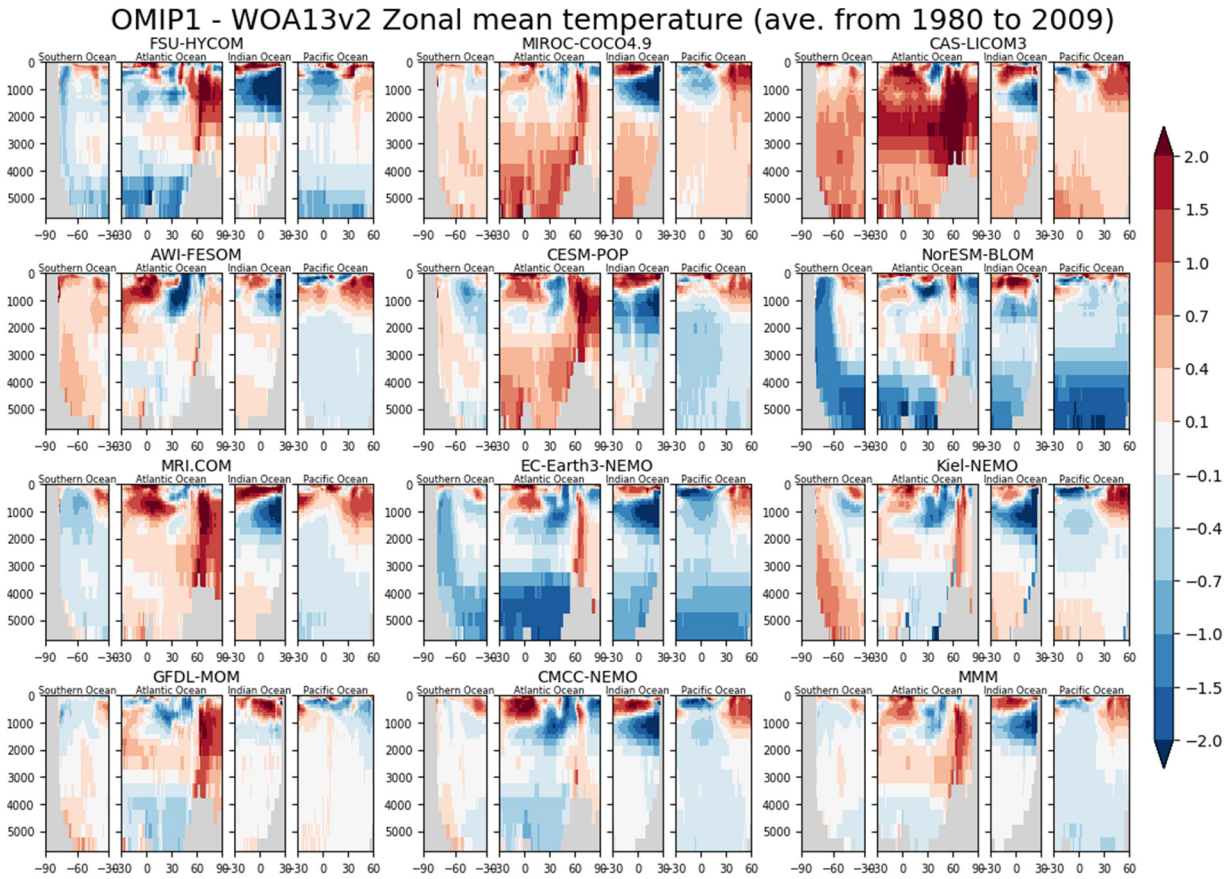

150 **Figure S33: Bias of 30-year (1980-2009) mean basin-wide zonally averaged temperature (°C) of the last cycle of OMIP-1 simulations relative to WOA13v2 (Locarnini et al. 2013).**

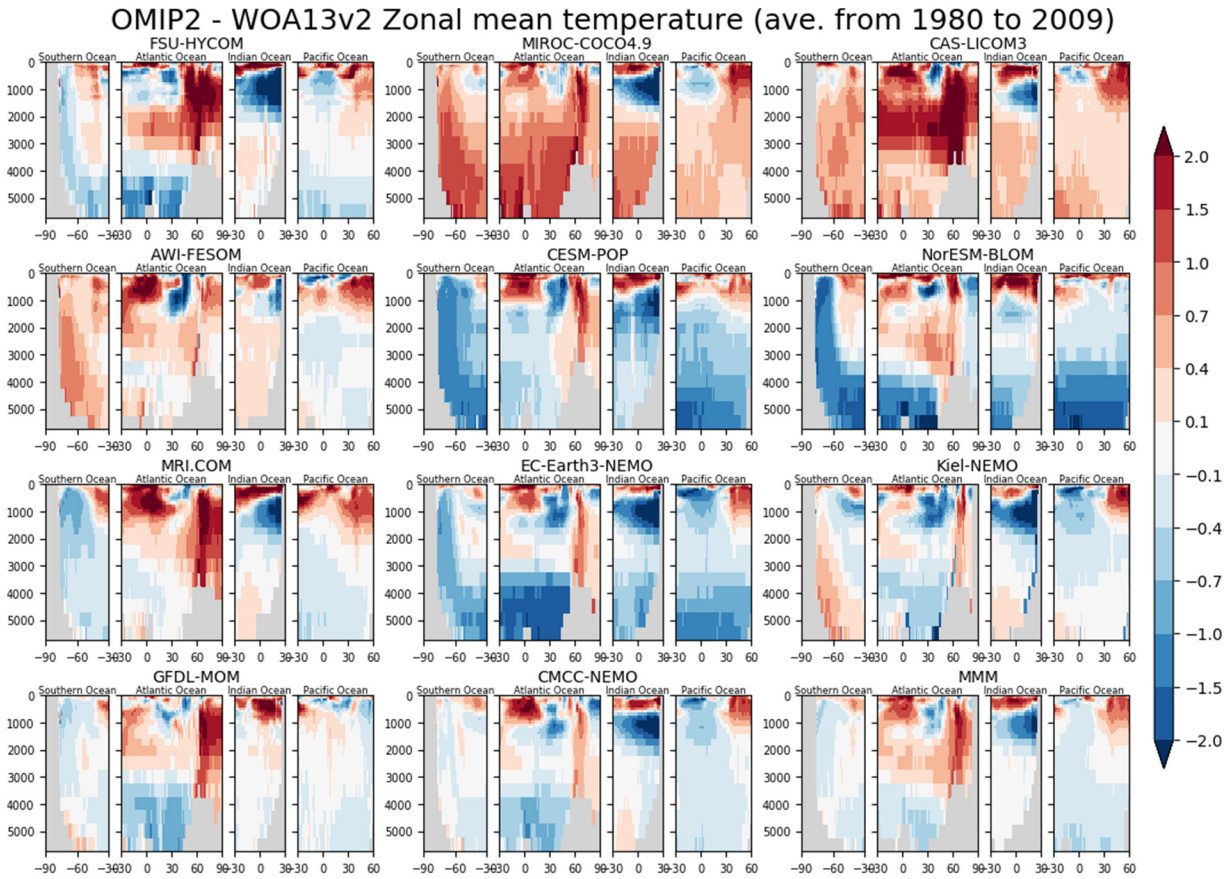

Figure S34: Same as Fig. S33 but for OMIP-2 simulations.

155

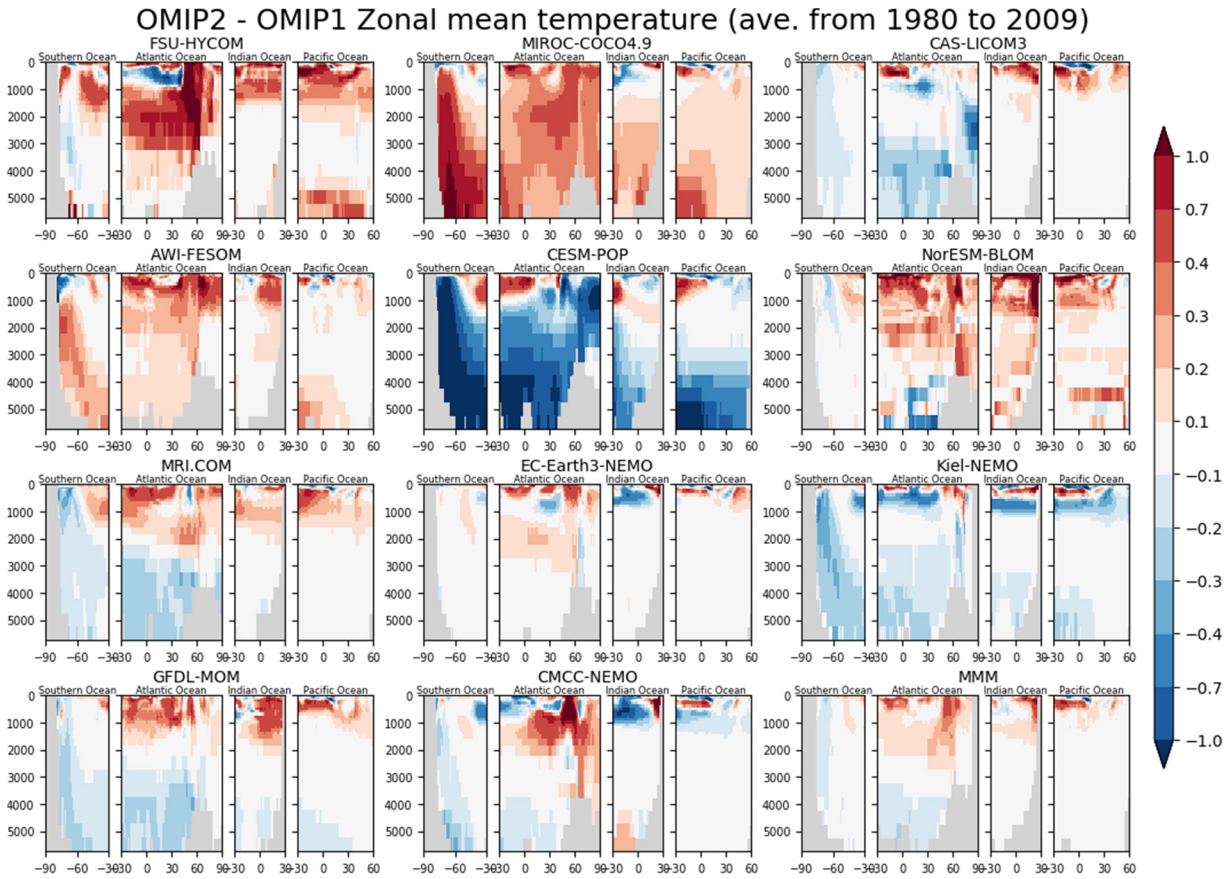

Figure S35: Difference of 30-year (1980-2009) mean basin-wide zonally averaged temperature (°C) of the last cycle between OMIP-1 and OMIP-2 simulations (OMIP-2 minus OMIP-1) for individual models.

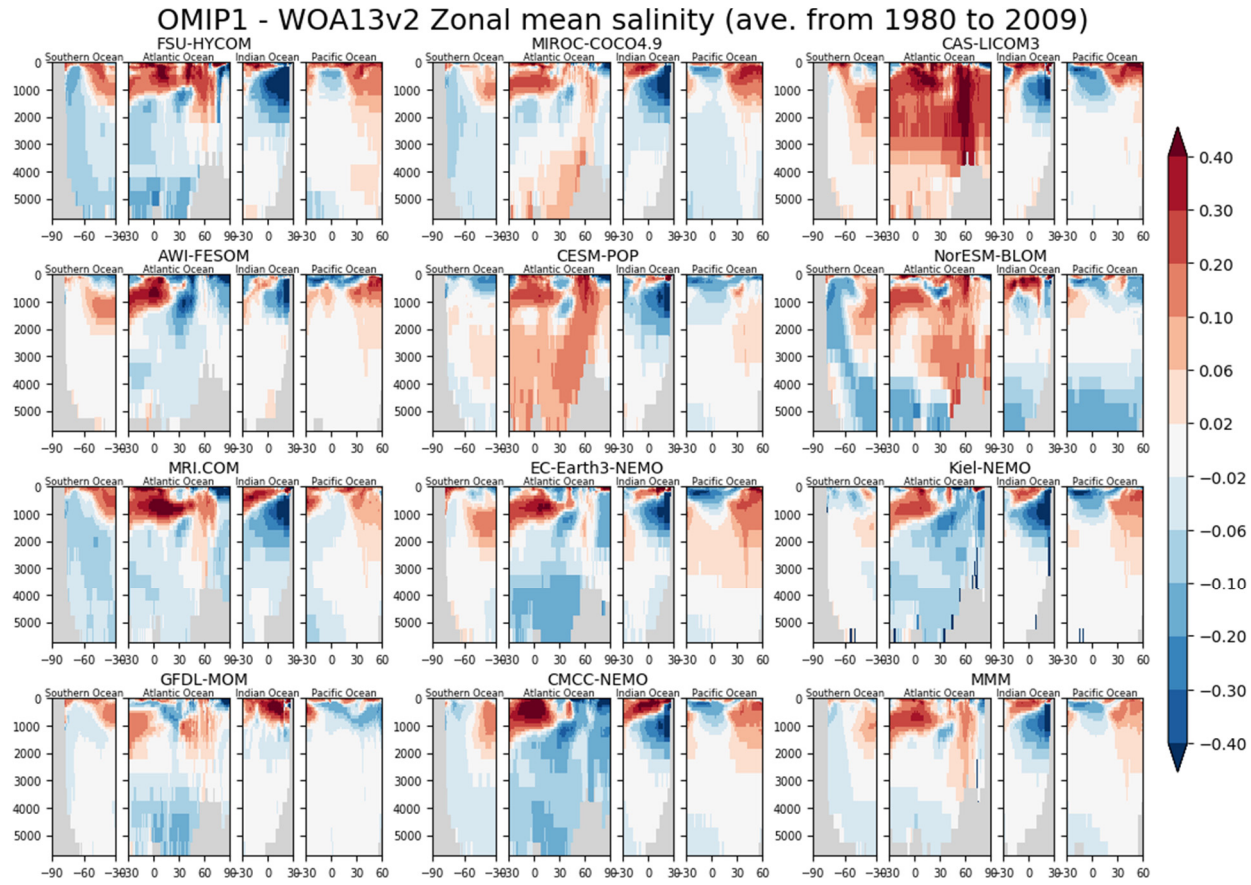

Figure S36: Bias of 30-year (1980-2009) mean basin-wide zonally averaged salinity (psu) of the last cycle of OMIP-1 simulations relative to WOA13v2 (Zweng et al. 2013).

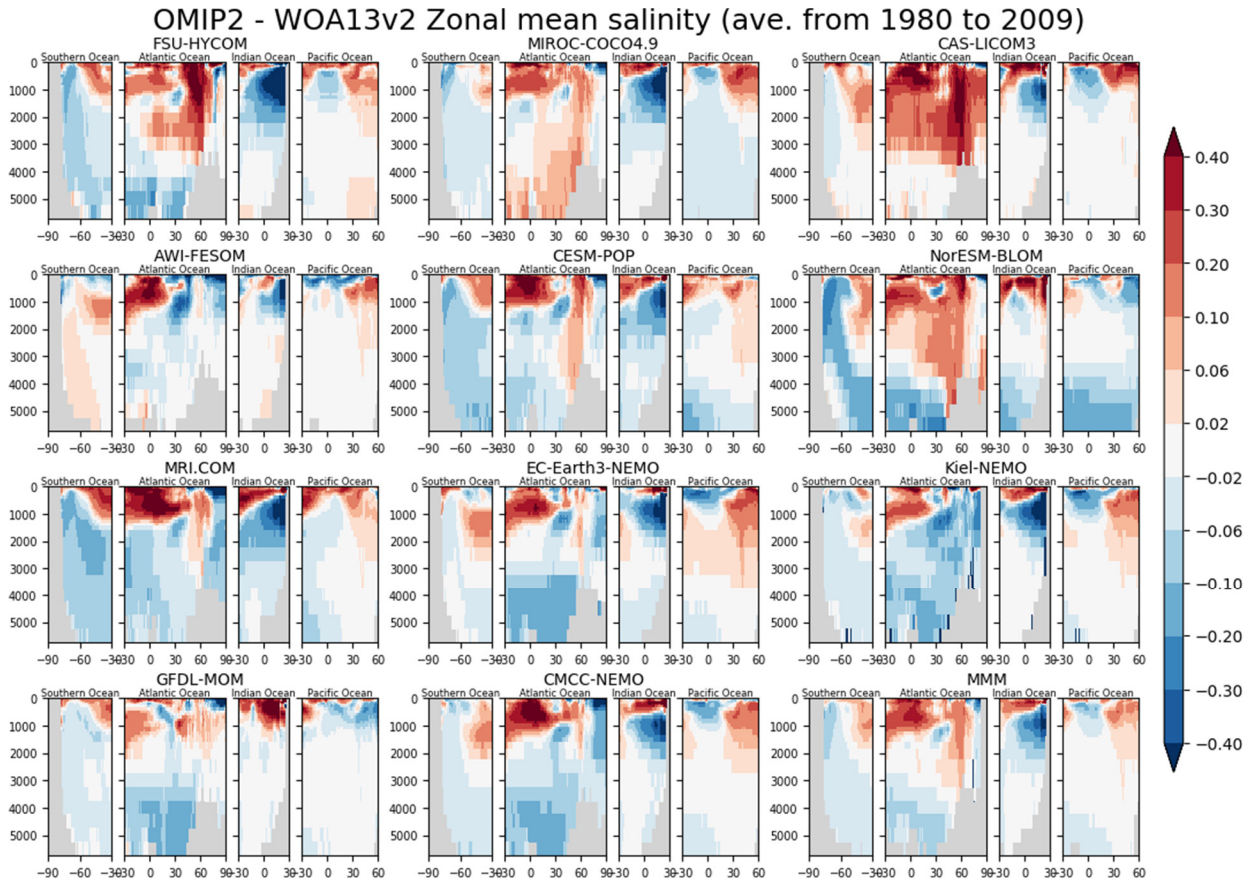

165 **Figure S37: Same as Fig. S36 but for OMIP-2 simulations.**

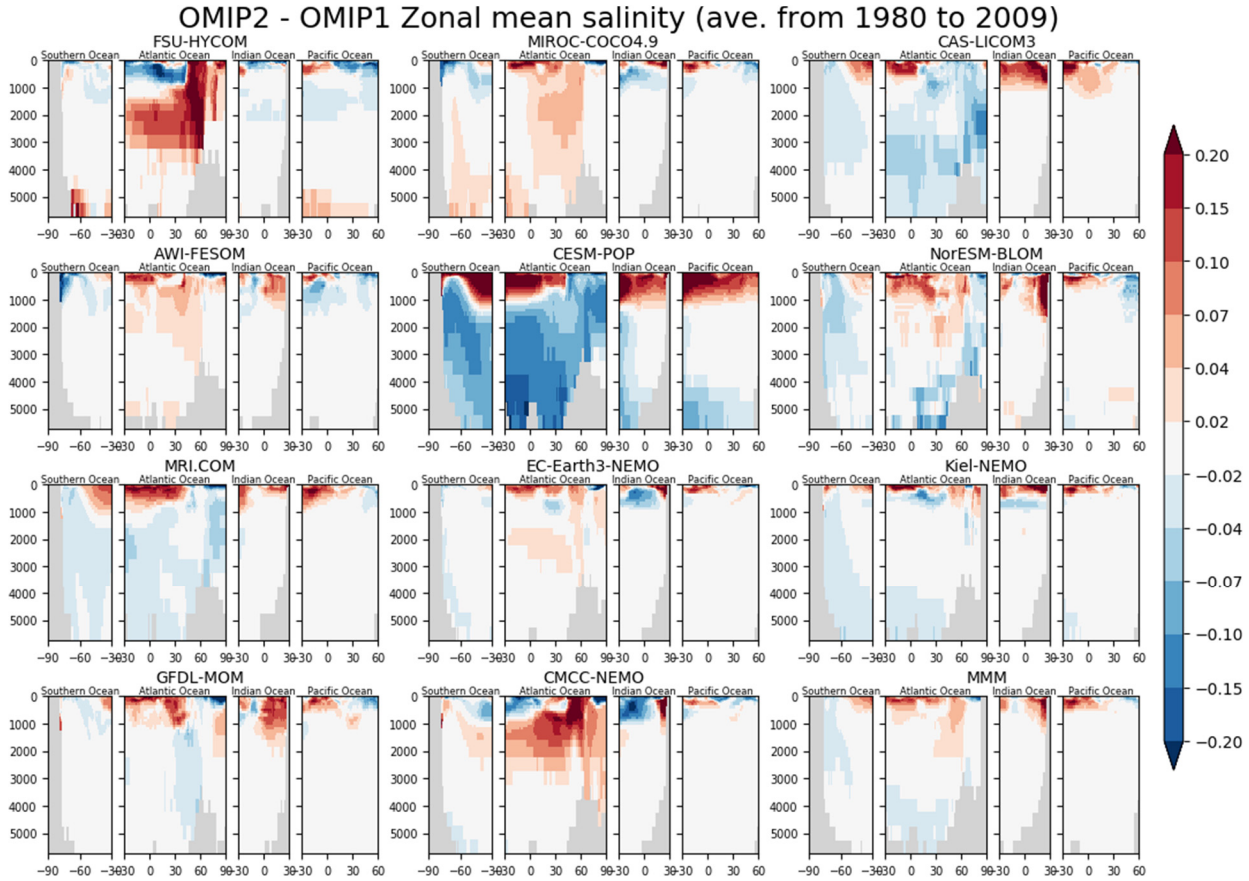

Figure S38: Difference of 30-year (1980-2009) mean basin-wide zonally averaged salinity (psu) of the last cycle between OMIP-1 and OMIP-2 simulations (OMIP-2 minus OMIP-1) for individual models.

170

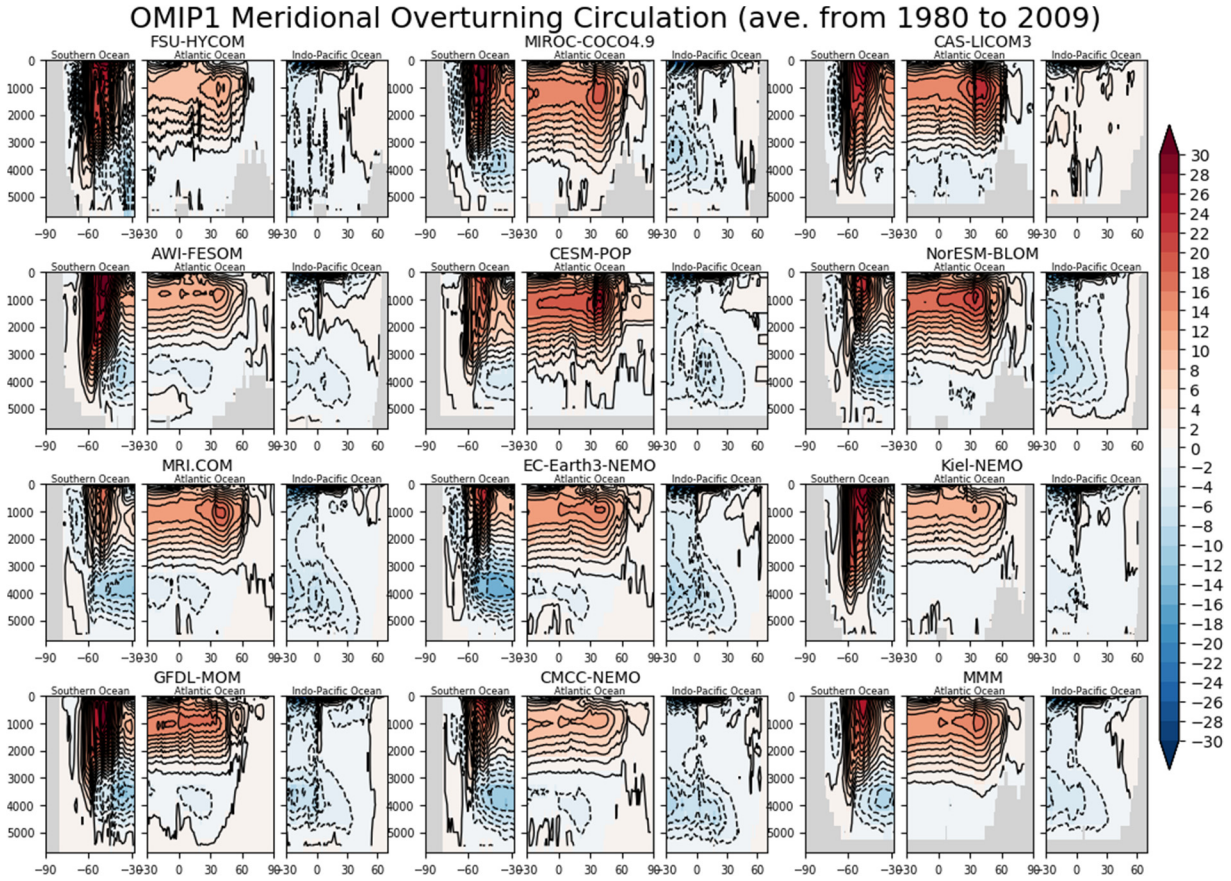

Figure S39: Thirty (30)-year (1980-2009) mean meridional overturning stream function in three oceanic basins of OMIP-1 simulations. Units are 10^9 kg s^{-1}. Clockwise circulations are implied around the positive extremes and vice versa.

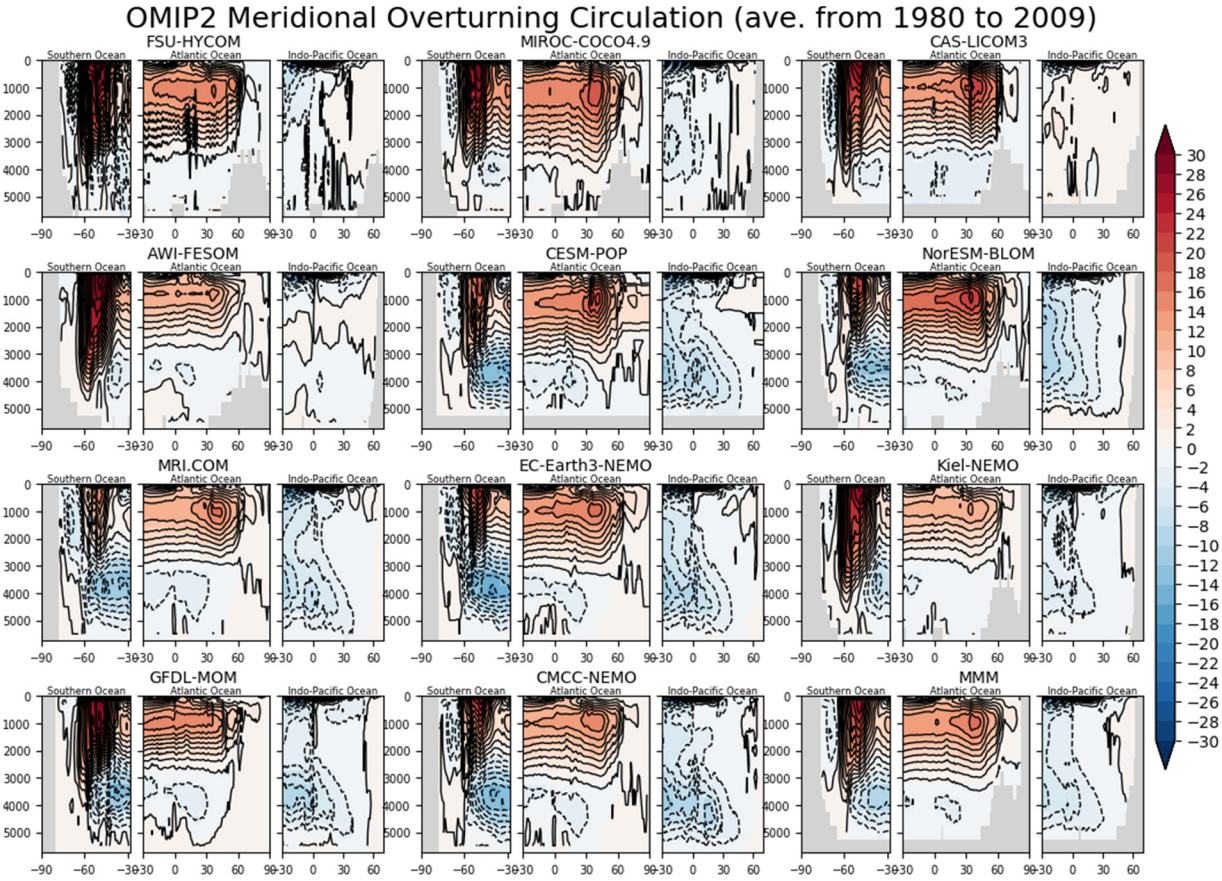

Figure S40: Same Fig. S39 but for OMIP-2 simulations.

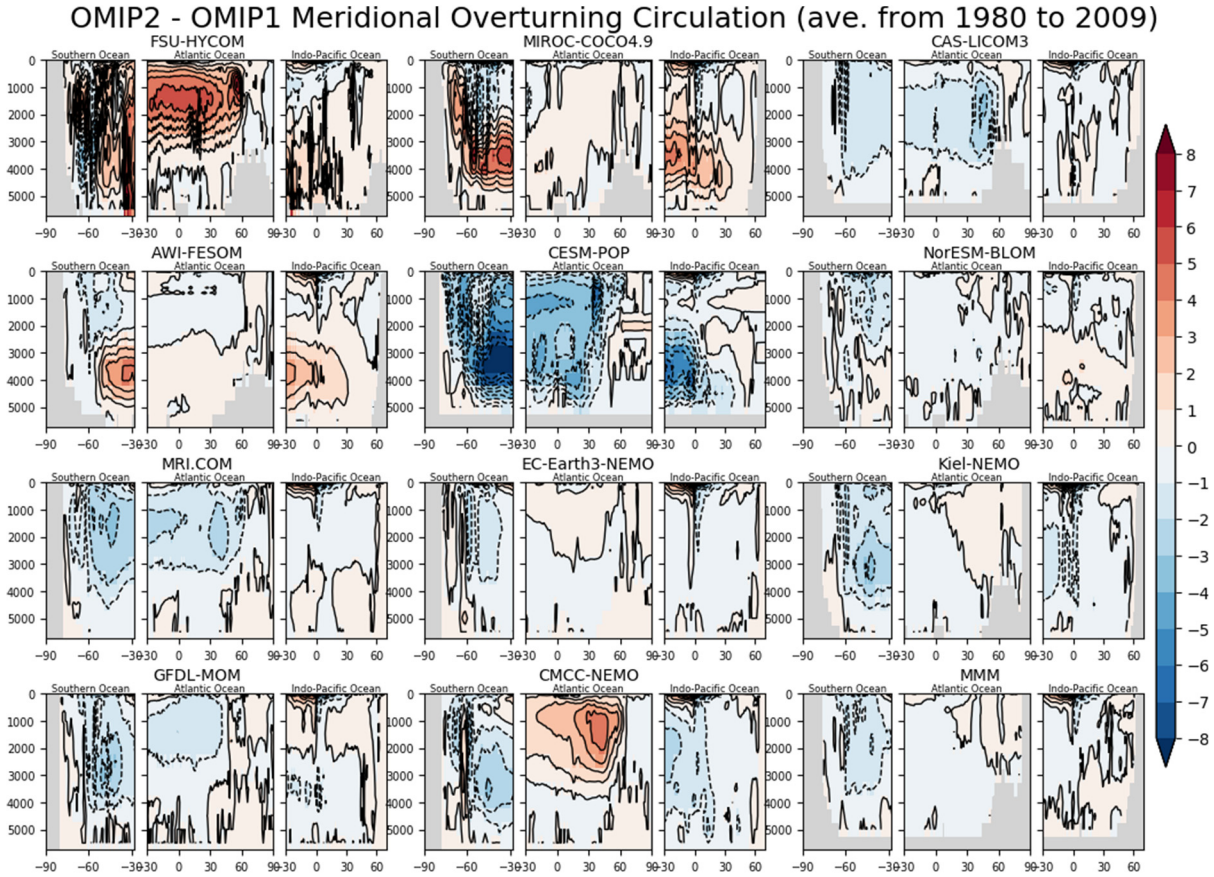

Figure S41: Difference of 30-year (1980-2009) mean meridional overturning stream function in three oceanic basins between OMIP-2 and OMIP-1 (OMIP-2 minus OMIP-1). Units are 10^9 kg s^{-1}.

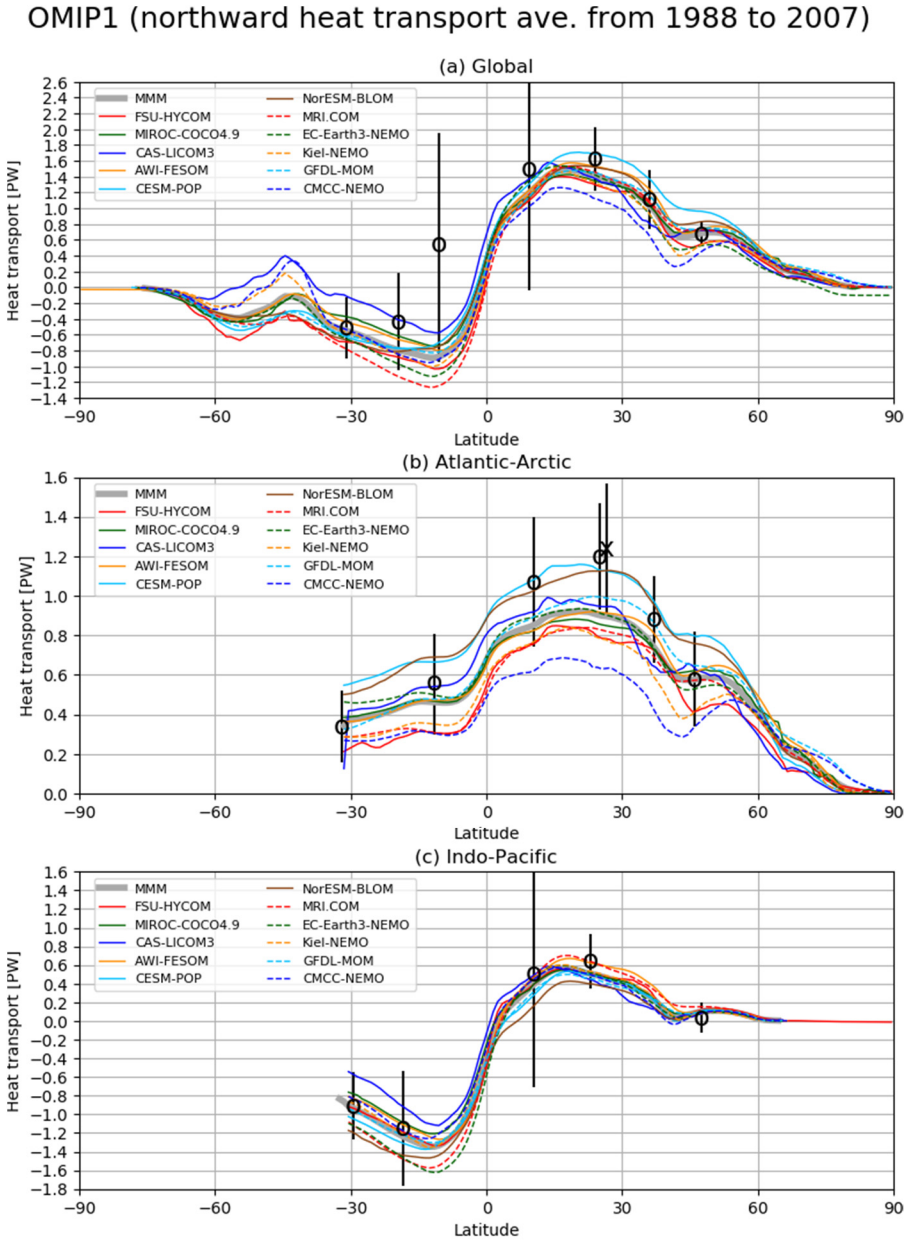

Figure S42: Twenty (20)-year (1988-2007) mean northward heat transport (PW = 10^{15} W m^{-2}) in three oceanic basins of OMIP-1 simulations. (a) Global, (b) Atlantic-Arctic, and (c) Indo-Pacific Ocean basins. The open circles are estimates from observations and assimilations compiled by Macdonald and Baringer (2013). The cross at 26.5°N in the Atlantic is an estimation from RAPID transport array reported by McDonagh et al. (2015).

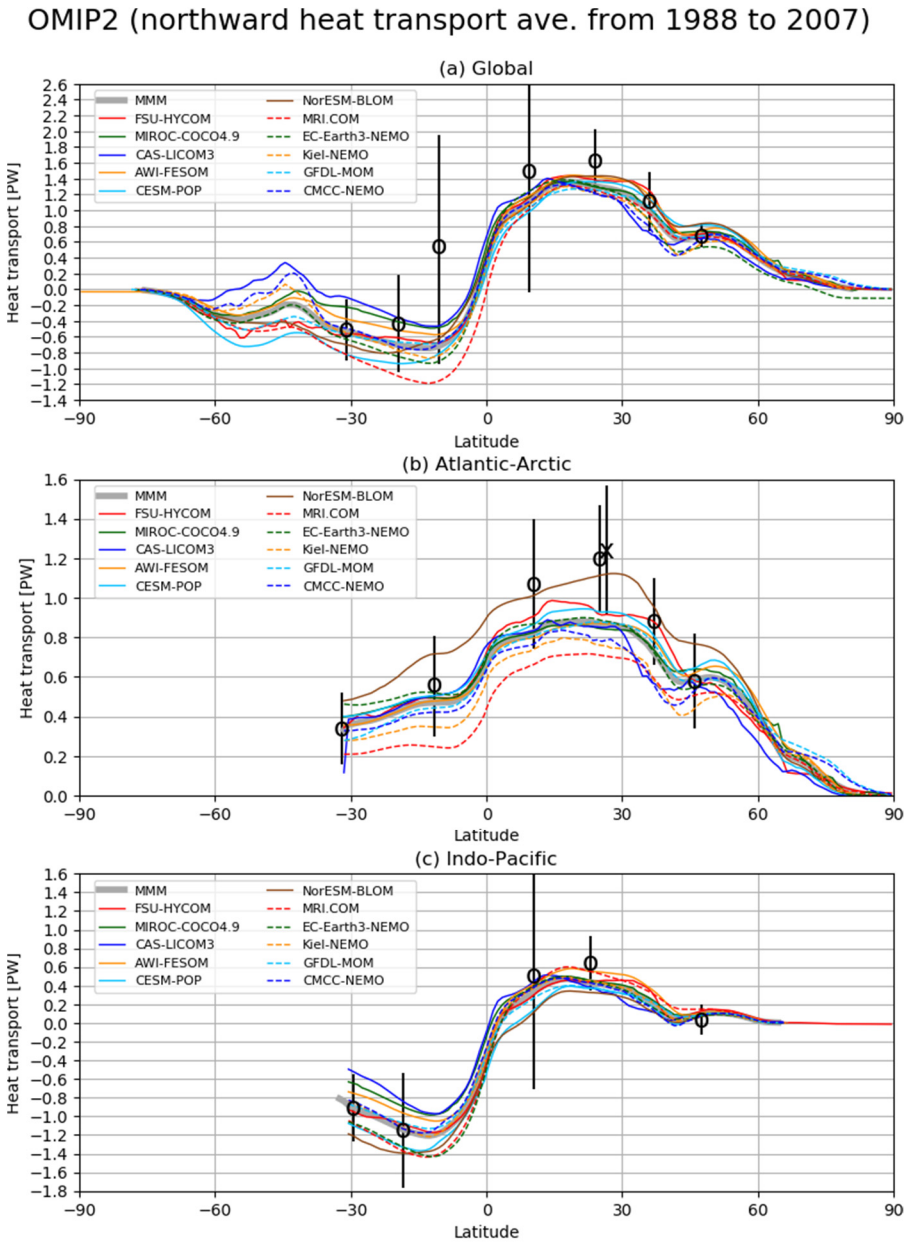

Figure S43: Same as Fig. S42 but for OMIP-2 simulations.

190

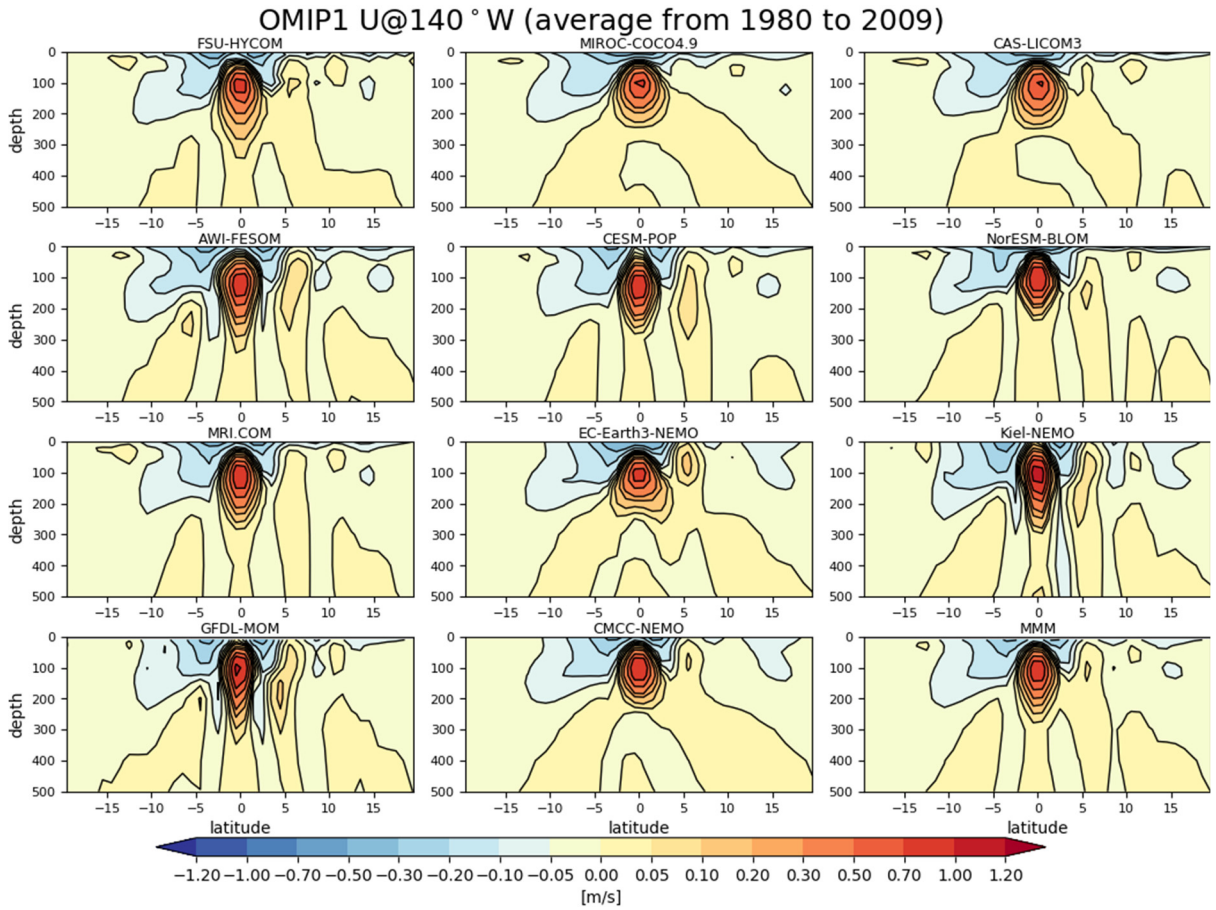

Figure S44: Thirty (30)-year (1980-2009) mean zonal velocity (m s^{-1}) across 140°W in the eastern tropical Pacific for OMIP-1 simulations.

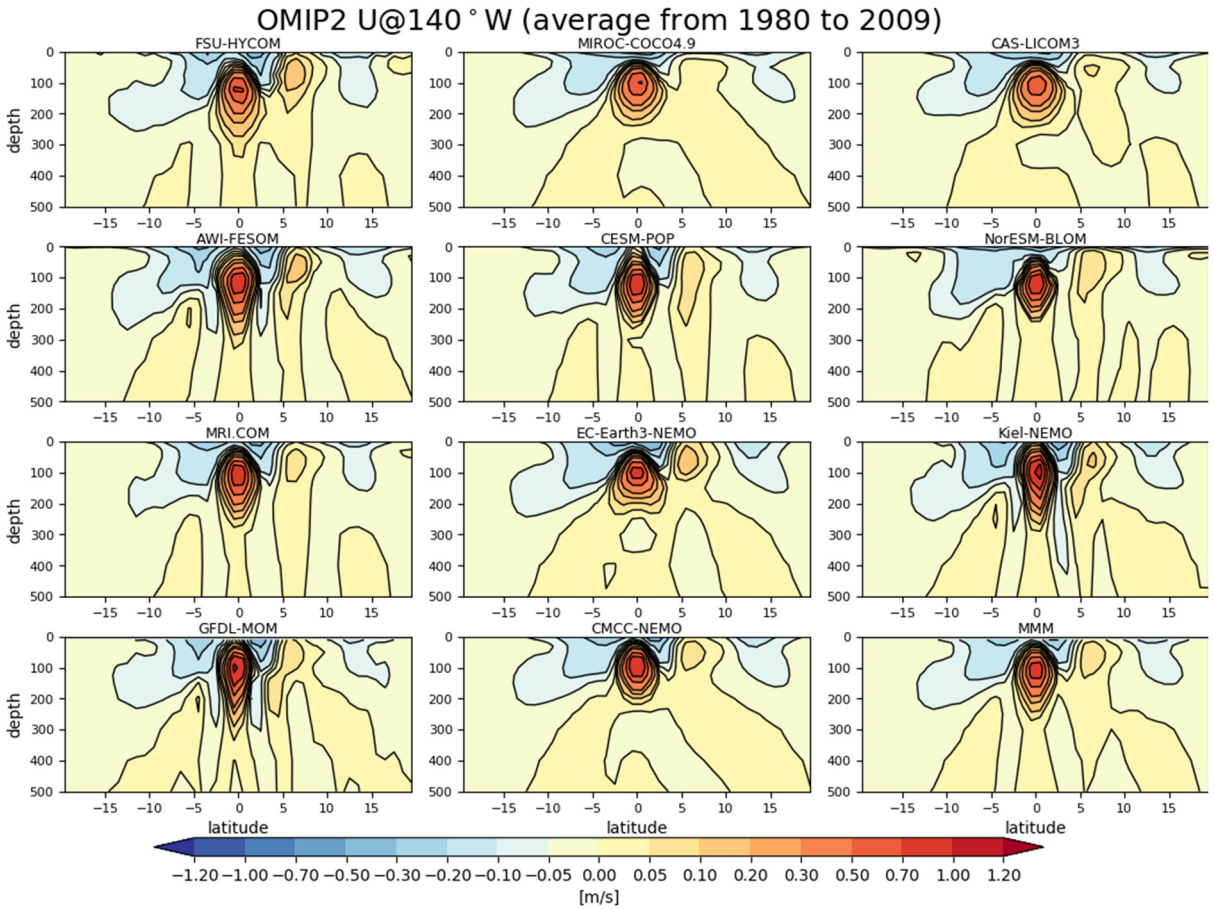

Figure S45: Same as Fig. S44 but for OMIP-2 simulations.

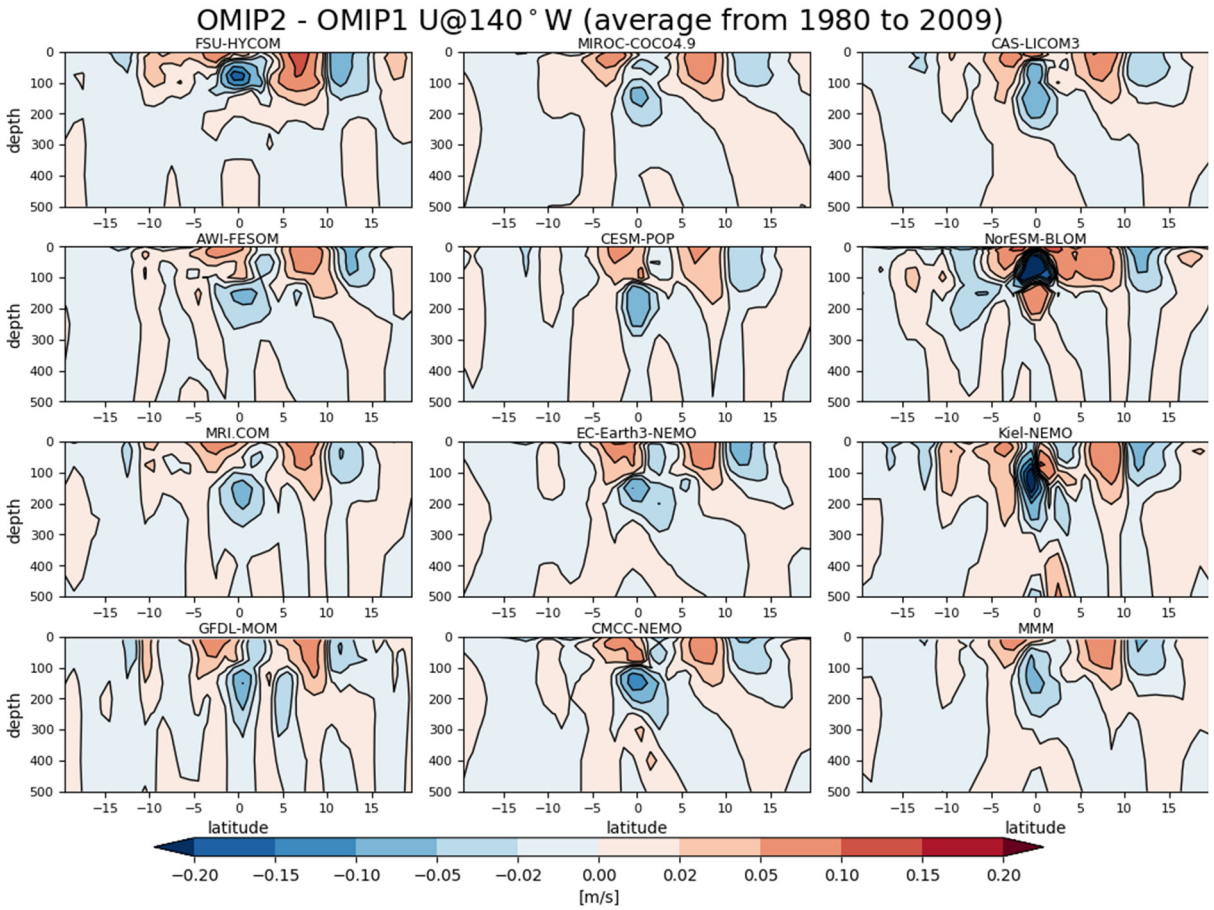

Figure S46: Difference of 30-year (1980-2009) mean zonal velocity (m s^{-1}) across 140°W in the eastern tropical Pacific between 200 **OMIP-1 and OMIP-2 simulations (OMIP-2 minus OMIP-1) for individual models.**

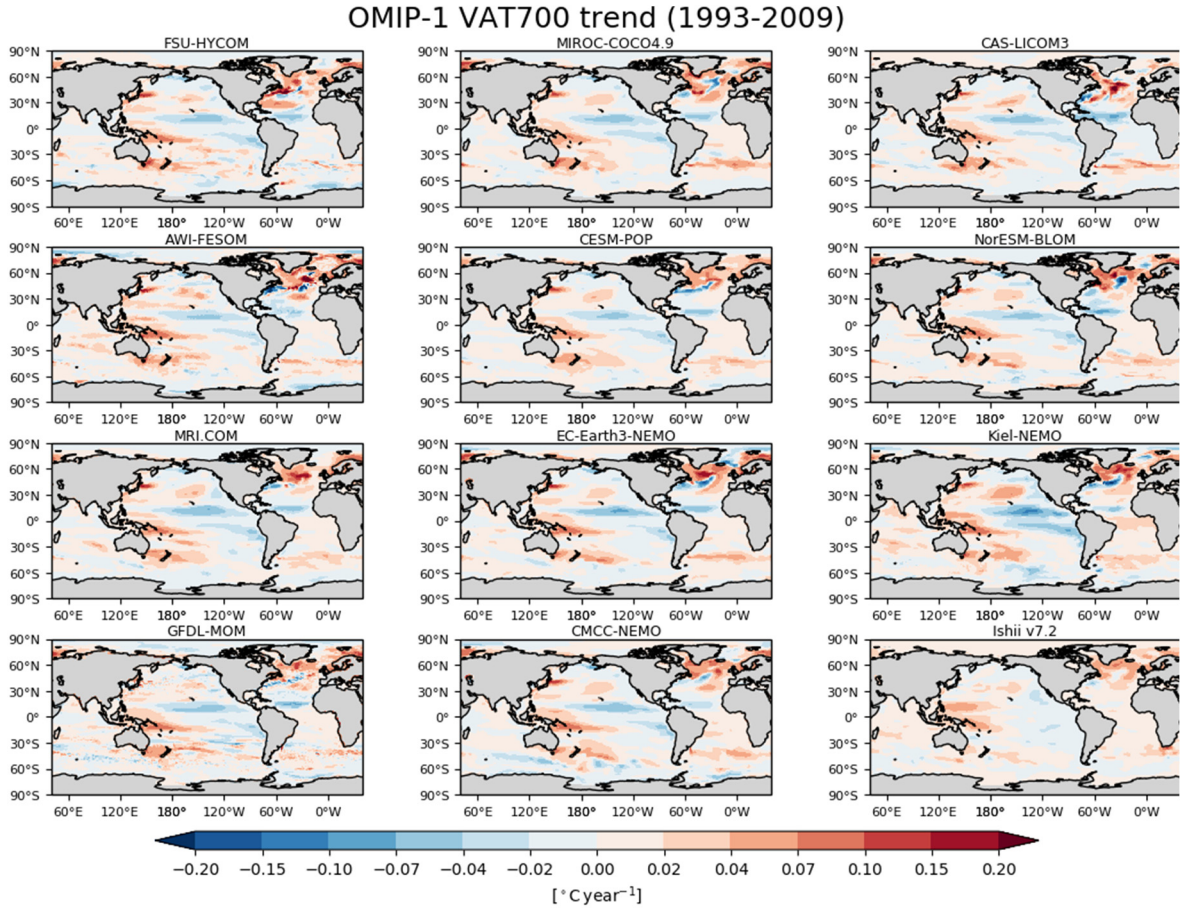

Figure S47: Seventeen (17)-year (1993-2009) trend of the upper 700 m temperature (°C year^{-1}) of OMIP-1 simulations. The lower right panel is based on an observational estimate by Ishii et al. (2017).

205

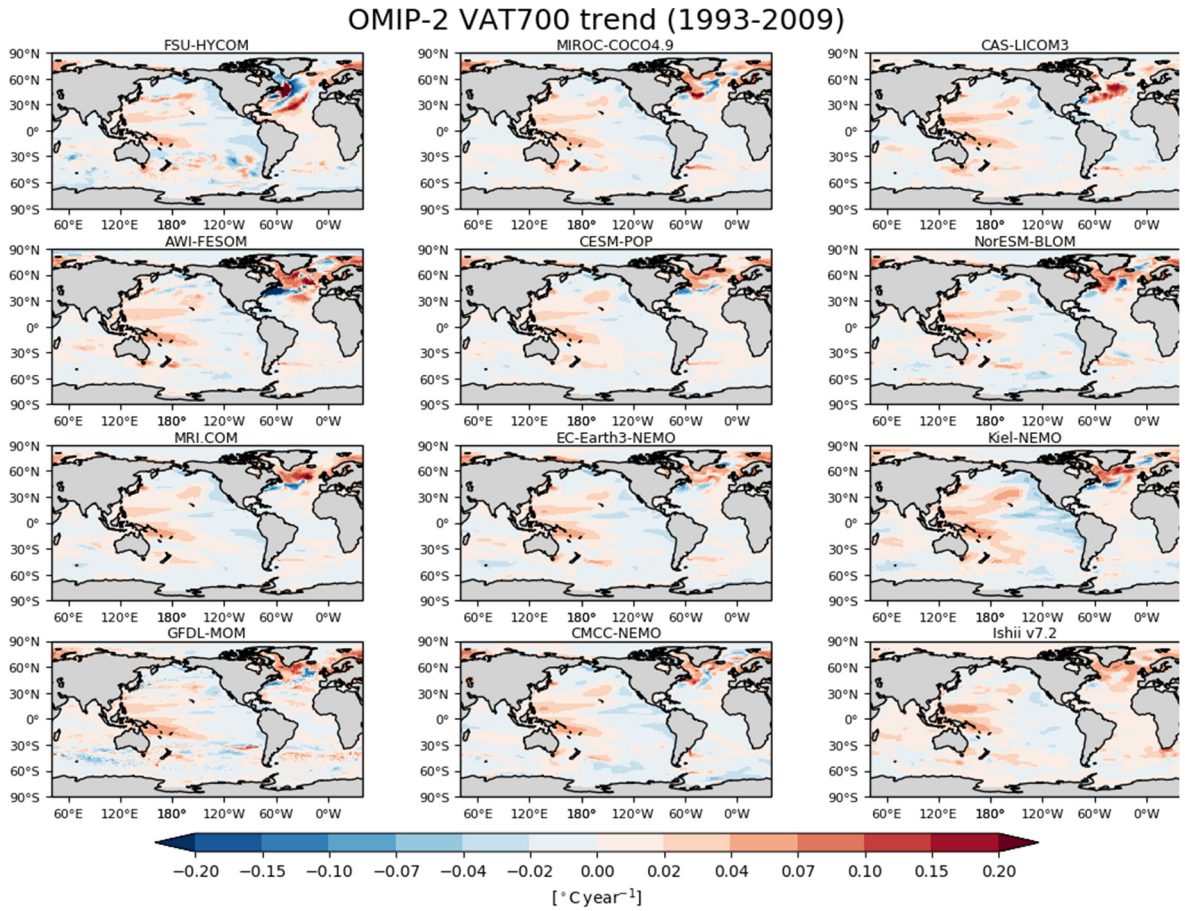

Figure S48: Same as Fig. S47 but for OMIP-2 simulations.

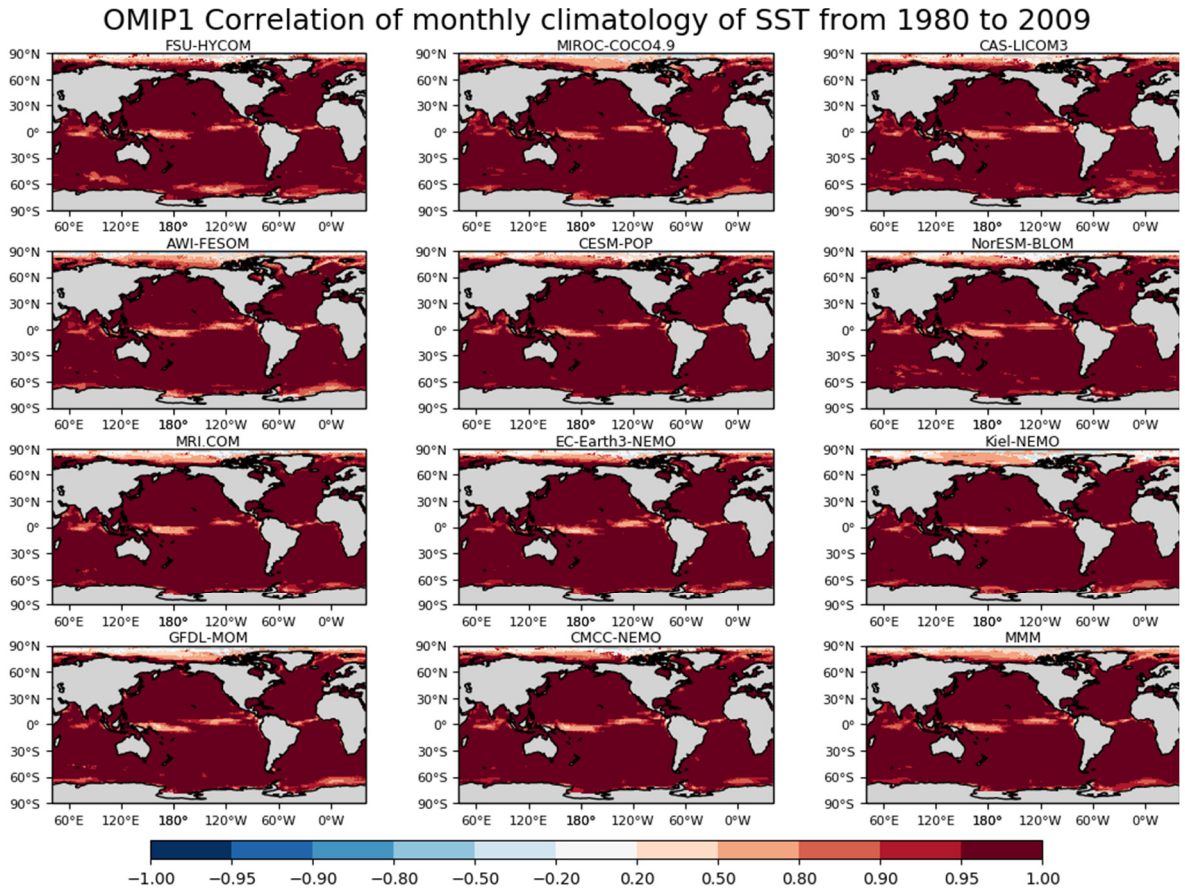

Figure S49: Correlation coefficients of monthly climatology of SST for the period 1980 – 2009 between OMIP-1 simulations and the PCMDI-SST dataset.

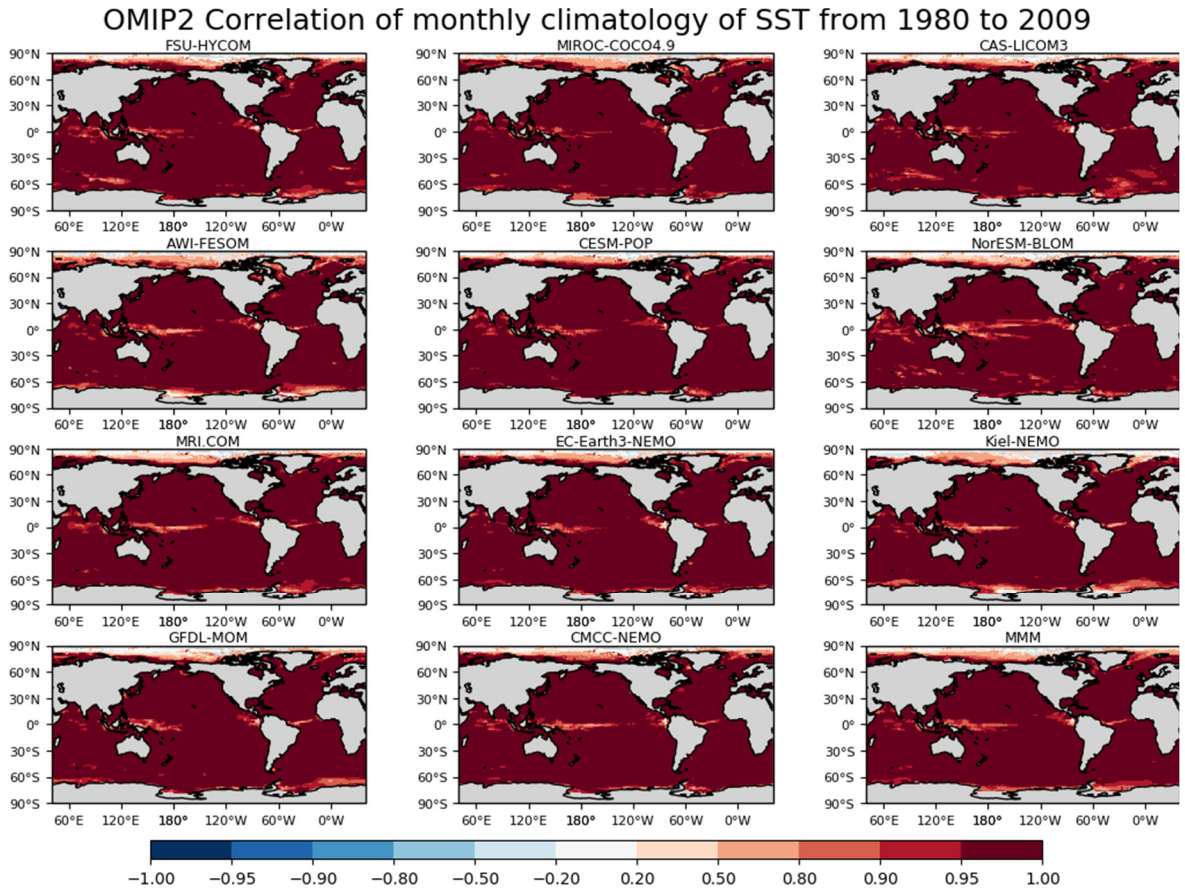

Figure S50: Same as Fig. S49 but for OMIP-2 simulations.

215

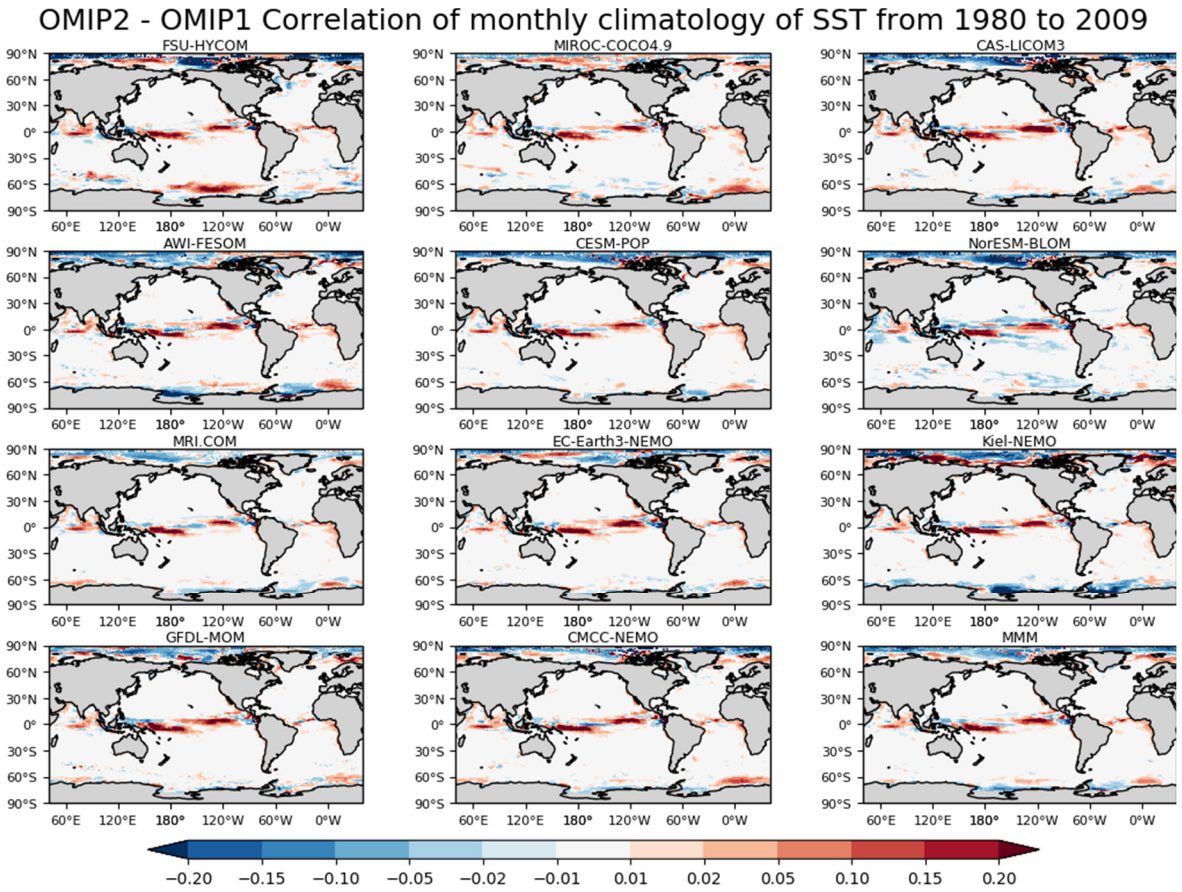

Figure S51: Difference between OMIP-1 and OMIP-2 simulations (OMIP-2 minus OMIP-1) of correlation coefficients of monthly climatology of SST for the period 1980 – 2009 between simulations and the PCMDI-SST dataset.

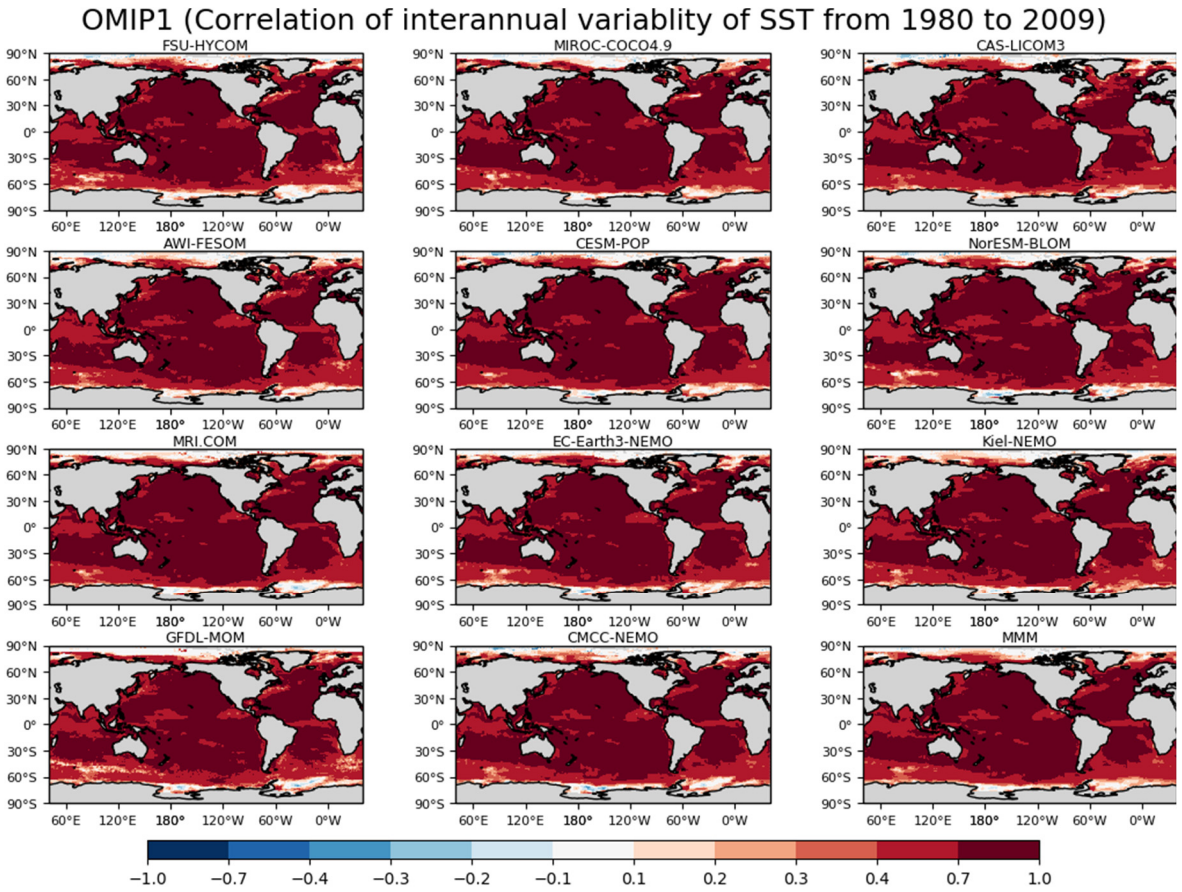

220

Figure S52: Correlation coefficients of monthly SST anomaly relative to the monthly climatology for the period 1980 – 2009 between OMIP-1 simulations and the PCMDI-SST dataset.

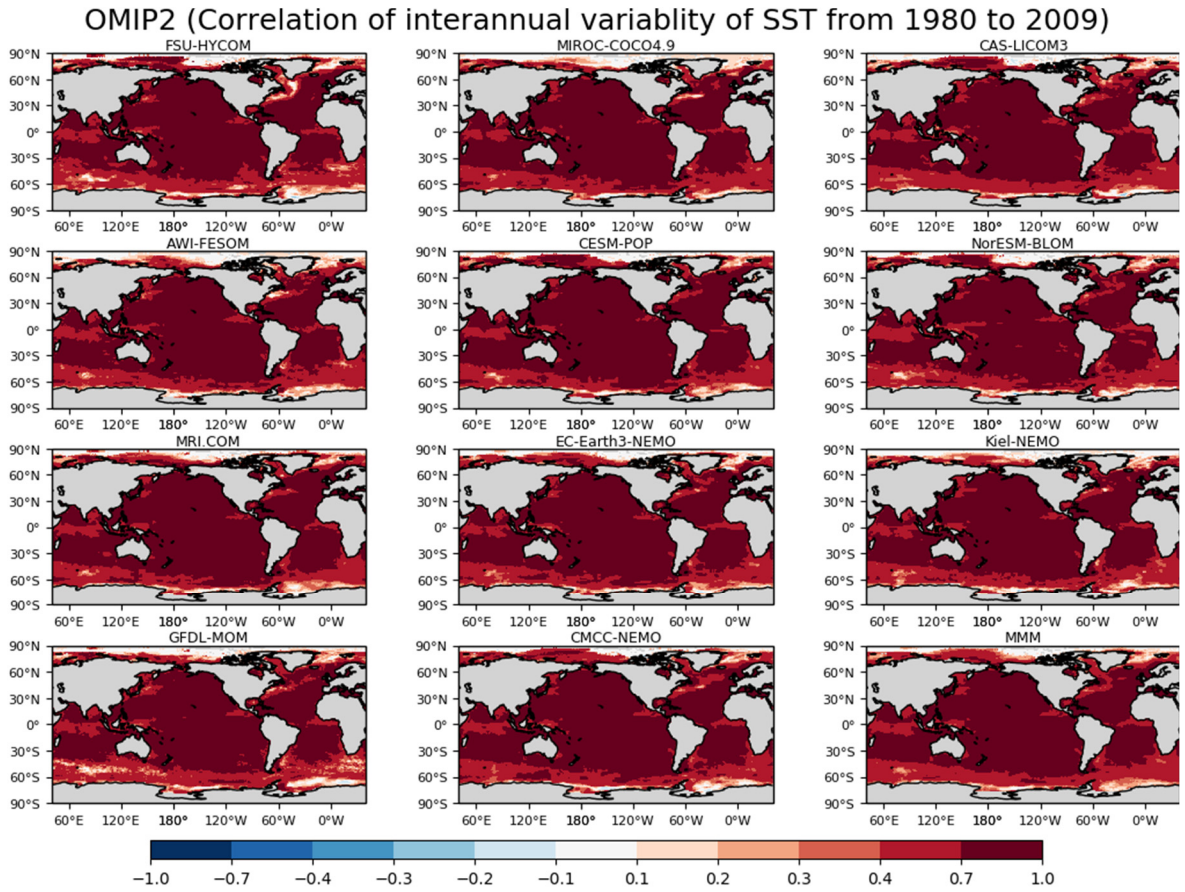

225 **Figure S53: Same as Fig. S52 but for OMIP-2 simulations.**

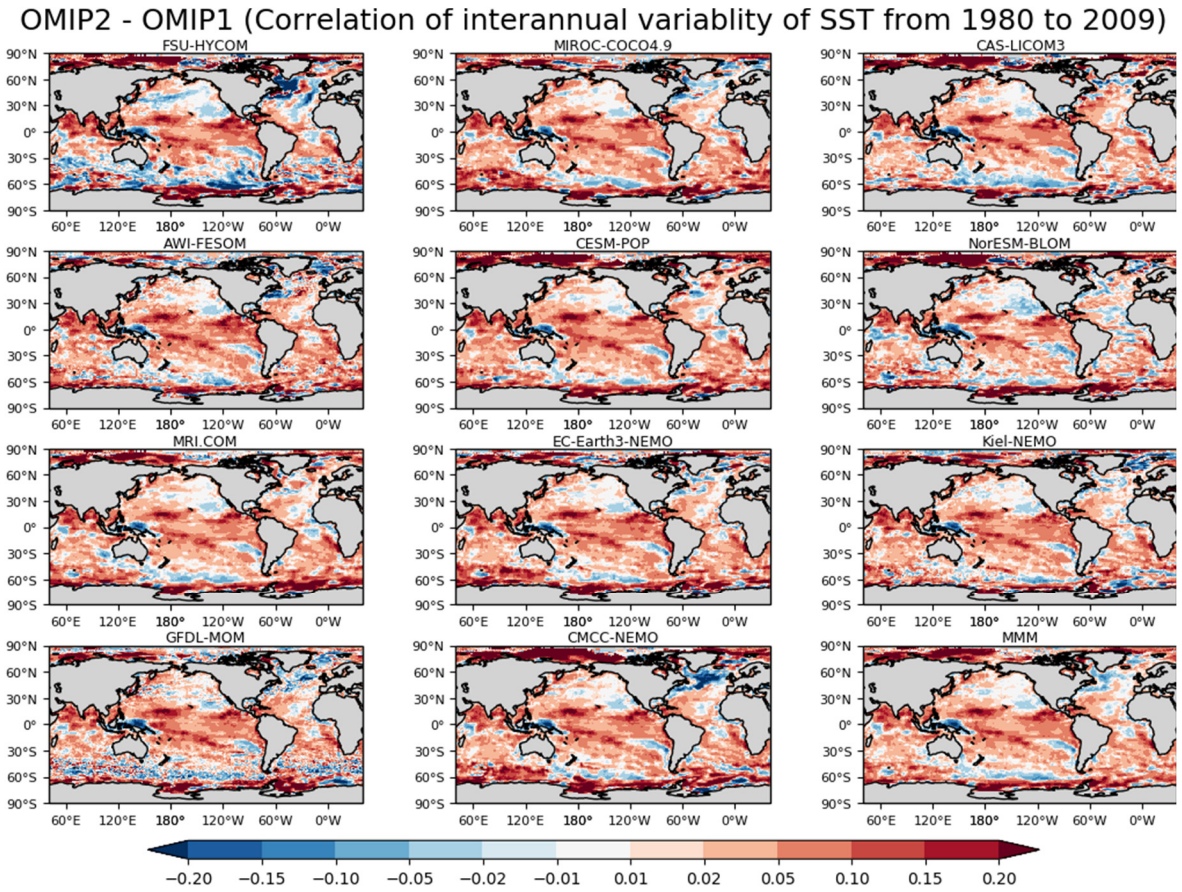

Figure S54: Difference between OMIP-1 and OMIP-2 simulations (OMIP-2 minus OMIP-1) of correlation coefficients of monthly anomaly relative to monthly climatology of SST for the period 1980 – 2009 between simulations and the PCMDI-SST dataset.

230

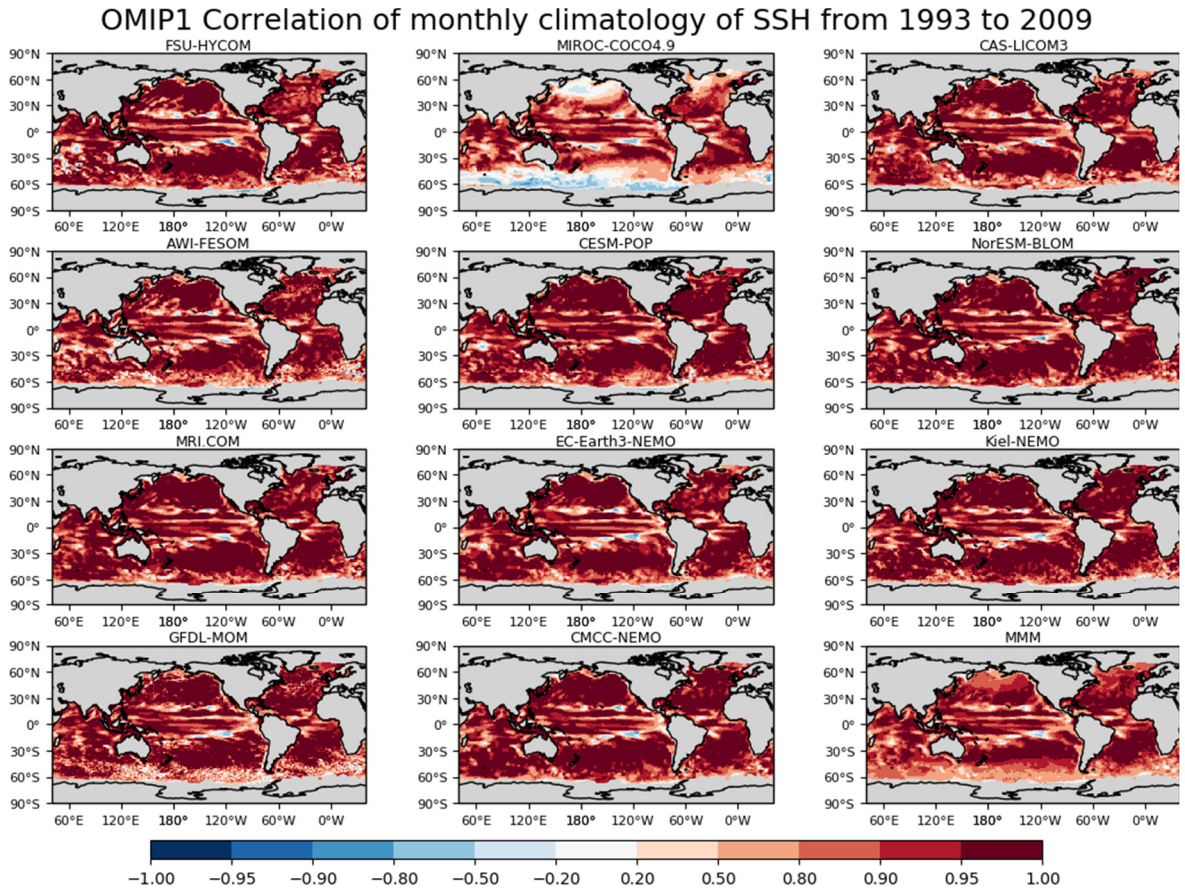

Figure S55: Correlation coefficients of monthly climatology of SSH for the period 1993 – 2009 between OMIP-1 simulations and CMEMS.

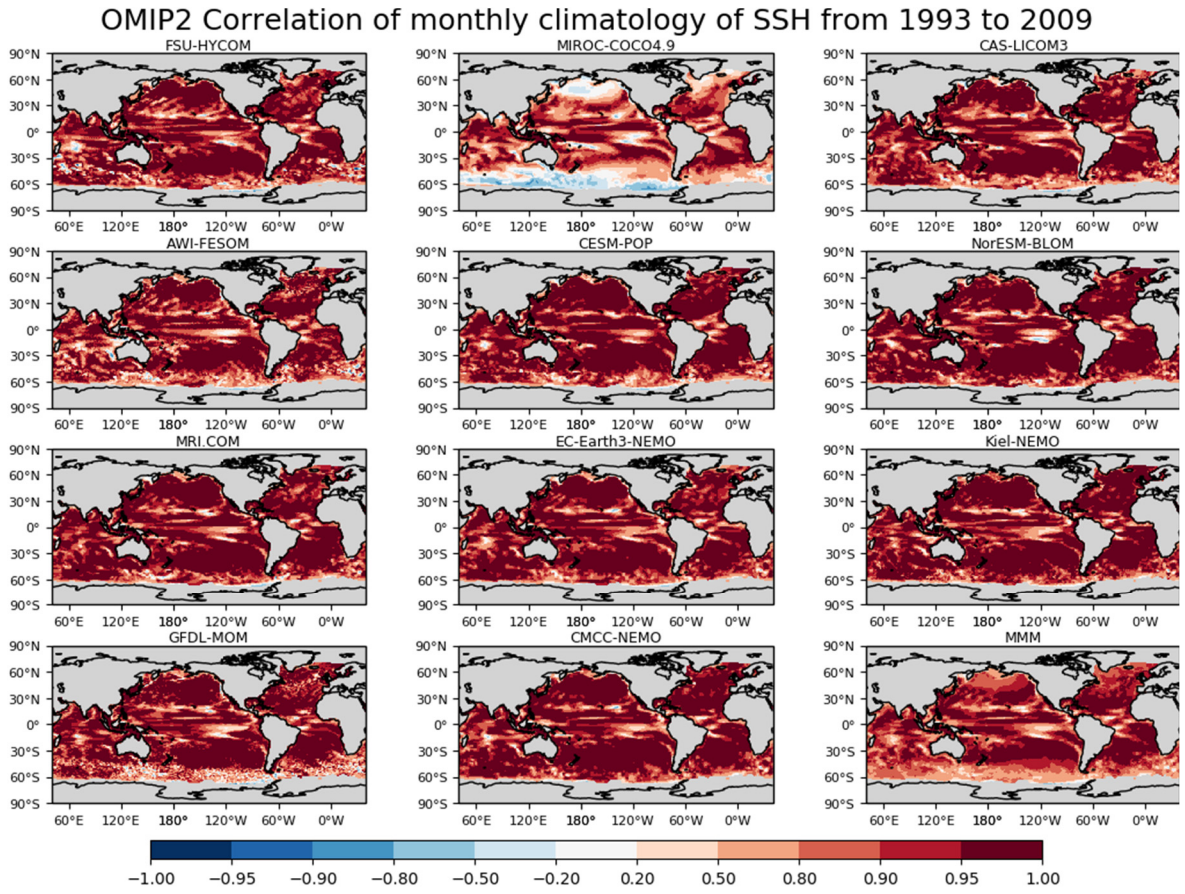

Figure S56: Same as Fig. S55 but for OMIP-2 simulations.

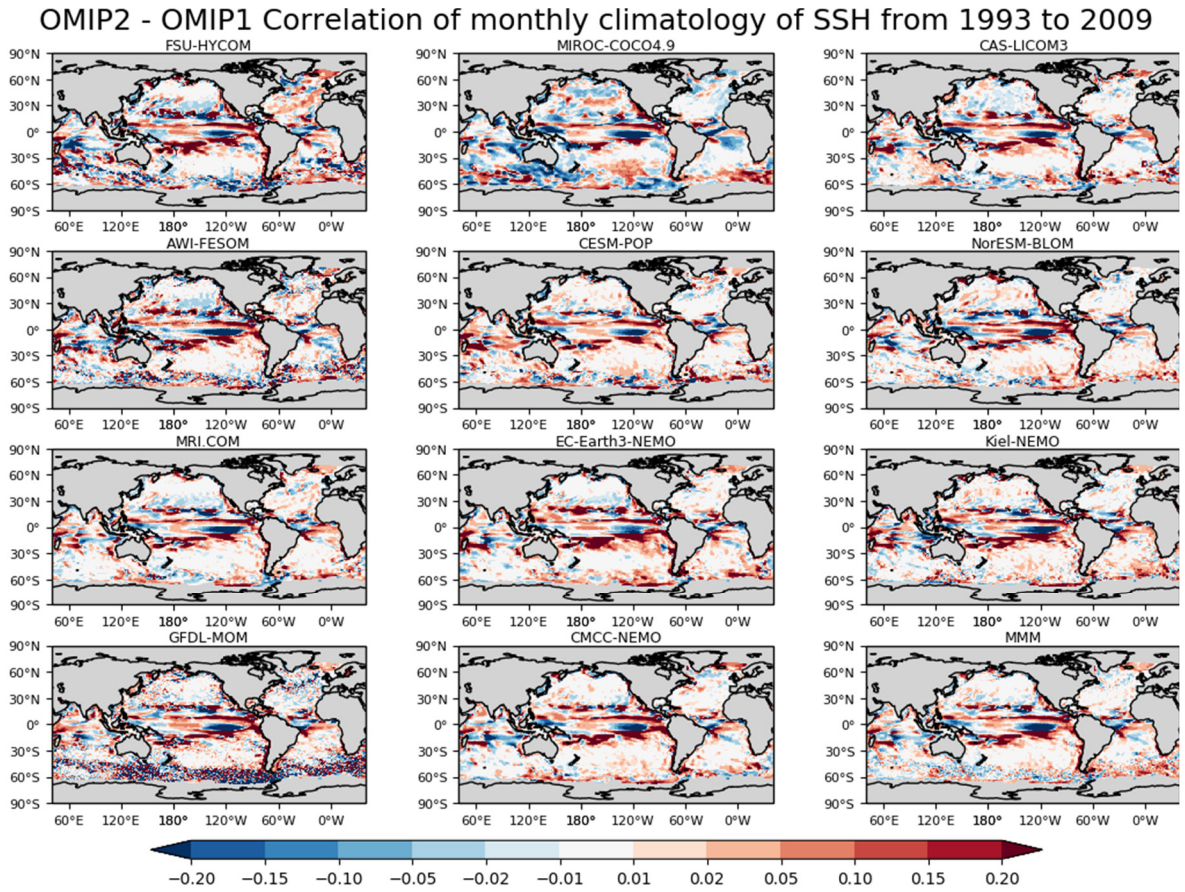

Figure S57: Difference between OMIP-1 and OMIP-2 simulations (OMIP-2 minus OMIP-1) of correlation coefficients of monthly climatology of SSH for the period 1993 – 2009 between simulations and CMEMS.

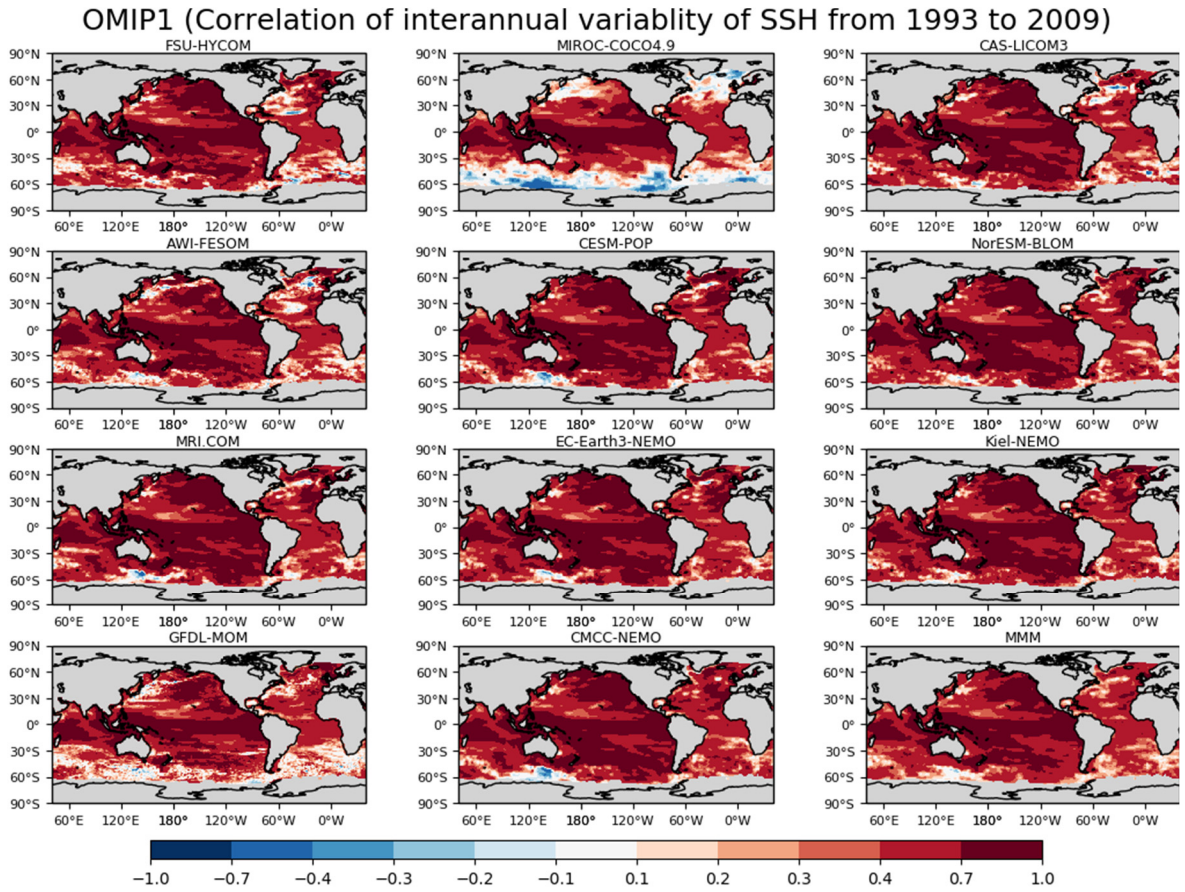

Figure S58: Correlation coefficients of monthly SSH anomaly relative to the monthly climatology for the period 1993 – 2009 between OMIP-1 simulations and CMEMS.

245

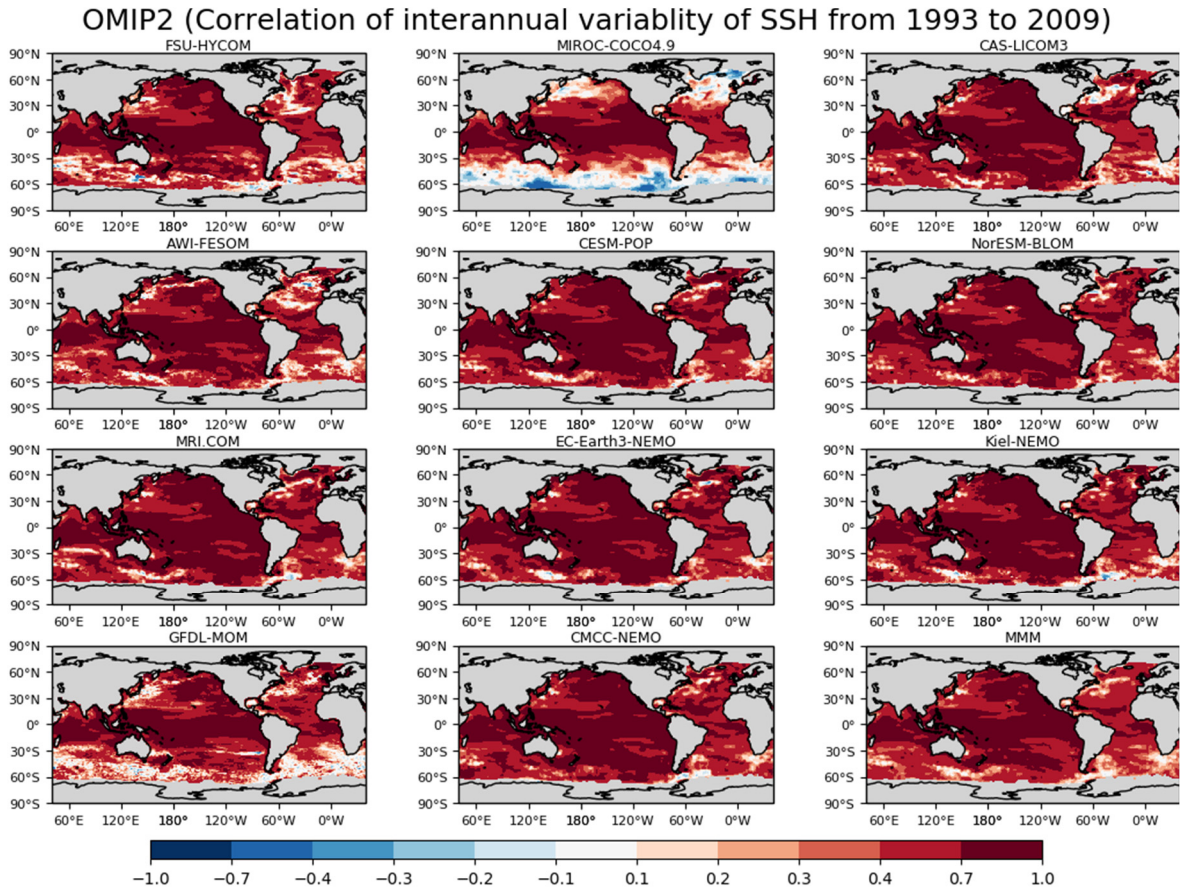

Figure S59: Same as Fig. S58 but for OMIP-2 simulations

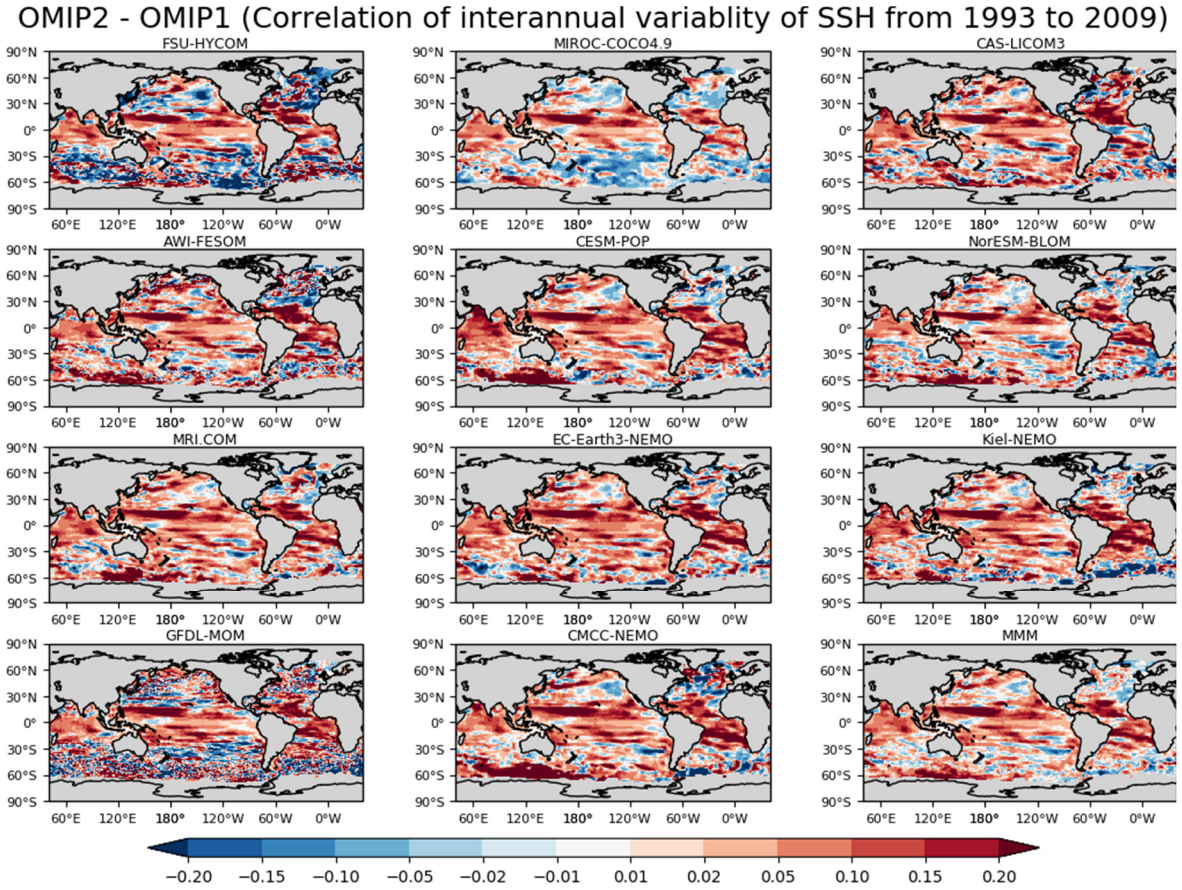

250 **Figure S60: Difference between OMIP-1 and OMIP-2 simulations (OMIP-2 minus OMIP-1) of correlation coefficients of monthly anomaly relative to monthly climatology of SSH for the period 1993 – 2009 between simulations and CMEMS.**

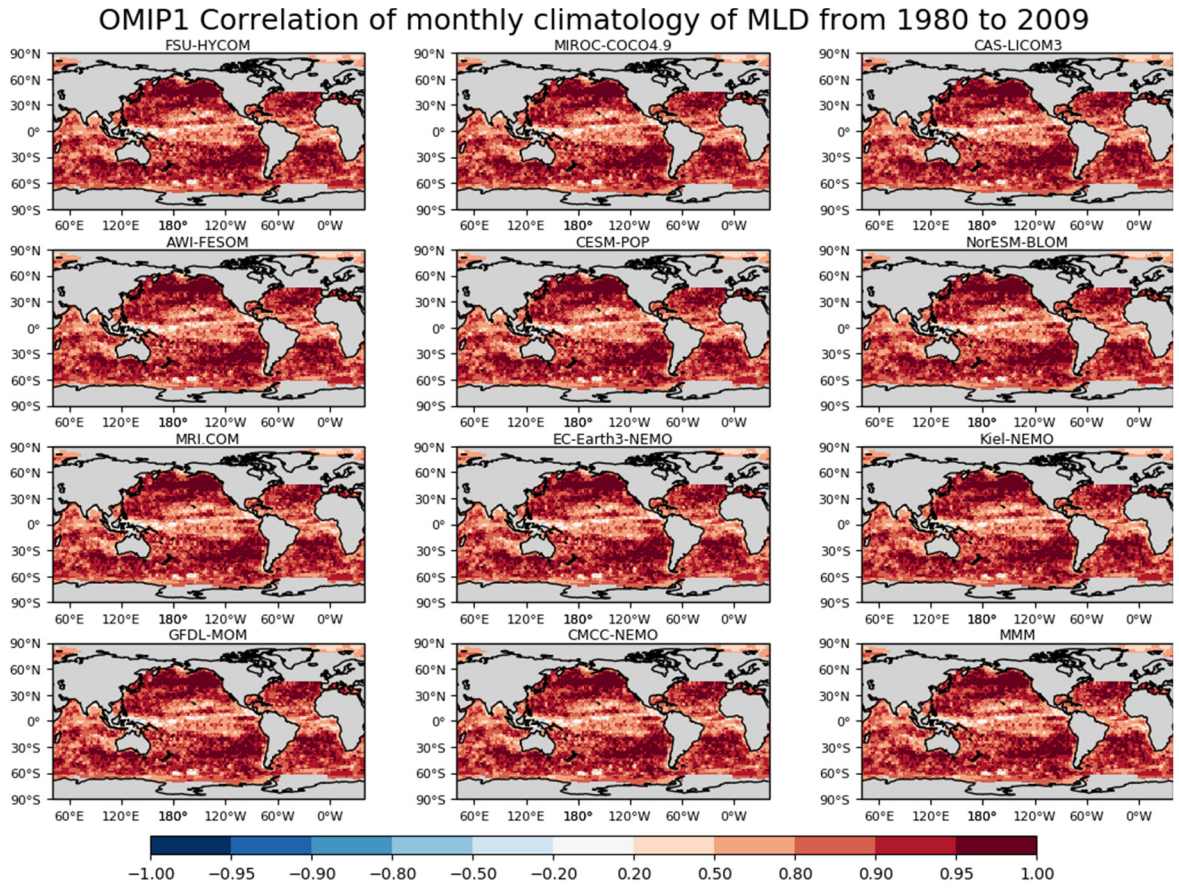

Figure S61: Correlation coefficients of monthly climatology of mixed layer depth (MLD) for the period 1980 – 2009 between OMIP-1 simulations and de Boyer Montégut et al. (2004).

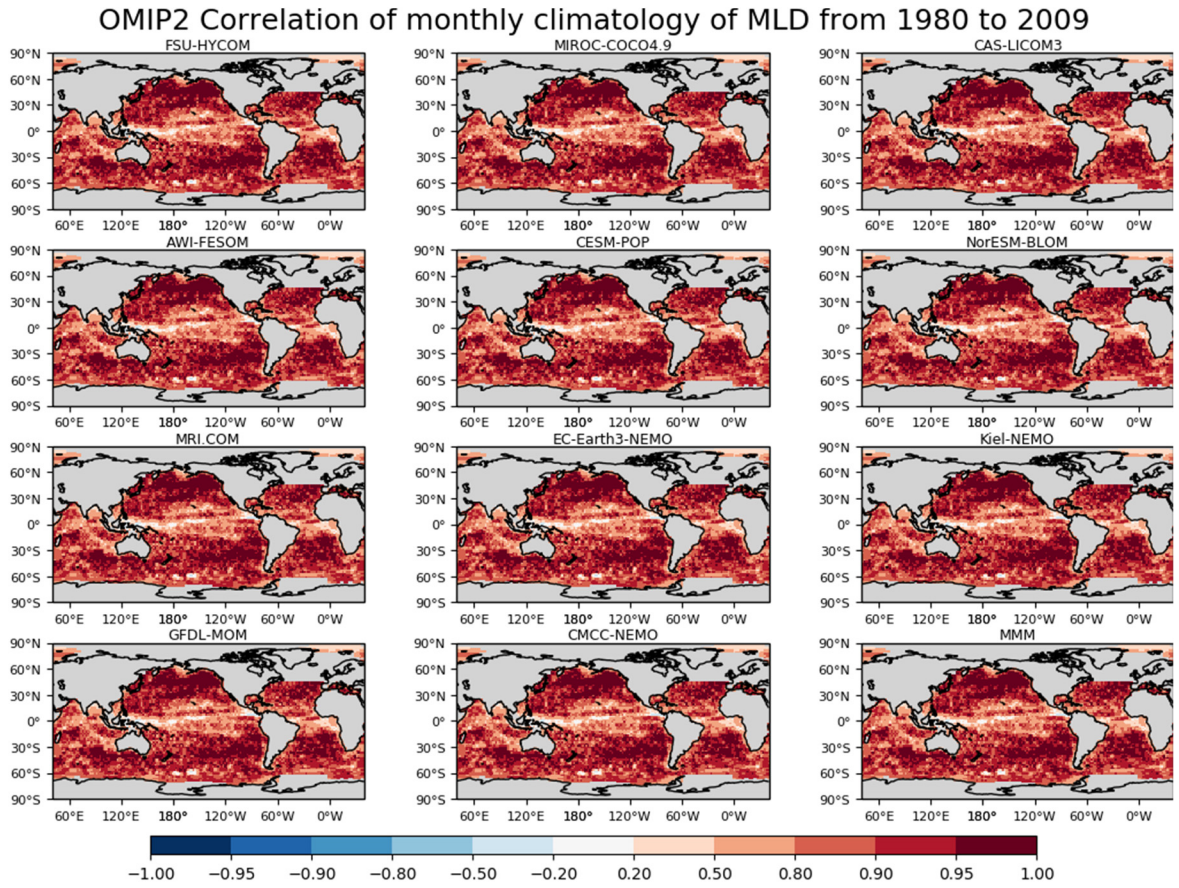

Figure S62: Same as Fig. S61 but for OMIP-2 simulations.

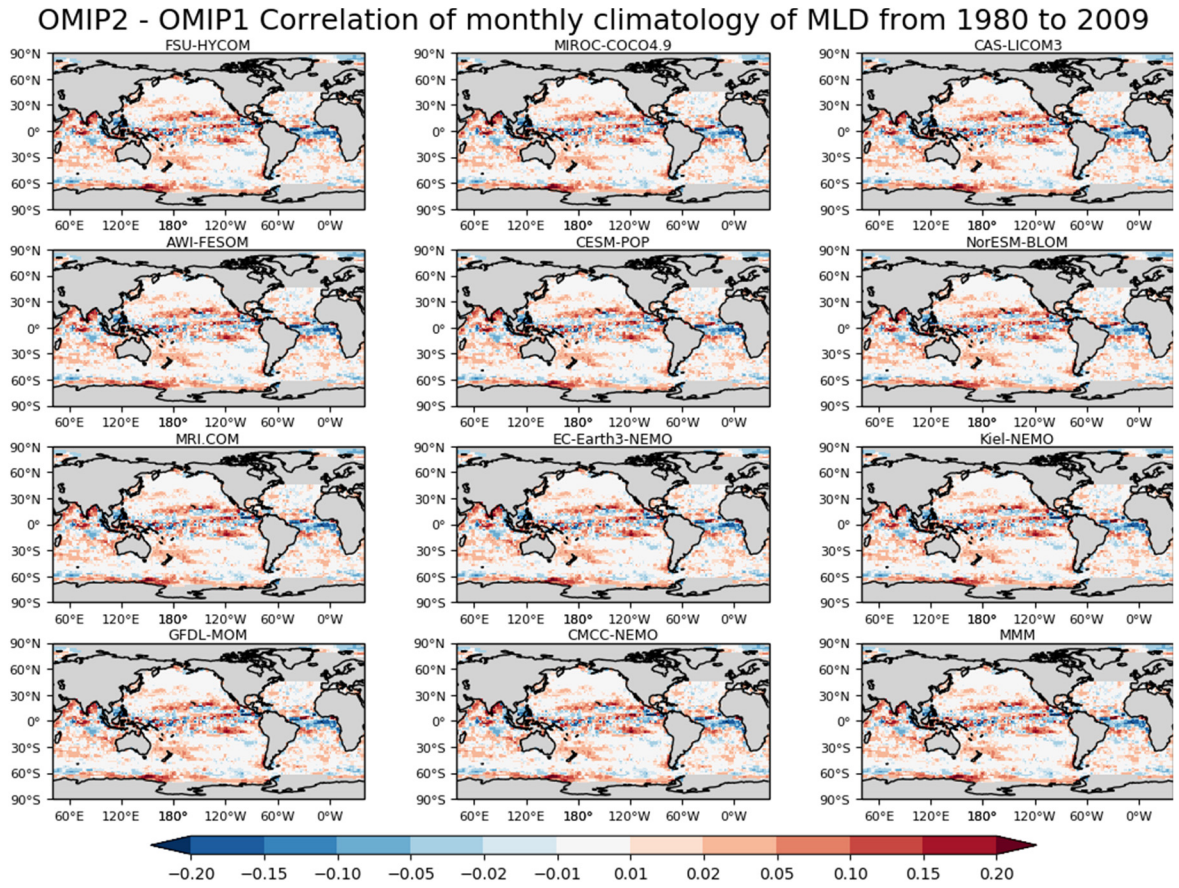

260

Figure S63: Difference between OMIP-1 and OMIP-2 simulations (OMIP-2 minus OMIP-1) of correlation coefficients of monthly climatology of mixed layer depth for the period 1980 – 2009 between simulations and the dataset compiled by de Boyer Montégut et al. (2004).